Nodal and periprostatic imaging in localized prostate cancer management

Nikolaos Grivas

Nodal and periprostatic imaging in localized prostate cancer management

Utrecht University, Utrecht, the Netherlands

ISBN: 978-90-393-7011-7

© N. Grivas, 2018, Utrecht, the Netherlands

No part of this thesis may be reproduced without prior permission of the author.

Nodal and periprostatic imaging in localized prostate cancer management

Beeldvorming van lymfklieren en periprostatische structuren bij de behandeling van gelokaliseerde prostaatkanker

(met een samenvatting in het Nederlands)

Proefschrift

ter verkrijging van de graad van doctor aan de Universiteit Utrecht op gezag van de rector magnificus, prof.dr. H.R.B.M. Kummeling, ingevolge het besluit van het college voor promoties in het openbaar te verdedigen op woensdag 7 november 2018 des middags te 2.30 uur

door

Nikolaos Grivas

geboren op 7 november 1981 te Agrinio, Griekenland

Promotor: Prof.dr. S. Horenblas

Copromotoren: Dr. H.G. van der Poel

Dr. S.W.T.P.J. Heijmink

CONTENTS

1

Introduction and outline

This first part of this thesis will analyze the current methods of detecting lymph node (LN) metastases in prostate cancer (PCa), focusing on the role of sentinel node (SN) biopsy (SNB). The second part will describe the role of Magnetic Resonance Imaging (MRI) both for detecting seminal vesicle (SV) invasion (SVI) and classifying benign prostate hyperplasia (BPH) as well as a method for improving the prediction of functional results erectile function and urinary incontinence) after Robot Assisted Radical Prostatectomy (RARP). At the end the aims and outline of this thesis are presented.

Diagnostic modalities in nodal staging of PCa-The role of SNB

The local LN status is a major prognostic factor in PCa (1). The risk of nodal metastases is 20–45% if any biopsy core has a predominant Gleason 4 pattern or more than three cores have any Gleason 4 pattern (2). Conventional cross-sectional imaging techniques such as Computed Tomography (CT) and MRI cannot accurately differentiate between benign and maligant LNs with a sensitivity for lymph node metatstases < 40% (3). Although higher, the sensitivity for ^{68}Ga–prostate-specific membrane antigen (PSMA) positron emission tomography (PET)/CT still remains between 49% and 66% and metastases smaller than 4 mm are likely to be missed (4-5).

According to the European Association of Urology (EAU) Guidelines the extended pelvic lymph node dissection (ePLND) is the gold standard method for the LN staging of intermediate and high-risk PCa with a risk of nodal metastases >5% (2). However, this template may not include all lymphatic drainage sites with a false negative rate of 13% for detecting metastatic LNs. Moreover it is correlated with increased morbidity and longer operating time (6-7). In addition, the oncological benefit of ePLND was not proven in a recent systematic review of the literature (8).

These limitations and the need to identify occult lymphatic metastases have encouraged the exploration of SN-technology. Selective SNB has the advantage of histopathologic examination and confirmation of metastatic and occult micro-metastatic nodal disease resulting in a more accurate staging, with

the potential to avoid the toxicity of ePLND (9). In urological tumors, the SN procedure was first (1977) described by Cabanas (10) in penile cancer while in PCa the first report was made by Wawroschek et al (11) in 1999. SNB in patients with clinically node negative tumors (cN0) is also a validated technique for accurate staging of nodal disease in breast cancer (12), penile cancer (13) and melanoma (14), while it is being used with promising results in gynecological cancers (15). In these malignancies SNB has become routine for nodal staging as it helps in distinguishing patients who need extensive nodal dissection from those who would not gain an oncologic benefit from such dissection.

SNB in PCa is still considered experimental, as the lymphatic drainage for the prostate gland is highly variable and complex. However, many recent studies suggest that sentinel lymph node dissection (SLND) combined with ePLND provides better lymph node staging in PCa. An improvement in biochemical recurrence free survival has also been reported (16-18). Two recent systematic reviews suggested a sensitivity of 94-95.2% of SLND) for detecting nodal metastases (19-20). This high sensitivity and low morbidity could make SLND the preferred nodal staging tool especially in low and intermediate risk patients. In these patient groups, the SN is often the only tumor-bearing node, and some have therefore suggested removal of only the SN in these cases (21-22). A recent SN consensus panel suggested that SNB could identify metastatic nodes outside the extended lymphadenectomy template but that it should be combined with ePLND especially in intermediate- and high-risk patients since often positive non-SNs were found besides the SNB (23). Recently, the detection rate of SNs has shown also further improvement with the application of new detection techniques, e.g by combining indocyanine green-99mTechnetium-nanocolloid with fluorescein (24). SNB has been also applied as a selection tool for the addition of pelvic radiotherapy and androgen deprivation therapy in patients with histologically positive nodes (pN1) (25).

Apart from diagnostic benefits, SNB may potentially have a therapeutic effect via removal of more metastatic LNs when compared with ePLND-only dissection. Wit et al. in their meta-analysis concluded that for one in 20 patients who undergo ePLND, metastatic LNs would have been left behind without SNB.

(20). Winter et al. detected more LN positive patients compared to the prediction of the Briganti nomogram when SLND was performed (22) and their SN based nomogram demonstrated a high predictive accuracy (26). In this context, SNB can increase the sensitivity of lymph node dissection.

MRI for primary diagnosis of prostate cancer and its role as predictor of functional results after radical prostatetctomy

Accurate PCa staging is critical in guiding a patient's treatment decision and it could prevent both under- and overtreatment. Local staging with multiparametric (mp)-MRI has become widely available and provides new diagnostic means to assess the local extent of prostate tumours. In the literature a wide range of sensitivity and specificity (27) for the detection of SVI is reported, mainly attributed to differences in technique, such as MR field strength, coil-type and variation in radiologist's' experience (28). Furthermore, in a previous study by Gupta et al. the superiority of mp 3T MRI for the diagnosis of organ confinement compared to the Partin Tables was shown, with an area under the curve of 0.82 versus 0.62, respectively (29). It is also known that the diagnostic accuracy of MRI for the detection of extraprostatic extension is higher for intermediate and high-risk cases (30) while a sensitivity of 50% has been reported in low risk disease (31).

Imaging with mpMRI has recently also shown to have a role in the evaluation of BPH patients. The often used transrectal ultrasound (TRUS) has the following limitations: it is user dependent, and it does under- or overestimate prostate volumes larger than 50 cm^3 or smaller than 30 cm^3. Central and anterior located tumors may be masked by the mixed echo pattern of BPH (32).These limitations have led to the increased use of mpMRI especially for Pca recently showing a diagnostic sensitivity of 95% for significant tumors (33). In BPH, prostate segmentation with MRI is an accurate technique for determining prostate and TZ volume, while it has been additionally used for choosing the optimal medical therapy, based on the stromal/glandular ratio and for the assessment of interventional procedures, including ablation and prostatic artery embolization (34-35). A new MRI classification of BPH patterns

was recently published by Wasserman et al. (36). This classification is of significant interest since it could be associated with patients' reported LUTS and determine treatment options (37). In clinical practice lower urinary tract symptoms (LUTS) often lead to serum PSA measurement with a subsequent possible diagnosis of PCa. Since a prostatectomy provides treatment of both BPH and PCa, many men opt for radical surgical removal of the prostate. However, there is limited knowledge on the effects of RARP on LUTS especially in men with both BPH and PCa.

The incidence of urinary incontinence (UI) after radical prostatectomy is variable and difficult to assess due to the lack of a common definition and differences in the time and methodology of assessment (38). The factors associated with postoperative urinary continence after RARP are only partly understood (39). To improve post-prostatectomy continence, it remains crucial to know which pelvic floor structures and prostate fascia areas are associated with urine control. Besides surgical factors such as extent of nerve preservation and reconstruction techniques, pelvic floor anatomical variables such as membranous urethral length (MUL), urethral wall thickness, levator muscle thickness and inner levator distance (ILD) were found to correlate with urinary continence recovery (40-41). A recent meta-analysis has shown that every extra millimeter of MUL is associated with 9% greater odd for return to continence (42). It is considered that an increased MUL could result in a greater amount of smooth muscle fibers and rhabdosphincter preservation potentially increasing the length of the urethral pressure profile and gaining muscle volume for postoperative training (43). mpMRI can be used to non-invasively investigate the morphology and anatomy of the pelvic floor and assess the thickness of the multilayered peri-prostatic fascia which contains the neurovascular bundles (NVBs) (44). Van der Poel et al. proposed an intraoperative scoring system that can be used by the urologist to document and to quantitatively assess the extent of fascia preservation (FP) at different radial segments of the prostate (45). Using this system, FP was found to be an independent predictor of continence recovery reducing the risk of UI at 6 months by >60% when the peri-prostatic fascia was preserved at the lateral locations.

Murphy et al reported that NVBs might not contain any somatic nerve supply while Strasser et al have shown that NVBs directly innervate the membranous urethra (46-47). In a multicenter study Steineck et al. (48) have recently demonstrated that the preservation of both NVBs during RARP decreased the rate of UI by 50% at 1 year after surgery. These findings suggest that not only erectile function but also continence may benefit from more extensive nerve sparing procedures.

Radical prostatectomy induces damage to nerves bundles surrounding the prostate and is often associated with ED. In an attempt to increase the quality of life of patients who value their erectile function (EF), a nerve-sparing prostatectomy is performed in confined PCa (49-51). Initially, the periprostatic nerves were considered to run mainly dorsolaterally to the prostate, but more recent studies have demonstrated that nerves exist in the entire circumference of the (multi-layered) periprostatic fascia (52-54). mpMRI could be helpful to virtually prepare the best nerve-sparing approach in a patient in order to improve EF (55-57). A thicker fascia may provide a better natural protection of periprostatic nerves during RARP and contain more periprostatic nerves. Both may result in better EF outcome. As such, a preoperative means of analysis with MRI of fascia thickness (FT) may have predictive value for postoperative EF.

Aims and outline of this thesis

The thesis will deal with two questions: 1) Imaging and detection of nodal metastases; are we removing the right nodes? and 2) MRI in primary diagnosis of PCa, "more than detecting extracapsular growth"?. In this thesis we will evaluate the diagnostic and oncological benefit of adding SNB to ePLND and the value of MRI both in oncological parameters such as the detection of SVI as well as functional parameters such as UI and ED.

The first part of the thesis includes three chapters. Chapter 2 is reporting the performance of SNB as a tool to select clinically node-negative prostate cancer patients for pelvic radiation therapy; the effect on biochemical recurrence and systemic progression is also analyzed. Chapter 3 reports the impact of adding

SNB to ePLND on the biochemical recurrence of patients treated with RARP. Chapter 4 is a validation study of three nomograms predicting the probability of lymph node invasion in patients undergoing extended and/or sentinel lymph node dissection.

The second part includes four chapters. Chapter 5 reports the diagnostic accuracy of MRI for the detection of seminal vesicle invasion based on the histopathology results of the radical prostatectomy specimen. Chapter 6 reports the correlations of MRI-based BPH patterns with LUTS and continence in men undergoing RARP. Chapter 7 reports the value of MRI-measured periprostatic FT as prognostic factor of EF after nerve-sparing RARP. Finally, Chapter 8 reports the value of MRI-assessed MUL, ILD and FT on continence outcome prediction after RARP.

References

1. Winter A, Kneib T, Rohde M, Henke RP, Wawroschek F. First Nomogram Predicting the Probability of Lymph Node Involvement in Prostate Cancer Patients Undergoing Radioisotope Guided Sentinel Lymph Node Dissection. Urol Int. 2015;95:422-428.
2. Mottet N, Bellmunt J, Bolla M, et al. EAU-ESTRO-SIOG Guidelines on Prostate Cancer. Part 1: Screening, Diagnosis, and Local Treatment with Curative Intent. Eur Urol. 2017 Apr;71(4):618-629.
3. Katz S, Rosen M. MR imaging and MR spectroscopy in prostate cancer management. Radiol Clin North Am. 2006;44:723-734.
4. Budäus L, Leyh-Bannurah SR, Salomon G, Michl U, Heinzer H, Huland H, et al. Initial experience of (68)Ga-PSMA PET/CT imaging in high-risk prostate cancer patients prior to radical prostatectomy. Eur Urol. 2016;69(3):393–6
5. van Leeuwen PJ, Emmett L, Ho B, et al. Prospective Evaluation of 68Gallium-PSMA Positron Emission Tomography/Computerized Tomography for Preoperative Lymph Node Staging in Prostate Cancer. BJU Int. 2016. doi: 10.1111/bju.13540.
6. Joniau S, Van den Bergh L, Lerut E, et al. Mapping of pelvic lymph node metastases in prostate cancer. Eur Urol. 2013;63:450-458.
7. Briganti, A., Chun, F.K., Salonia, A. et al. Complications and other surgical outcomes associated with extended pelvic lymphadenectomy in men with localized prostate cancer. Eur Urol. 2006; 50: 1006–1013.
8. Fossati N, Willemse PM, Van den Broeck T, van den Bergh RC, Yuan CY, Briers E, et al. The benefits and harms of different extents of lymph node dissection during radical prostatectomy for prostate cancer: a systematic review. Eur Urol. 2017;72(1):84–109.
9. van der Poel, H.G., Buckle, T., Brouwer, O.R., Valdes Olmos, R.A., and van Leeuwen, F.W. Intraoperative laparoscopic fluorescence guidance to the sentinel lymph node in prostate cancer patients: clinical proof of concept of an integrated functional imaging approach using a multimodal tracer. Eur Urol. 2011; 60: 826–833.

10. Cabanas RM. An approach for the treatment of penile carcinoma. Cancer. 1977;39:456-466.
11. Wawroschek F, Vogt H, Weckermann D, Wagner T, Harzmann R. The sentinel lymph node concept in prostate cancer - first results of gamma probe-guided sentinel lymph node identification. Eur Urol. 1999;36:595-600.
12. Veronesi U, Paganelli G, Viale G, et al. A randomized comparison of sentinel-node biopsy with routine axillary dissection in breast cancer. N Engl J Med. 2003;349:546-553.
13. Sadeghi R, Gholami H, Zakavi SR, Kakhki VR, Tabasi KT, Horenblas S. Accuracy of sentinel lymph node biopsy for inguinal lymph node staging of penile squamous cell carcinoma: systematic review and meta-analysis of the literature. J Urol. 2012;187:25-31
14. Morton DL, Thompson JF, Cochran AJ, et al. Final trial report of sentinel-node biopsy versus nodal observation in melanoma. N Engl J Med. 2014;370:59.
15. Belhocine TZ, Prefontaine M, Lanvin D, et al. Added-value of SPECT/CT to lymphatic mapping and sentinel lymphadenectomy in gynaecological cancers. Am J Nucl Med Mol Imaging. 2013;3:182–193.
16. KleinJan GH, van den Berg NS, Brouwer OR, et al. Optimisation of fluorescence guidance during robot-assisted laparoscopic sentinel node biopsy for prostate cancer. Eur Urol. 2014;66:991-998.
17. Acar C, Kleinjan GH, van den Berg NS, Wit EM, van Leeuwen FW, van der Poel HG. Advances in sentinel node dissection in prostate cancer from a technical perspective. Int J Urol. 2015;22:898-909.
18. Grivas N, Wit EMK, Kuusk T, et al. The Impact of Adding Sentinel Node Biopsy to Extended Pelvic Lymph Node Dissection on Biochemical Recurrence in Prostate Cancer Patients Treated with Robot-Assisted Radical Prostatectomy. J Nucl Med. 2018q;59(2):204-209.
19. Sadeghi R, Tabasi KT, Bazaz SM, et al. Sentinel node mapping in the prostate cancer. Meta-analysis. Nuklearmedizin. 2011;50:107-115.
20. Wit EMK, Acar C, Grivas N, et al. Sentinel Node Procedure in Prostate Cancer: A Systematic Review to Assess Diagnostic Accuracy. Eur Urol. 2017;71:596-605.

21. Holl, G., Dorn, R., Wengenmair, H., Weckermann, D., and Sciuk, J. Validation of sentinel lymph node dissection in prostate cancer: experience in more than 2,000 patients. Eur J Nucl Med Mol Imaging. 2009; 36: 1377–1382.
22. Winter, A., Kneib, T., Henke, R.P., and Wawroschek, F. Sentinel lymph node dissection in more than 1200 prostate cancer cases: rate and prediction of lymph node involvement depending on preoperative tumor characteristics. Int J Urol. 2014; 21: 58–63.
23. van der Poel HG, Wit EM, Acar C, et al. Sentinel node biopsy for prostate cancer: report from a consensus panel meeting. BJU Int. February 10, 2017
24. van den Berg NS, Buckle T, KleinJan GH, van der Poel HG, van Leeuwen FW. Multispectral fluorescence imaging during robot-assisted laparoscopic sentinel node biopsy: a first step towards a fluorescence-based anatomic roadmap. Eur Urol. June 23, 2016 [Epub ahead of print].
25. Grivas N, Wit E, Pos F, et al. Sentinel Lymph Node Dissection to Select Clinically Node-negative Prostate Cancer Patients for Pelvic Radiation Therapy: Effect on Biochemical Recurrence and Systemic Progression. Int J Radiat Oncol Biol Phys. 2017 Feb 1;97(2):347-354.
26. Winter A, Kneib T, Rohde M, Henke RP, Wawroschek F. First nomogram predicting the probability of lymph node involvement in prostate cancer patients undergoing radioisotope guided sentinel lymph node dissection. Urol Int. 2015;95:422-428.
27. Otto, G. Thörmer, M. Seiwerts, et al., Value of endorectal magnetic resonance imaging at 3T for the local staging of prostate cancer, Rofo 186 (8) (2014) 795–802.
28. M. Hoeks, J.O. Barentsz, T. Hambrock, et al., Prostate cancer: multiparametric MR imaging for detection, localization, and staging, Radiology 261 (1) (2011 46–66.
29. R.T. Gupta, K.F. Faridi, A.A. Singh, et al., Comparing 3-T multiparametric MRI and the Partin tables to predict organ-confined prostate cancer after radical prostatectomy. Urol. Oncol. 32 (8) (2014) 1292–1299.

30. P. Radtke, B.A. Hadaschik, M.B. Wolf, et al., The impact of magnetic resonance imaging on prediction of extraprostatic extension and prostatectomy outcome in patients with low-, intermediate- and high-Risk prostate cancer: try to find a standard, J.Endourol 29 (12) (2015) 1396–1405.
31. F. Cornud, T. Flam, L. Chauveinc, et al., Extraprostatic spread of clinically localized prostate cancer: factors predictive of pT3 tumor and of positive endorectal MR.
32. Matthews GJ, Motta J and Fracehia JA. The accuracy of transrectal ultrasound prostate volume estimation: clinical correlations. J Clin Ultrasound. 1996; 24: 501-505.
33. Ahmed HU, El-Shater Bosaily A, Brown LC, et al. Diagnostic accuracy of multiparametric MRI and TRUS biopsy in prostate cancer (PROMIS): a paired validating confirmatory study. Lancet. 2017 Feb 25;389(10071):815-822.
34. Turkbey B, Fotin SV, Huang RJ, et al. Fully automated prostate segmentation on MRI: comparison with manual segmentation methods and specimen volumes. AJR Am J Roentgenol. 2013; 201: W720-729.
35. Kisilevzky N and Faintuch S. MRI assessment of prostatic ischaemia: best predictor of clinical success after prostatic artery embolisation for benign prostatic hyperplasia. Clin Radiol. 2016; 71: 876-882.
36. Wasserman NF, Spilseth B, Golzarian J, et al. Use of MRI for Lobar Classification of Benign Prostatic Hyperplasia: Potential Phenotypic Biomarkers for Research on Treatment Strategies. AJR Am J Roentgenol. 2015; 205: 564-571.
37. Guneyli S, Ward E, Thomas S, et al. Magnetic resonance imaging of benign prostatic hyperplasia. Diagn Interv Radiol. 2016; 22: 215-219.
38. Eastham JA, Kattan MW, Rogers E, et al. Risk factors for urinary incontinence after radical prostatectomy. J Urol. 1996;156:1707–1713.
39. Sandhu JS, Eastham JA. Factors predicting early return of continence after radical prostatectomy. Curr Urol Rep. 2010;11:191–197.
40. Tienza A, Hevia M, Benito A, et al. MRI factors to predict urinary incontinence after retropubic/laparoscopic radical prostatectomy. Int Urol Nephrol. 2015;47:1343–1349.

41. von Bodman C, Matsushita K, Savage C, et al. Recovery of urinary function after radical prostatectomy: predictors of urinary function on preoperative prostate magnetic resonance imaging. J Urol. 2012;187:945–950.
42. Mungovan SF, Sandhu JS, Akin O, et al. Preoperative membranous urethral length measurement and continence recovery following radical prostatectomy: a systematic review and meta-analysis. Eur Urol. 2017;71:368–378
43. Chang JI, Lam V, Patel MI. Preoperative pelvic floor muscle exercise and postprostatectomy incontinence: a systematic review and meta-analysis. Eur Urol. 2016;69:460–467
44. Sievert KD, Hennenlotter J, Laible I, et al. The periprostatic autonomic nerves-bundle or layer? Eur Urol. 2008;54:1109–1116.
45. van der Poel HG, de Blok W, Joshi N, van Muilekom E. Preservation of lateral prostatic fascia is associated with urine continence after robotic-assisted prostatectomy. Eur Urol. 2009;55:892–900.
46. Murphy DG, Costello AJ. How can the autonomic nervous system contribute to urinary continence following radical prostatectomy? A “boson-like“ conundrum. Eur Urol. 2013;63:445–447.
47. Strasser H, Bartsch G. Anatomic basis for the innervation of the male pelvis. Urologe A. 2004;43:128–132.
48. Steineck G, Bjartell A, Hugosson J, et al. Degree of preservation of the neurovascular bundles during radical prostatectomy and urinary continence 1 year after surgery. Eur Urol. 2015;67: 559–568.
49. Savera AT, Kaul S, Badani K, et al. Robotic radical prostatectomy with the "Veil of Aphrodite" technique: histologic evidence of enhanced nerve sparing. Eur Urol. 2006;49:1065-73.
50. Stolzenburg JU, Rabenalt R, Do M, et al. Intrafascial nerve-sparing endoscopic extraperitoneal radical prostatectomy. Eur Urol. 2008;53:931-40.
51. Tewari A, Peabody JO, Fischer M, et al. An operative and anatomic study to help in nerve sparing during laparoscopic and robotic radical prostatectomy. Eur Urol. 2003;43:444-54.

52. Villeirs GM, L Verstraete K, De Neve WJ, De Meerleer GO. Magnetic resonance imaging anatomy of the prostate and periprostatic area: a guide for radiotherapists. Radiother Oncol. 2005;76:99-106.
53. Secin FP, Bianco FJ. Surgical anatomy of radical prostatectomy: periprostatic fascial anatomy and overview of the urinary sphincters. Arch Esp Urol. 2010;63:255-66.
54. Eichelberg C, Erbersdobler A, Michl U, et al. Nerve distribution along the prostatic capsule. Eur Urol. 2007;51:105-10.
55. de Rooij M, Hamoen EH, Fütterer JJ, et al. Accuracy of multiparametric MRI for prostate cancer detection: a meta-analysis. AJR Am J Roentgenol. 2014;202:343-51.
56. McClure TD, Margolis DJ, Reiter RE, et al. Use of MR imaging to determine preservation of the neurovascular bundles at robotic-assisted laparoscopic prostatectomy. Radiology. 2012;262:874-83.
57. Tanaka K, Shigemura K, Muramaki M, et al. Efficacy of using three-tesla magnetic resonance imaging diagnosis of capsule invasion for decision-making about neurovascular bundle preservation in robotic-assisted radical prostatectomy. Korean J Urol. 2013;54:437-41.

Part I

Imaging and detection of nodal metastases; “are we removing the right nodes?"

2

Sentinel Lymph Node Dissection to Select Clinically Node-negative Prostate Cancer Patients for Pelvic Radiation Therapy: Effect on Biochemical Recurrence and Systemic Progression.

Grivas N, Wit E, Pos F, de Jong J, Vegt E, Bex A, Hendricksen K, Horenblas S, KleinJan G, van Rhijn B, van der Poel H.

Int J Radiat Oncol Biol Phys. 2017 Feb 1;97(2):347-354.

Abstract

Purpose - To assess the efficacy of robotic-assisted laparoscopic sentinel lymph node (SLN) dissection (SLND) to select those patients with prostate cancer (PCa) who would benefit from additional pelvic external beam radiation therapy and long-term androgen deprivation therapy (ADT).

Methods and Materials - Radioisotope-guided SLND was performed in 224 clinically node-negative patients scheduled to undergo external beam radiation therapy. Patients with histologically positive SLNs (pN1) were also offered radiation therapy to the pelvic lymph nodes, combined with 3 years of ADT. Biochemical recurrence (BCR), overall survival, and metastasis-free (including pelvic and nonregional lymph nodes) survival (MFS) rates were retrospectively calculated. The Briganti and Kattan nomogram predictions were compared with the observed pN status and BCR.

Results - The median prostate-specific antigen (PSA) value was 15.4 ng/mL (interquartile range [IQR] 8-29). A total number of 834 SLNs (median 3 per patient; IQR 2-5) were removed. Nodal metastases were diagnosed in 42% of the patients, with 150 SLNs affected (median 1; IQR 1-2). The 5-year BCR-free and MFS rates for pN0 patients were 67.9% and 87.8%, respectively. The corresponding values for pN1 patients were 43% and 66.6%. The PSA level and number of removed SLNs were independent predictors of BCR and MFS, and pN status was an additional independent predictor of BCR. The 5-year overall survival rate was 97.6% and correlated only with pN status. The predictive accuracy of the Briganti nomogram was 0.665. Patients in the higher quartiles of Kattan nomogram prediction of BCR had better than expected outcomes. The complication rate from SLND was 8.9%.

Conclusions - For radioisotope-guided SLND, the high staging accuracy is accompanied by low morbidity. The better than expected outcomes observed in the lower quartiles of BCR prediction suggest a role for SLN biopsy as a potential selection tool for the addition of pelvic radiation therapy and ADT intensification in pN1 patients.

Introduction

The local lymph node (LN) status is a major prognostic factor in prostate cancer (PCa) (1). According to the European Association of Urology (EAU) guidelines, extended pelvic LN dissection (ePLND) is the reference standard method for LN staging of patients with intermediate- and high-risk PCa (2). In addition, ePLND has been associated with a survival advantage in some retrospective series. However, this potential benefit has been limited by the selection bias and the Will Rogers phenomenon observed in these studies (3). Moreover, this extended template might not include all lymphatic drainage sites, and resection has been correlated with increased morbidity and longer operating times (4).

These limitations and the need to identify occult lymphatic metastases have encouraged the exploration of the sentinel lymph node (SLN). Selective SLN biopsy (SLNB) has the advantage of histopathologic examination and confirmation of metastatic and occult micrometastatic nodal disease, with the potential of avoiding the toxicity of ePLND. In urologic tumors, the SLNB procedure was first described by Cabanas (5) in 1977 for penile cancer. In PCa, the first study was reported by Wawroschek et al (6) in 1999. SLNB in patients with clinically node-negative tumors (cN0) is also a validated technique for accurate staging of nodal disease in breast cancer (7), penile cancer (8), and melanoma (9). It is also being used with promising results in gynecologic cancers (10). Many recent studies have suggested that SLN dissection (SLND), combined with ePLND, also provides better LN staging in PCa (11, 12). The EAU guidelines suggest SLND as an experimental method with the aim of improving diagnostic accuracy and reducing the morbidity associated with ePLND (2).

With the aim of identifying the low-risk cases, numerous nomograms based on preoperative variables have been developed to predict LN invasion (LNI) and biochemical recurrence (BCR) in PCa. The updated nomogram by Briganti et al (13) is the most commonly used nomogram for predicting LNI status. It includes the clinical stage, pretreatment prostate-specific antigen (PSA) level, primary and secondary Gleason grade, and percentage of positive cores. The

most frequently used nomogram for predicting BCR is the Kattan nomogram, which includes the PSA level, clinical stage, and Gleason grade (14).

The Radiation Therapy Oncology Group for pelvic irradiation recommends the irradiation of the distal common iliac, presacral, external and internal iliac, and obturator LNs (15). The EAU guidelines do not recommend prophylactic whole pelvic irradiation, suggesting that ePLND should be used to guide the selection of patients who should undergo additional pelvic radiation therapy (RT) (2). Müller et al (16) proposed selective RT according to the single-photon emission computed tomography (SPECT)-identified SLN template. They reported favorable results, with 4 patients required to undergo treatment to avoid 1 regional relapse.

Obtaining histologic confirmation of nodal metastases by surgical sampling of the SLN might allow the tailoring of pelvic RT to those men with LN-positive (pN1) disease and avoid unnecessary RT for men without nodal invasion. The aim of our study was to assess the efficacy of robotic-assisted laparoscopic SLND to select those patients with PCa who would benefit from additional pelvic RT and long-term androgen deprivation therapy (ADT). The observed LNI and BCR-free rates were compared using the Briganti and Kattan nomogram predictions, respectively.

Methods and Materials

Patients

From February 2005 to February 2016, 224 patients who had opted for external beam RT (EBRT) for localized, biopsy-proven PCa were offered a pre-RT robotic-assisted laparoscopic SLND. All the data were prospectively gathered but were retrospectively analyzed. The primary tumor was staged using digital rectal examination and transrectal ultrasonography and classified using the 2009 TNM staging system. PSA was measured using standard assays. Only patients with a risk of ≥5% for LN metastases, according to the Briganti nomogram, were included. Additional selection criteria were patient consent for

SLNB, no bone metastasis on bone scan, no pelvic LN enlargement on abdominopelvic imaging (ie, no LN ≥8 mm in the transverse dimension), World Health Organization performance status <2, no previous hormonal therapy or prostatectomy, and no previous or other malignancy.

RT technique

From 2005 to 2007, the patients were treated with 3-dimensional conformal RT to a dose of 50 Gy in 25 fractions of 2 Gy to the pelvis and a sequential boost dose to the prostate and seminal vesicles of 20 Gy in 10 fractions. The pelvis was irradiated using a 3-field technique. The clinical target volume for the sequential boost dose was the prostate and seminal vesicles, and the clinical target volume was expanded with a 1-cm uniform margin to reach the planning target volume. From 2007 onward, the patients underwent 7-field intensity-modulated RT (IMRT) using 3 dose levels and a simultaneous integrated boost technique. In the case of positive findings from the SLN procedure, the pelvic LN template received a dose of 52.5 Gy in 35 fractions of 1.5 Gy, and the prostate and seminal vesicles received a dose of 70 Gy in 35 fractions of 2 Gy.

SLND technique

99mTc-nanocolloid was used as a tracer from 2005 until 2012, and indocyanine green-99mTc-nanocolloid was used from 2012 onward (11). Both were transrectally injected into the peripheral zone of each quadrant of the prostate under ultrasound guidance. Static planar lymphoscintigraphy was performed 15 minutes and 2 hours after injection, followed by SPECT and low-dose computed tomography (CT) for all patients. The images were fused, and a reconstructed image was created using OsiriX medical imaging software (Pixmeo, Geneva, Switzerland). The results were analyzed by an experienced nuclear medicine.

Surgery was performed by a urologist experienced in laparoscopic or robotic-assisted surgery using either a standard laparoscopic setup or the da Vinci Si Surgical System (Intuitive Surgical Inc, Sunnyvale, CA). Preoperatively acquired SPECT-CT images were used as a virtual roadmap for the localization

of the individual SLNs. Intraoperatively, the SLNs were initially pursued using a laparoscopic gamma probe (Europrobe 2; Eurorad, Eckbolsheim, France), followed by confirmatory fluorescence imaging using the TricamSLII with D-Light C system or the Image 1 HUB HD with D-Light P system (both KARL STORZ GmbH & Co KG, Tuttlingen, Germany). LNs other than the SLNs that were directly adhering to the SLNs were also removed if in situ separation was not possible. In the case of unilateral nonvisualization of the SLNs on preoperative imaging, LN dissection of the LNs to the ureter vessel crossing was performed ipsilaterally.

Pathologic examination

The SLNs were formalin fixed, cut into 2-mm sections, and stained with hematoxylin and eosin. A CAM5.2 antibody was used for immunohistochemical analysis (catalogue no. 345779; Becton Dickinson Biosciences, San Jose, CA).

Androgen deprivation therapy

All patients started ADT before the initiation of RT. LN-negative patients were offered ADT for 6 months. Patients with high-risk disease and/or positive LNs were offered 3 years of ADT.

Follow-up examinations

The follow-up examinations after EBRT consisted of serum PSA analysis every 4 months for 3 years. Thereafter, the patients were evaluated every 6 months. BCR was defined as a PSA nadir plus 2 ng/mL in accordance with the recommendations of the Radiation Therapy Oncology Group and American Society for Therapeutic Radiation Oncology Phoenix consensus (17). Imaging for metastases included routine CT and bone scanning in the case of a PSA level >10 ng/mL or with symptomatic progression. Metastasis-free survival (MFS) and overall survival (OS) were recorded as the interval from the end of RT to the occurrence of metastasis (including pelvic and nonregional LN

metastasis) and death from any cause, respectively. Postoperative complications (within 90 days after surgery) were scored using the Clavien-Dindo score (18).

Statistical analysis

The Mann-Whitney U nonparametric test was used to compare the median values. Kaplan-Meier statistics were used to report on the 5-year BCR, MFS, and OS for patients with pN1 versus pN0 PCa, and the log-rank test was used to test for significance. Cox multivariate regression analysis was used to compare the factors associated with BCR, OS, and MFS. The area under the curve of the receiver operating characteristics analysis was used to quantify the accuracy of the updated Briganti nomogram to predict the probability of LNI in the cohort. The concordance index of Harrell et al (19) was used to compare Kattans' nomogram prediction for BCR and actual outcomes. $P<.05$ was considered statistically significant. SPSS software, version 22.0 (SPSS Inc, Chicago, IL), was used to perform the statistical analysis.

Results

The patient characteristics are listed in Table 1. A total of 834 SLNs (median 3 per patient; interquartile range [IQR] 2-5) and 994 non-SLNs (median 3 per patient; IQR 1-7) were removed surgically. Nodal metastases were diagnosed in 94 patients (42%), with 150 positive SLNs (median 1; IQR 1-2) in 83 patients (37%) and 41 positive non-SLNs (median 0; IQR 0-1) in 27 patients (12.1%). In 11 patients, no positive SLNs were found, although the removed non-SLNs were positive (false-negative rate 4.9%). Nonvisualization occurred in 8 patients (SLN detection rate 96.5%). In 40 patients (17.8%), SLNs were identified and excised outside the ePLND template at the following locations: Cloquet's node, inguinal, presacral, pararectal, para-aortic, and behind the common iliac artery. In 12 patients, these LNs were positive for tumor (12.7% of node-positive patients and 5.3% of all patients). Solitary SLN metastases outside the ePLND template were found in 5 patients (5.3% of node-positive

patients). Representative pathologic and SPECT images and the axial dose distributions are shown in Figure E1.

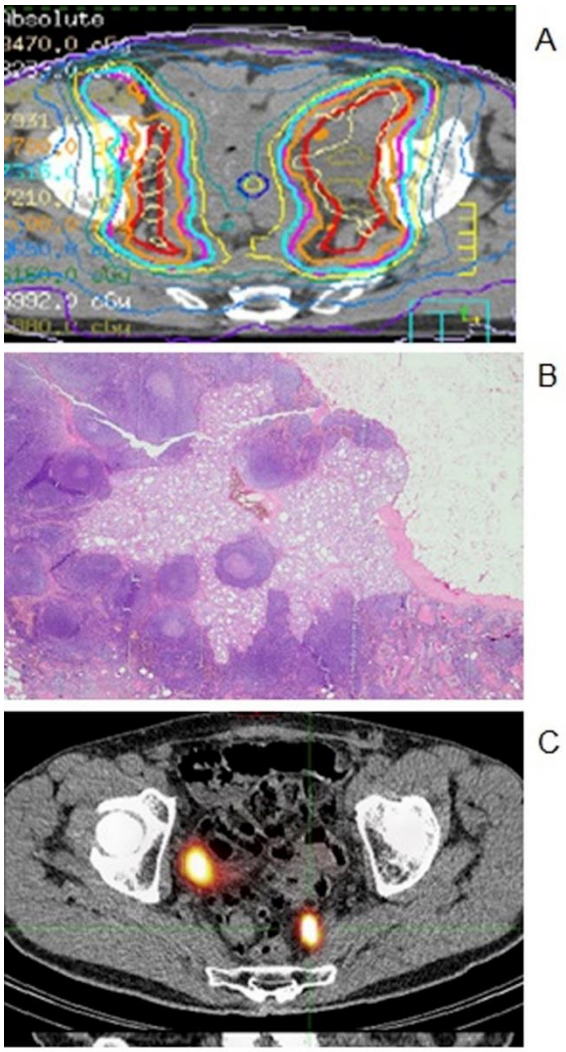

Figure E1. (A) Axial, preoperative single photon emission computed tomography image demonstrating pathologic indocyanine green-99mTc-nanocolloid uptake in 1 right obturator and 1 left internal iliac lymph node in a 72-year-old man with prostate cancer. (B) The pathology image showed a positive right obturator lymph node (metastatic size 5 mm). (C) Image showing the corresponding intensity-modulated radiation therapy plan.

Table 1. Characteristics of patients stratified by pathologic node (pN) status				
Characteristic	Overall (n=224)	pN0 (n=133)	pN1 (n=91)	P value
Age (y)				.76
Mean	64.3	64.6	63.92	

Median	65	65	64	
IQR	61-68	61-69	62-67	
PSA level (ng/mL)				.025
Mean	27.6	25.1	31.22	
Median	15.4	15.2	16	
IQR	8-29	9-29	8.5-31	
Clinical stage (n)				<.01
T1c	15 (6.7)	8 (6)	7 (7.7)	
T2	51 (22.8)	34 (25.6)	17 (18.7)	
T3	158 (70.5)	91 (68.4)	67 (73.6)	
Primary Gleason grade (n)				.064
≤3	99 (48.1)	64 (52.8)	35 (41.1)	
≥4	107 (51.9)	57 (47.2)	50 (58.9)	
Secondary Gleason grade (n)				.536
≤3	48 (23.3)	30 (24.8)	18 (21.2)	
≥4	158 (76.7)	91 (75.2)	67 (78.8)	
Overall Gleason score (n)				.018
2-6	22 (9.9)	18 (13.5)	4 (4.5)	
7	93 (42.1)	58 (43.6)	35 (39.8)	
8-10	106 (48)	57 (42.9)	49 (55.7)	
Biopsy cores taken (n)				.44
Mean	8.98	8.85	9.16	
Median	9	9	10	
IQR	8-12	8-12	8-12	
Positive biopsy cores (%)				.042
Mean	45.96	41.33	51.71	
Median	50	40	50	
IQR	30-60	30-50	33-75	
Patients with positive SLN/non-SLNs (n)				NA
Positive SLNs	83 (37)	NA	83 (37)	

Positive non-SLNs	27 (12.1)	NA	27 (12.1)	
Positive non-SLNs and negative SLNs	11 (4.9)	NA	11 (4.9)	
Removed and examined SLNs (n)				.76
Mean	3.7	3.8	3.5	
Median	3	3	3	
IQR	2-5	2-5	2-5	
Positive SLNs (n)				NA
Mean	1.6	NA	1.6	
Median	1	NA	1	
IQR	1-2		1-2	
Removed and examined non-SLNs (n)				.59
Mean	4.5	4.6	4.4	
Median	3	4	3	
IQR	1-7	2-7	1-7	
Positive non-SLNs with negative SLNs (n)				NA
Mean	0.12	NA	0.12	
Median	0	NA	0	
IQR	0-0		0-0	
D'Amico risk group (n)				<.001
Intermediate	15 (6.7)	12 (9)	3 (3.2)	
High	209 (93.3)	121 (91)	88 (96.8)	

The 5-year BCR-free rate was significantly greater (*P*<.001) for node-negative than for node-positive patients (67.9% and 43%, respectively; Fig. 1). On Cox multivariate regression analysis, pathologic lymph node (pN) status (*P*=.011), PSA level (*P*=.018), and the number of removed SLNs (*P*=.043) were independent predictors of the BCR interval (Table 2). The 5-year OS rate was 97.6% and only correlated with pN status (all patients who died had pN1

disease). The 5-year MFS rate was greater (*P*<.001) for node-negative (pN0) compared with node-positive (pN1) patients (87.8% and 66.6%, respectively). On multivariate analysis, MFS correlated only with PSA level (*P*=.02) and the number of removed SLNs (*P*=.012), and no correlation (*P*=.196) was observed with pN status. The complications of the procedure are listed in Table 3. The rate of severe complications (Clavien grade 3) was 5.3% (Clavien grade 3a, 2.2%; Clavien grade 3b, 3.1%) and the rate of Clavien grade 1 and 2 complications was 0.8% and 2.6%, respectively.

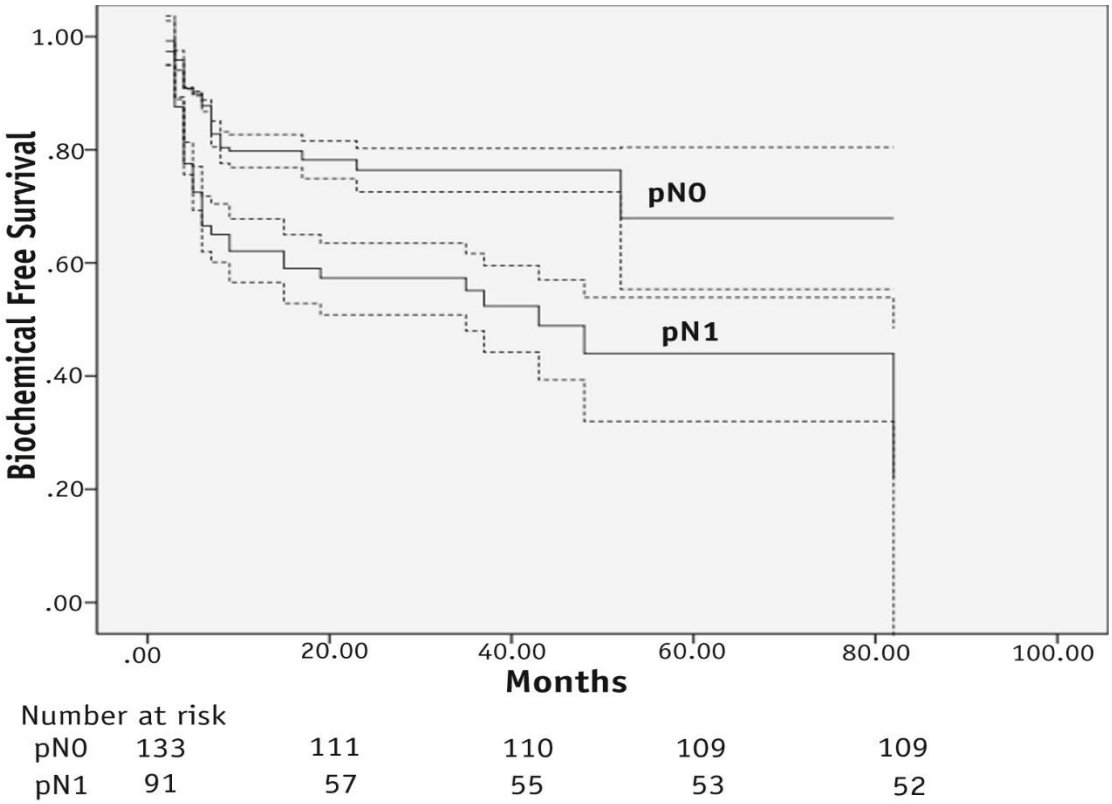

Fig. 1. Kaplan-Meier survival curves of biochemical-free survival according to pathologic lymph node (pN) status showing 95% confidence intervals (dashed lines) and patients at risk.

Table 2. Characteristics predicting biochemical recurrence rate						
Prediction of BCR	Univariate analysis			Multivariate analysis		
	OR	95% CI	*P* value	OR	95% CI	*P* value
pN status	3.685	2.066-6.571	.000	3.247	1.310-8.050	.011
PSA level before RT	1.005	1.001-1.008	.007	1.006	1.001-1.010	.018
cT	1.123	0.920-1.371	.255	0.968	0.766-1.223	.785
Biopsy Gleason score	1.123	0.818-1.542	.474	0.981	0.673-1.429	.919
No. of removed SLNs	0.809	0.698-0.938	.005	0.832	0.696-0.994	.043
No. of positive SLNs	1.352	1.117-1.636	.002	1.040	0.725-1.493	.831
No. of non-SLNs	0.985	0.917-1.059	.690	0.919	0.838-1.007	.072
No. of positive non-SLNs	1.346	1.114-1.625	.002	1.276	0.944-1.723	.112

Table 3. Complications after sentinel lymph node dissection using the Clavien-Dindo classification system		
Grade	**Complication**	**Patients (n)**
1	Ileus	1
	Wound hematoma	1
2	Urinary tract infection	3
	Lymphocele	2
	Ureteral injury	1
3a	Ureteral stricture	1
	Urine incontinence	1
	Lymphocele	2
	Ureteric injury	1
3b	Incisional hernia	1
	Wound hematoma	2
	Postoperative bleeding	1
	Bowel injury	1
	Ureteric injury	2

Nomogram prediction

The median follow-up period according to the reverse Kaplan-Meier method was 52 months (range 2-82). The overall mean expected rate of LN metastasis according to the Briganti nomogram (Fig. E2) was 43.6% (median 52.5%, IQR 10.7%-84.6%), and the mean observed rate for LN metastasis was 43.7% (median 55.3%; IQR 19.5%-57.4%). For the intermediate-risk group, the mean expected and observed rates were 10.7% and 19.56% (P>.05), and in the high-risk group, the corresponding rates were 56.2% and 49.5% (P=.01). The overall predictive accuracy of the Briganti nomogram, as measured by the area under the receiver operating characteristics curve was 0.665 (95% confidence interval 0.587-0.744). Harrell's concordance index for the overall prediction of the BCR-free rate using the Kattan nomogram was 0.72 (Fig. E3). The nomogram

seemed to have better accuracy with pN1 patients (Fig. E4), and the pN0 and pN1 patients in the lower quartiles of the predicted BCR had better outcomes than predicted (Fig. E5).

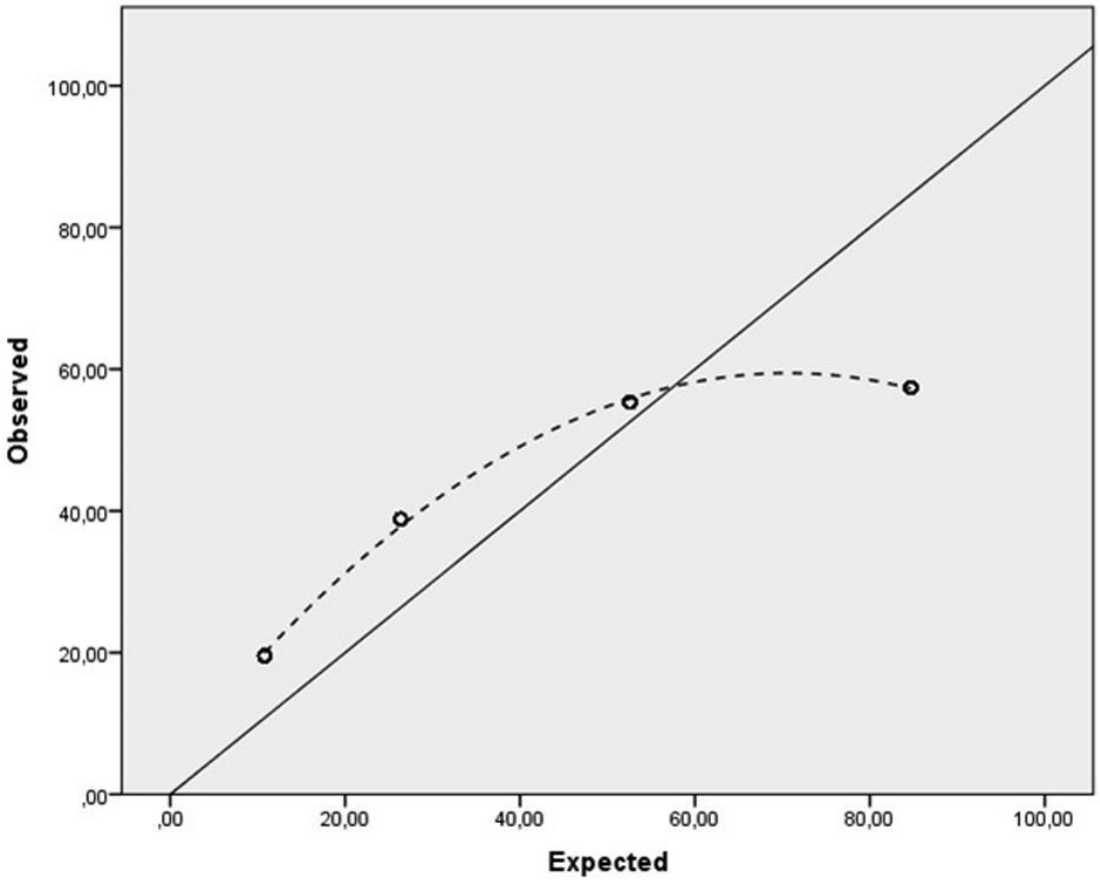

Figure E2. Correlation between Briganti nomogram prediction of lymph node invasion and actual positive lymph nodes stratified by quartile

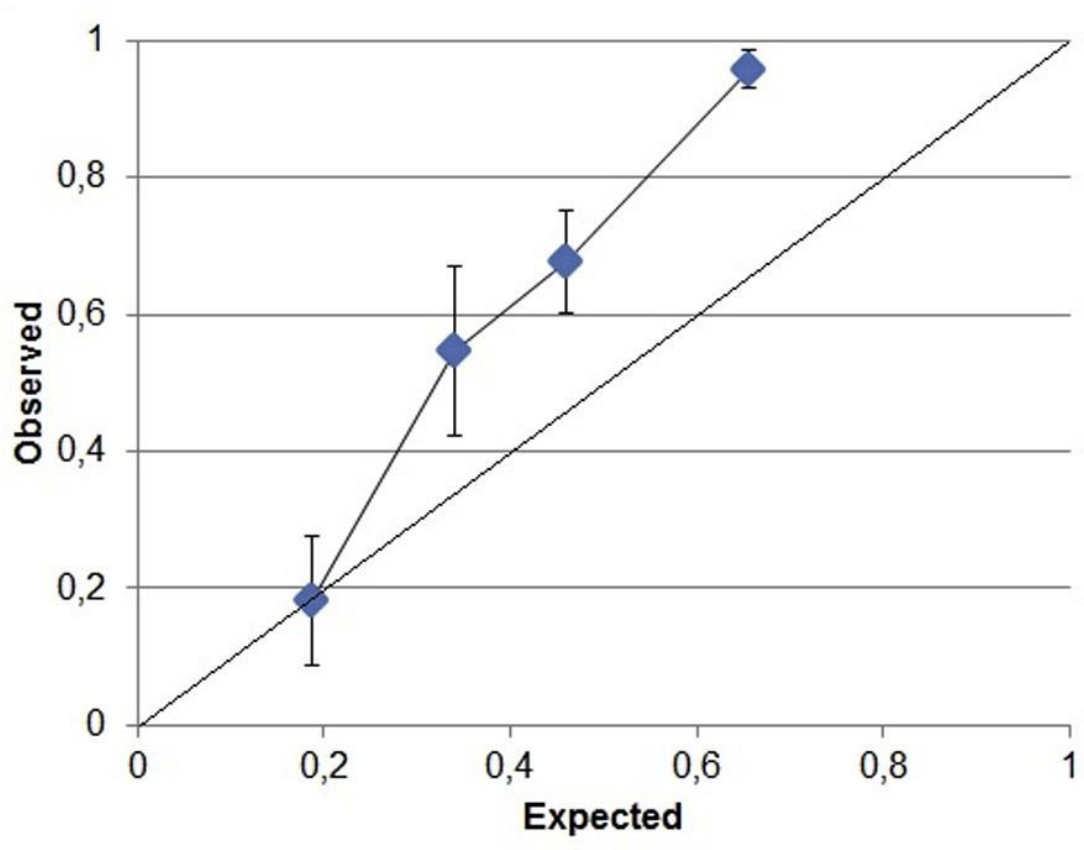

Fig. E3 Correlation between Kattan nomogram prediction of biochemical-free survival and actual survival rate stratified by quartile for overall study population.

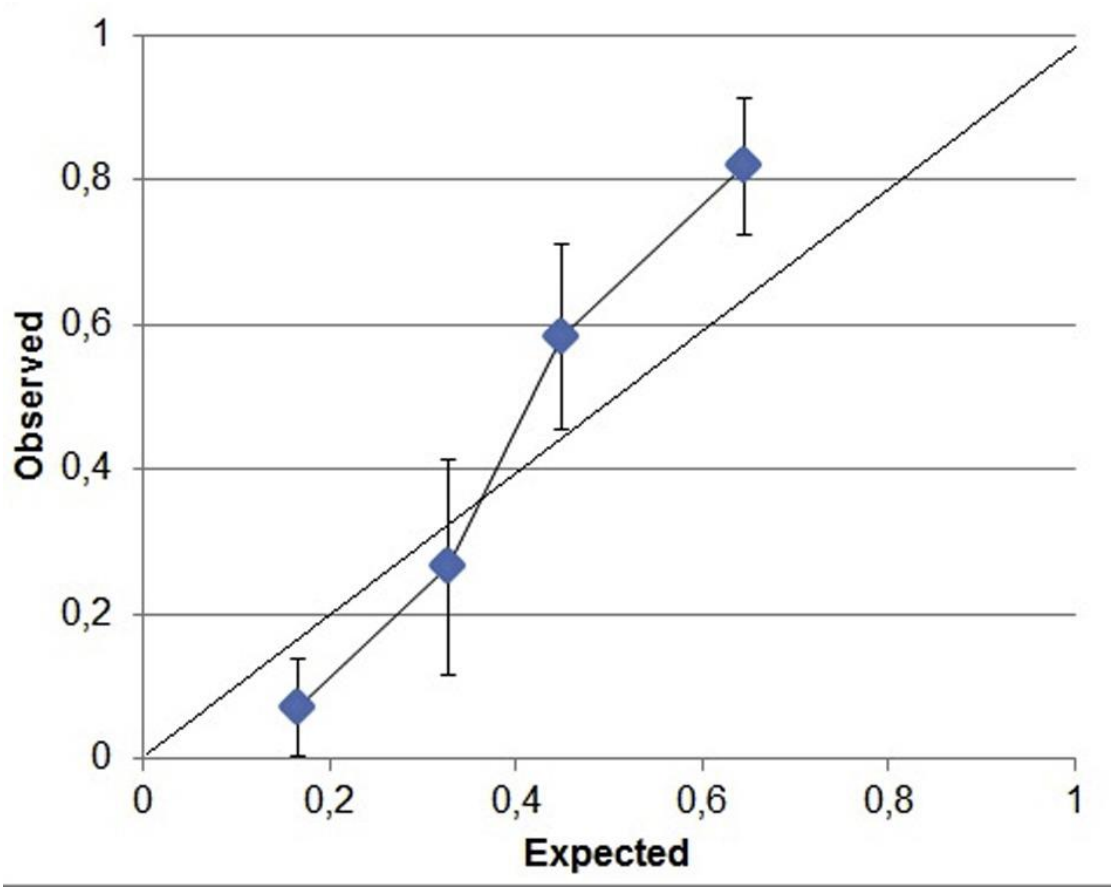

Figure E4. Correlation between Kattan nomogram prediction of biochemical-free survival and actual survival rate for patients with node-positive disease.

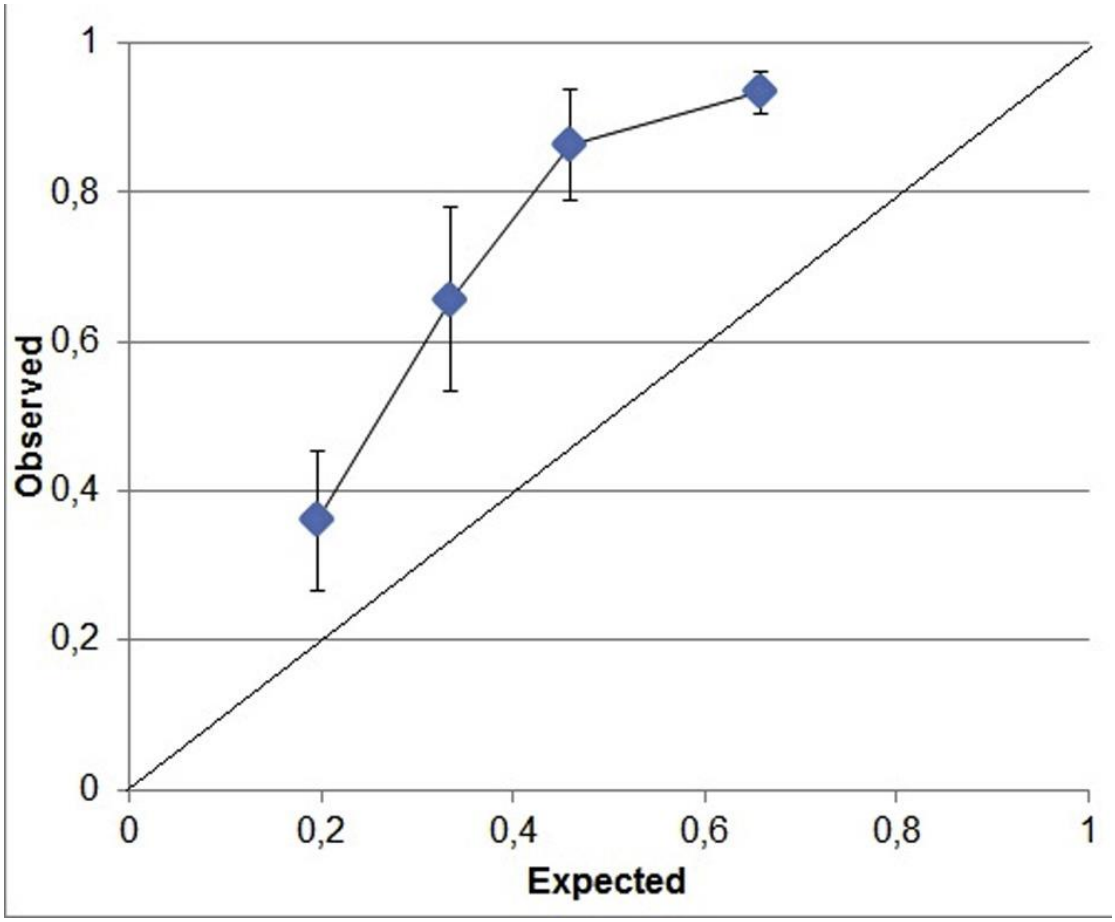

Figure E5. Correlation between Kattan nomogram prediction of biochemical-free survival and actual survival rate for patients with node-negative disease.

Discussion

To the best of our knowledge, our study is the first to explore the prognostic value of robotic-assisted laparoscopic SLN technique when applied to EBRT-treated patients offered additional pelvic irradiation with the finding of histologically positive SLNs. Despite negative preoperative imaging findings, 42% of our patients had nodal metastases. Conventional cross-sectional imaging techniques such as CT and magnetic resonance imaging cannot accurately differentiate between benign and malignant lymph nodes (20. Although greater sensitivity for diffusion-weighted magnetic resonance imaging and 68Ga–prostate-specific membrane antigen–positron emission tomography have been reported, the sensitivity remained <90% (21, 22). ePLND, the

current reference standard for nodal staging, was recently reported to have a false-negative rate of 13% for metastatic LNs (4).

From our data, no clear statement can be made regarding the sensitivity of SLND, because no additional ePLND was performed. In 2006, Corvin et al (23) described their experience with laparoscopic SLND in 28 patients considered for EBRT. Although the sample size was small, they reported no complications and an acceptable intraoperative and preoperative identification rate, with 23% of patients with positive findings. Two recent systematic reviews suggested a sensitivity of 94% to 95.2% of SLND for detecting nodal metastases (24, 25). This high sensitivity and low morbidity could make SLND the preferred nodal staging tool.

Regarding the distribution of SLNs, our findings were in accordance with previous mapping studies (26). However, in 17.8% of our patients, SLNs were identified and excised outside the ePLND template. In 8 of our patients, no SLN was visualized, all had a Gleason score >8. Six of these patients had LNs harboring cancer. A possible explanation for the nonvisualization of the SLN could be blockage of LN channels by macrometastases, highly aggressive (Gleason score >8) tumors, or a too-low count rate for intraoperative detection owing to a low dose of tracer or leakage of the tracer out of the peripheral zone after injection (27). This finding confirms that in cases with nonvisualization, nodal dissection should not be omitted, and an ePLND template is the preferred nodal staging approach.

Although overall the concordance between the predicted and observed incidence of nodal metastases by the Briganti nomogram was high (c-index 0.72) on the basis of our calibration plot, the Briganti nomogram tended to underestimate the risk of SLN metastasis for the intermediate-risk group. In contrast, SLNB can underestimate the presence of nodal metastases in high- or higher-risk patients. In accordance with our observation, Weckermann et al (28) found that when SLNs were positive, the incidence of positive non-SLNs was greater in patients with high-risk PCa. Moreover, Winter et al (29) recently proposed a SLN-based prediction model, which showed a greater predicted incidence of positive LNs for low- and intermediate-risk tumors compared with

a routine prediction nomogram. In contrast, this predicted incidence of pN1 was similar in high-risk tumors, suggesting that SLND might be particularly interesting for lower risk disease.

Müller et al (16) used the SLN template as obtained by SPECT-CT imaging to guide pelvic IMRT in men with mainly high-risk PCa, with the advantage of avoiding LN dissection. The observed BCR-free survival rate at 5 years was 73.8% compared with 67.9% and 43% in our LN-negative and -positive patients, respectively. However, tailoring of pelvic IMRT only to pN1 disease prevented pelvic radiation in >50% of cases without nodal metastases.

The LN-positive patients in our series had lower BCR-free rates than the LN-negative patients despite pelvic RT and longer androgen ablation. Similar outcomes were found for OS and MFS. This strengthens the theory that LN-positive patients have a greater relative risk of harboring or developing systemic disease (30).

When comparing the expected (Kattan nomogram) to the observed 5-year BCR rates, men with pN0 disease showed better than predicted outcomes. This was not surprising, because the Memorial Sloan Kettering Cancer Center series included in the Kattan nomogram did not have nodal sampling. It is, therefore, remarkable that the observed outcomes of men in the more favorable quartiles with pN1 were better than the nomogram prediction. This might imply that the longer ADT and pelvic RT applied in these men could have improved their outcomes. In men with worse predicted outcomes in the lowest 2 quartiles, no difference between the predicted and observed outcomes was noted. This might have resulted from a possible therapeutic effect of longer ADT and pelvic RT in men with positive LNs but a lower predicted risk of BCR. This notion is supported by the observation that of the patients who presented with LN metastases at a mean follow-up point of 52.8 months after positive SLNB findings, all had developed recurrence in nonpelvic locations (ie, para-aortal and interaortocaval). Neither ePLND nor pelvic RT would have included these LNs and recurrence would not have been avoided. Our observations are in accordance with those from Winter et al (29) indicating that SLNB should mainly be used in lower-risk patients in whom it might improve diagnostic efficacy and

potentially aid in identifying men who might benefit from longer ADT and pelvic RT. In particular, patients with a predicted 5-year BCR-free survival of >40% seemed to benefit from SLND.

Complications

The overall complication rate in our cohort was 8.9%. Our observed complication rate was much lower than that reported by Briganti et al (31) for ePLND (19.8%), with lymphocele and urinary anastomotic leakage the most common complications (10.3% and 3.1%, respectively). In the published data, the most common complications related to laparoscopic SLN procedures were lymphocele (0%-15%), neuropraxia (0%-5%), deep vein thrombosis (0%-5%), and mild leg edema (0%-5.7%) (32, 33).

Study limitations

The limitations of our analysis were the retrospective setting and the relatively short follow-up period. Despite the prospective data, a sampling bias in the selection of patients for SLND and EBRT could not be excluded. Another limitation was the lack of a control group. This made it impossible for us to assess the role of pelvic RT in men with a positive SLN. That in 2 men pelvic nodal recurrence developed despite pelvic RT suggests that pelvic RT might not prevent nodal recurrence in all patients.

Conclusions

SLN identification has the potential to accurately determine nodal staging of PCa with the advantage of lower morbidity compared with ePLND. In addition, positive SLN status correlates with an adverse prognosis and reduced survival. The result of SLND would allow radiation oncologists to tailor the planning target volume, in particular, to ensure that patients with pN0 disease do not undergo pelvic irradiation. With the design of our single-arm cohort analysis, we were unable to confirm the therapeutic effects of pelvic RT in men with

proven nodal metastases. In particular, men with LN-positive disease and a lower nomogram-predicted BCR might benefit most from SLND, 3 years of ADT, and pelvic RT, given the improved outcomes observed in the present analysis compared with the Kattan BCR nomogram predictions. Prospective randomized studies are required to confirm the added benefit of SLND and the use of SLND as a selection tool for the addition of pelvic RT and ADT intensification.

References

1. Winter A, Kneib T, Rohde M, Henke RP, Wawroschek F. First Nomogram Predicting the Probability of Lymph Node Involvement in Prostate Cancer Patients Undergoing Radioisotope Guided Sentinel Lymph Node Dissection. Urol Int. 2015;95:422-428.

2. Mottet N, Bellmunt J, Bolla M, et al. EAU-ESTRO-SIOG Guidelines on Prostate Cancer. Part 1: Screening, Diagnosis, and Local Treatment with Curative Intent. Eur Urol. 2016. doi: 10.1016/j.eururo.2016.08.003.

3. Gofrit ON, Zorn KC, Steinberg GD, et al. The Will Rogers phenomenon in urological oncology. J Urol. 2008;179:28-33.

4. Joniau S, Van den Bergh L, Lerut E, et al. Mapping of pelvic lymph node metastases in prostate cancer. Eur Urol. 2013;63:450-458.

5. Cabanas RM. An approach for the treatment of penile carcinoma. Cancer.

1977;39:456-466.

6. Wawroschek F, Vogt H, Weckermann D, Wagner T, Harzmann R. The sentinel lymph node concept in prostate cancer - first results of gamma probe-guided sentinel lymph node identification. Eur Urol. 1999;36:595-600.

7. Veronesi U, Paganelli G, Viale G, et al. A randomized comparison of sentinel-node biopsy with routine axillary dissection in breast cancer. N Engl J Med. 2003;349:546-553.

8. Sadeghi R, Gholami H, Zakavi SR, Kakhki VR, Tabasi KT, Horenblas S. Accuracy of sentinel lymph node biopsy for inguinal lymph node staging of penile squamous cell carcinoma: systematic review and meta-analysis of the literature. J Urol. 2012;187:25-31

9. Morton DL, Thompson JF, Cochran AJ, et al. Final trial report of sentinel-node biopsy versus nodal observation in melanoma. N Engl J Med. 2014;370:599-609.

10. Belhocine TZ, Prefontaine M, Lanvin D, et al. Added-value of SPECT/CT to lymphatic mapping and sentinel lymphadenectomy in gynaecological cancers. Am J Nucl Med Mol Imaging. 2013;3:182–193

11. KleinJan GH, van den Berg NS, Brouwer OR, et al. Optimisation of fluorescence guidance during robot-assisted laparoscopic sentinel node biopsy for prostate cancer. Eur Urol. 2014;66:991-998.

12. Acar C, Kleinjan GH, van den Berg NS, Wit EM, van Leeuwen FW, van der Poel HG. Advances in sentinel node dissection in prostate cancer from a technical perspective. Int J Urol. 2015;22:898-909.

13. Briganti A, Larcher A, Abdollah F, et al. Updated nomogram predicting lymph node invasion in patients with prostate cancer undergoing extended pelvic lymph node dissection: the essential importance of percentage of positive cores. Eur Urol. 2012;61:480-487.

14. Zelefsky MJ, Kattan MW, Fearn P, et al. Pretreatment nomogram predicting ten-year biochemical outcome of three-dimensional conformal radiotherapy and intensity modulated radiotherapy for prostate cancer. Urology. 2007;70:283-287.

15. Lawton CA, Michalski J, El-Naqa I, et al. RTOG GU Radiation oncology specialists reach consensus on pelvic lymph node volumes for high-risk prostate cancer. Int J Radiat Oncol Biol Phys. 2009;74:383-387.

16. Müller AC, Eckert F, Paulsen F et al. Nodal Clearance Rate and Long-Term Efficacy of Individualized Sentinel Node-Based Pelvic Intensity Modulated Radiation Therapy for High-Risk Prostate Cancer. Int J Radiat Oncol Biol Phys. 2016;94:263-271.

17. Roach M 3rd, Hanks G, Thames H Jr, et al. Defining biochemical failure following radiotherapy with or without hormonal therapy in men with clinically localized prostate cancer: recommendations of the RTOG-ASTRO Phoenix Consensus Conference. Int J Radiat Oncol Biol Phys. 2006;65:965-974.

18. Dindo D, Demartines N, Clavien PA. Classification of surgical complications: a new proposal with evaluation in a cohort of 6336 patients and results of a survey. Ann Surg. 2004;240:205-213.

19. Harrell FE Jr, Califf RM, Pryor DB, Lee KL, Rosati RA. Evaluating the yield of medical tests. JAMA. 1982;247:2543-2546.

20. Katz S, Rosen M. MR imaging and MR spectroscopy in prostate cancer management. Radiol Clin North Am. 2006;44:723-734.

21. Vallini V, Ortori S, Boraschi P, et al. Staging of pelvic lymph nodes in patients with prostate cancer: Usefulness of multiple b value SE-EPI diffusion-weighted imaging on a 3.0 T MR system. Eur J Radiol Open. 2015;3:16-21.

22. van Leeuwen PJ, Emmett L, Ho B, et al. Prospective Evaluation of 68Gallium-PSMA Positron Emission Tomography/Computerized Tomography for Preoperative Lymph Node Staging in Prostate Cancer. BJU Int. 2016. doi: 10.1111/bju.13540.

23. Corvin S, Schilling D, Eichhorn K, et al. Laparoscopic sentinel lymph node

dissection--a novel technique for the staging of prostate cancer. Eur Urol.

2006;49:280-285.

24. Sadeghi R, Tabasi KT, Bazaz SM, et al. Sentinel node mapping in the prostate cancer. Meta-analysis. Nuklearmedizin. 2011;50:107-115.

25. Wit EM, Acar C, Grivas N, et al. Sentinel Node Procedure in Prostate Cancer: A Systematic Review to Assess Diagnostic Accuracy. Eur Urol. 2016. doi: 10.1016/j.eururo.2016.09.007.

26. Mattei A, Fuechsel FG, Bhatta Dhar N, et al. The template of the primary lymphatic landing sites of the prostate should be revisited: results of a multimodality mapping study. Eur Urol. 2008;53:118-125.

27. Buckle T, Brouwer OR, Valdés Olmos RA, van der Poel HG, van Leeuwen FW. Relationship between intraprostatic tracer deposits and sentinel lymph node mapping in prostate cancer patients. J Nucl Med. 2012;53:1026-1033.

28. Weckermann D, Dorn R, Holl G, Wagner T, Harzmann R. Limitations of radioguided surgery in high-risk prostate cancer. Eur Urol. 2007;51:1549-1556.

29. Winter A, Kneib T, Henke RP, Wawroschek F. Sentinel lymph node dissection in more than 1200 prostate cancer cases: rate and prediction of lymph node involvement depending on preoperative tumor characteristics. Int J Urol. 2014;21:58-63.

30. Chaffer CL, Weinberg RA. A perspective on cancer cell metastasis. Science. 2011;331:1559-1564.

31. Briganti A, Chun FK, Salonia A, et al. Complications and other surgical outcomes associated with extended pelvic lymphadenectomy in men with localized prostate cancer. Eur Urol. 2006;50:1006-1013.

32. Meinhardt W, Valdés Olmos RA, van der Poel HG, Bex A, Horenblas S. Laparoscopic sentinel node dissection for prostate carcinoma: technical and anatomical observations. BJU Int. 2008;102:714-717.

33. Jeschke S, Beri A, Grüll M, et al. Laparoscopic radioisotope-guided sentinel lymph node dissection in staging of prostate cancer. Eur Urol. 2008;53:126-132.

3

The Impact of Adding Sentinel Node Biopsy to Extended Pelvic Lymph Node Dissection on Biochemical Recurrence in Prostate Cancer Patients Treated with Robot-Assisted Radical Prostatectomy.

Grivas N, Wit EMK, Kuusk T, KleinJan GH, Donswijk ML, van Leeuwen FWB, van der Poel HG.

J Nucl Med. 2018 Feb;59(2):204-209.

Abstract

Introduction: The benefit of adding sentinel node biopsy (SNB) to extended pelvic lymph node dissection (ePLND), remains controversial. Aim of our study was to evaluate biochemical recurrence (BCR) after robot-assisted radical prostatectomy (RARP) and ePLND in prostate cancer (PCa) patients, stratified by the application of SNB. The results were compared with the predictions of the updated Memorial Sloan Kettering Cancer Center (MSKCC) nomogram. **Methods:** Between January 2006 and November 2016, 920 patients underwent RARP with ePLND combined with or without SNB (184 and 736 patients, respectively). BCR was defined as two consecutive prostate-specific antigen (PSA) rises ≥ 0.2 ng/ml. The Kaplan-Meier method and Cox regression analyses were used to identify predictors of BCR. **Results:** Median follow up was 28 months (interquartile range: 13-56.7). The 5-year BCR-free survival rate was 80.5% and 69.9% in the ePLND+SNB and ePLND group, respectively. At multivariate analysis PSA, primary Gleason grade > 3, seminal vesicle invasion and higher number of removed and positive nodes were independent predictors of BCR in the ePLND group. In the ePLND+SNB group only the number of positive nodes was independent predictor of BCR. The overall accuracy of MSKCC nomogram was higher in the ePLND+SNB compared to the ePLND group. However, the nomogram was underestimating the probability of BCR-free status in the ePLND+SNB group, while the ePLND group was performing as predicted. **Conclusion:** Adding SNB to ePLND improves BCR-free survival, although it remains speculation on the precise explanation of this observation. Our results should be interpreted cautiously, given the non-randomized nature and the selection bias of the study.

Introduction

Approximately one quarter of prostate cancer (PCa) patients undergoing radical prostatectomy develop biochemical recurrence (BCR) (1). The natural history after the occurrence of BCR is highly variable mainly due to the heterogeneity of the disease and the differences observed on its biological behavior. The

interval until the development of clinical disease is 5-8 years and half of these patients will die within 15 years (2).

To assist patient counseling and treatment decision-making several nomograms have been developed and validated. These nomograms help calculate the individual risk of BCR based on pre- and post-operative clinico-pathological data (1,3-8). The recently updated postoperative Memorial Sloan Kettering Cancer Center (MSKCC) nomogram replaced the covariate of lymph node (LN) invasion, by the number of positive nodes, categorized as none, one or two, and three or more (9). The full updated model also includes prostate-specific antigen (PSA), primary and secondary pathologic Gleason grade, seminal vesicle invasion, extracapsular extension and positive surgical margin. The additional stratification by the number of positive nodes showed favorable accuracy for predicting BCR (9).

Given the low sensitivity (49%-66%) of even the newest imaging methods like ^{68}gallium Prostate Specific Membrane Antigen-Positron Emission/Computed Tomography, European Association of Urology Guidelines suggest the extended pelvic lymph node dissection (ePLND) as the gold standard for LN staging of intermediate and high-risk (>5%) PCa patients (10,11). The concept of selective sentinel node (SN) biopsy (SNB) was mainly developed to avoid the toxicity of ePLND and to improve detection rates for positive SNs. SNB is a standard procedure in melanoma, breast and penile cancer and is increasingly applied also in PCa (12-14). Although SNB is still considered experimental a recent systematic review has shown a diagnostic accuracy comparable to ePLND (15). Moreover the combination of ePLND+SNB can increase the detection rate of affected nodes (15). Nevertheless, one open question is the ability of the procedure to increase the removal of metastatic LNs which could result on better oncologic outcomes when compared with ePLND-only dissection.

Aim of this study was to evaluate the BCR outcomes after robot-assisted radical prostatectomy (RARP) in PCa patients, stratified by the additional application of SNB. The observed results were validated with the predictions of the updated MSKCC nomogram.

Materials and Methods

Study Population

After obtaining institutional approval we retrospectively reviewed data of 920 consecutive PCa patients who underwent RARP along with pelvic lymphadenectomy for clinically organ-confined PCa from January 2006 until November 2016. In 736 patients (80%) ePLND alone was applied. In 184 patients (20%) ePLND was combined with additional SNB (ePLND+SNB) within the scope of a clinical study approved by the local ethical committee (Dutch trial register NL41285.031.12). Written informed consent was obtained from all patients participating in this study. Patients who declined participation were offered only ePLND. Patients who received salvage prostatectomy, adjuvant treatment or with missing data were excluded. The indication for LN dissection was based on guidelines' recommendations at the year of diagnosis.

The primary tumor was staged by digital rectal examination, trans-rectal ultrasound or magnetic resonance imaging and classified per the 2009 TNM staging system. PSA was measured using standard assays. All patients were subjected to trans-rectal ultrasound-guided prostate biopsy and the total number of cores, the number and the percentage of positive cores, the primary and secondary Gleason grade, the number of removed and positive LNs and the presence of seminal vesicle invasion, extracapsular extension or positive surgical margin were prospectively recorded. The number of positive nodes was categorized in accordance with the updated MSKCC nomogram (9). Follow-up after RARP consisted of serum PSA analyses every 4 months for the first 3 years and every 6 months thereafter.

SN and ePLND Technique

The RARP, ePLND, SNB technique and the pathology examination were performed as described earlier (16). In brief, surgery was performed by a urologist experienced in laparoscopic or robotic-assisted surgery using either a standard laparoscopic set-up or the da Vinci S(i) Surgical system (Intuitive

Surgical Inc., Sunnyvale, CA, USA). The ePLND included the removal of the nodes along the external and internal iliac artery and vein, the obturator nodes and the nodes overlying the common iliac vessels up to the ureteral crossing. All SNs were identified using the hybrid tracer indocyanine green-99mTechnetium-nanocolloid, which was trans-rectally injected into the peripheral zone of the prostate under ultrasound guidance. Preoperatively acquired Single-Photon Emission Computed Tomography and low-dose Computed Tomography images were used to generate a roadmap for the intraoperative localization of the individual SNs (16).

Outcome Assessment

BCR was defined as two consecutive PSA rises ≥ 0.2 ng/ml (11). Two groups of patients were compared i.e. patients who were submitted to RARP and ePLND and those who were offered RARP combined with ePLND+SNB. The observed BCR results were validated with the predictions of updated MSKCC nomogram. Finally we did an additional subgroup analysis in a cohort of patients with ≥ 14 LNs removed.

Statistical Analysis

The Mann-Whitney U nonparametric test was used to compare the median values of baseline characteristics. The Kaplan Meier plot was used to present BCR-free survival data and the log rank assay to test significance. The Cox multivariate regression analysis was used to compare factors associated with BCR. Covariates included preoperative PSA, clinical stage, primary and secondary biopsy Gleason grade, extracapsular extension, positive surgical margin, seminal vesicle invasion, number of removed nodes, number of positive nodes (0 vs 1-2 or ≥ 3) and removal or not of SNs. The area under the curve (AUC) as well as calibration plots were used to compare actual outcome and nomogram prediction between the two groups. Decision curve analyses were perfomed to examine the relationship between the threshold probability of BCR and the relative value of false-positive and negative results. Values of $p < 0.05$

were considered statistically significant. SPSS software ver. 22.0 (SPSS Inc., Chicago, IL) and the R statistical package (R Foundation for Statistical Computing, Vienna, Austria) were used to perform the statistical analysis.

RESULTS

Baseline Characteristics

Baseline characteristics are presented in Supplemental Table 1. Median follow up was 28 months (interquartile range: 13–56.7). The median number of removed LNs and the percentage of node positive patients were significantly higher in the ePLND+SNB group (14 vs 9, $p < 0.001$ and 25% vs 15.8%, $p = 0.003$) while median preoperative PSA was significantly higher in the ePLND group (9.3 vs 8.3, $p = 0.004$). Stratified by the number of positive nodes, one or two and more than three positive nodes were significantly more common in the ePLND+SNB group compared to the ePLND (17.9% vs 11.8% and 7.1% vs 3.9% ($p = 0.003$) of the patients, respectively).

Table 1. Patients characteristics stratified by the performance of sentinel node biopsy.

	Overall (n=920)	ePLND (n = 736)	ePLND+SNB (n=184)	p Value
Age, years:				
Mean (median)	63.4 (64)	63.4 (64)	63.6 (64)	0.785
IQR	60-68	60-68	60-68	
Preoperative PSA level, ng/ml:				
Mean (median)	13.1 (9.2)	13.4 (9.3)	11.1 (8.3)	**0.004**

IQR	6.6-15	6.7-16	6.2-12.1	
No. clinical stage (%):		0.192		
T1c	152 (16.5)	127 (17.3)	25 (13.6)	
T2a	104 (11.3)	84 (11.4)	20 (10.9)	
T2b	193 (21)	153 (20.8)	40 (21.7)	
T2c	215 (23.4)	175 (23.8)	40 (21.7)	
T3	256 (27.8)	197 (26.7)	59 (32.1)	
No. primary Gleason grade (%):		0.78		
≤ 3	593 (64.5)	476 (64.7)	117 (63.6)	
≥ 4	327 (35.5)	260 (35.3)	67 (36.4)	
No. secondary Gleason grade (%):		0.09		
≤ 3	303 (32.9)	252 (34.2)	51 (27.7)	
≥ 4	617 (67.1)	484 (65.8)	133 (72.3)	
No. biopsy cores taken:				
Mean (median)	9.3 (10)	9.3 (9.5)	9.6(10)	0.29
IQR	8-12	8-12	8-12	
% percentage of positive biopsy cores:				
Mean (median)	48.7 (45.8)	49.1 (50)	47.2 (38.4)	0.299
IQR	25-66.6	25-66.6	25-62.5	
No. LN invasion (%):	162 (17.6%)	116 (15.8)	46 (25)	**0.003**

No. removed and examined LNs:				
Mean (median)	11.1 (10)	10.1 (9)	15.1 (14)	**<0.001**
IQR	6-15	6-14	10-20	
No. patients (%):				**0.003**
0 positive nodes	758 (82.4)	620 (84.6)	138 (75)	
1-2 positive nodes	120 (13.1)	87 (11.8)	33 (17.9)	
≥3 positive nodes	42 (4.5)	29 (3.9)	13 (7.1)	
No. extracapsular extension (%):	393 (42.7)	327 (44.4)	66 (35.9)	0.066
No. seminal vesicle invasion (%):	186 (20.2)	158 (21.5)	28 (15.2)	0.059
No. positive surgical margin (%):	336 (36.5)	280 (38)	56 (30.4)	0.055

Survival Analysis

The 5-year BCR-free survival rate was significantly higher ($p = 0.03$) in the ePLND+SNB group compared to the ePLND group (80.5% vs 69.9%, respectively) (Fig 1A). When patients were stratified according to LN stage BCR-free survival rates were again in favor of the ePLND+SNB group (both $p \leq 0.016$; Fig. 1B and 1C).

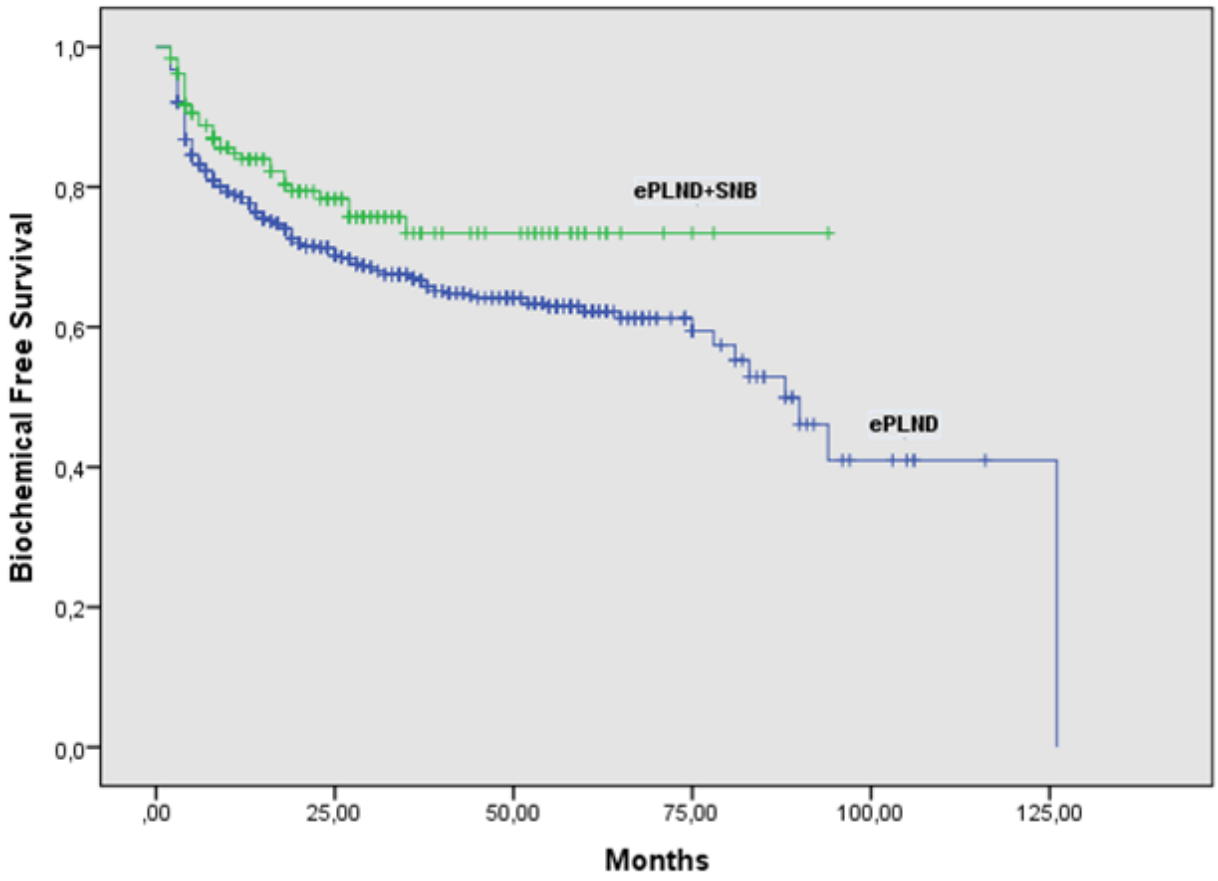

Number at risk					
ePLND+SNB	184	144	135	135	135
ePLND	736	515	472	438	301

FIGURE 1A. Kaplan-Meier survival curves of biochemical recurrence-free survival, stratified by the performance of sentinel node biopsy, in overall cohort (long rank; p = 0.03).

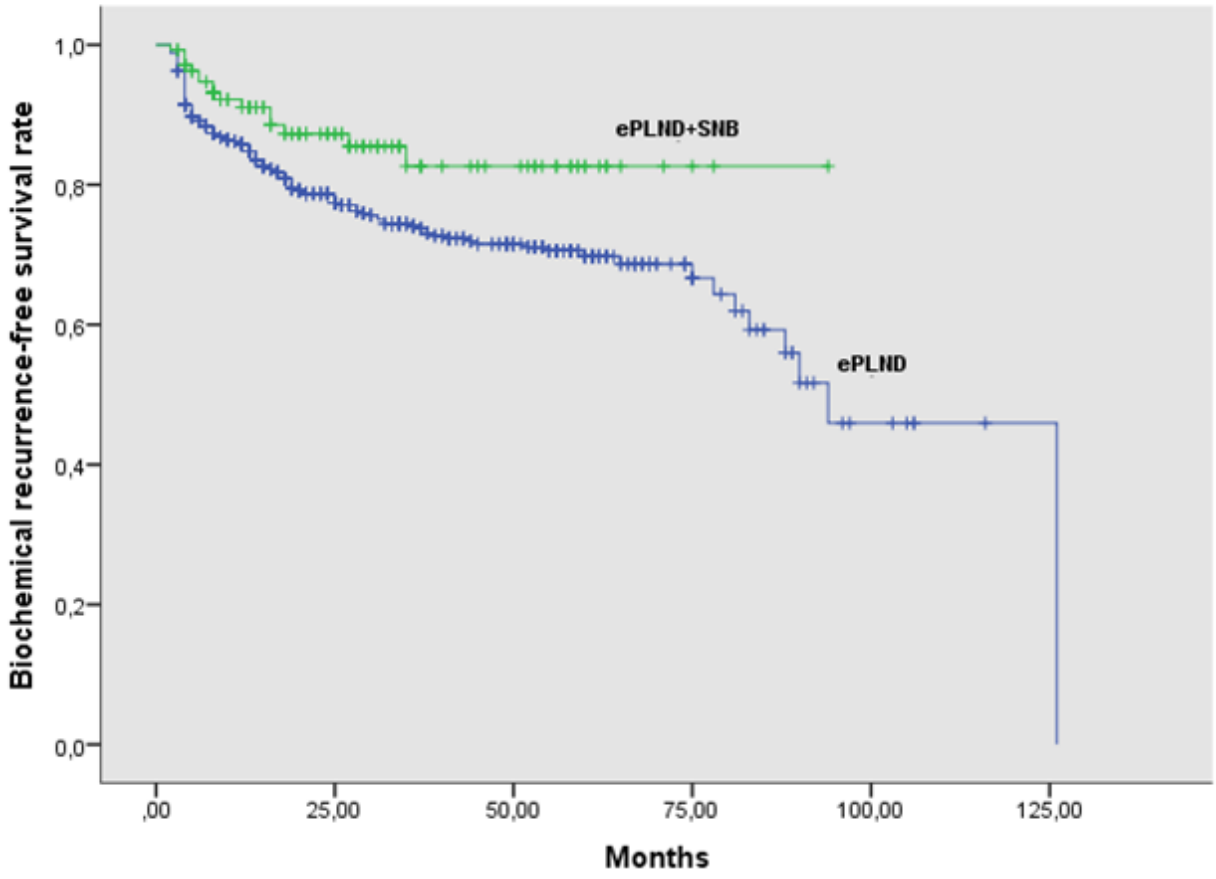

Number at risk					
ePLND+SNB	138	52	21	2	-
ePLND	620	292	165	33	6

FIGURE 1B. Kaplan-Meier survival curves of biochemical recurrence-free survival, stratified by the performance of sentinel node biopsy, in node negative patients (long rank; p = 0.016). ePLND = extended pelvic lymph node dissection; SNB = sentinel node biopsy.

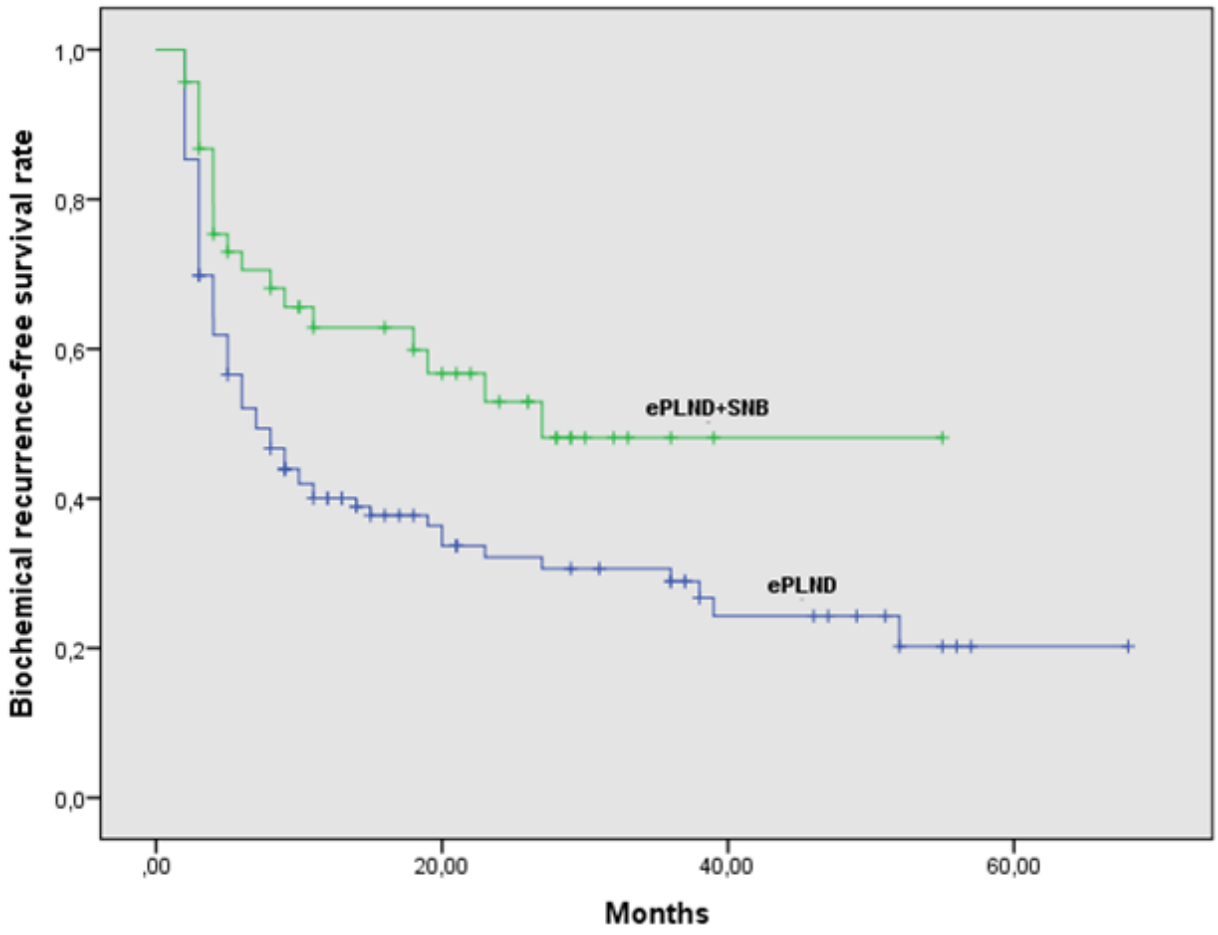

FIGURE 1C. Kaplan-Meier survival curves of biochemical recurrence-free survival, stratified by the performance of sentinel node biopsy, in node positive patients (long rank; p = 0.011). ePLND = extended pelvic lymph node dissection; SNB = sentinel node biopsy.

Subgroup Analysis

In the subgroup analysis of patients with ≥ 14 LNs removed, the 5-year BCR-free survival rate remained significantly higher in the ePLND+SNB group compared the to ePLND group (82.7% vs 63.9%, respectively; p = 0.001). Similar results were observed when patients were stratified according to LN

stage (node negative: 91.3% vs 76.2%, p = 0.026; node positive: 62.1% vs 24.1%, p = 0.001).

Univariate and Multivariate Cox Regression Models Predicting BCR

The univariate and multivariate analyses for the entire cohort are shown in Table 2. In the univariate analysis, higher preoperative PSA (odds ratio [OR], 1.014; 95% CI, 1.010–1017; p < 0.001), advanced clinical stage (p < 0.001), primary pathological Gleason grade > 3 (OR, 3.746; 95% CI, 2.923–4.801; p < 0.001), positive surgical margin (OR, 2.111; 95% CI, 1.657–2.688; p < 0.001), extracapsular extension (OR, 3.314; 95% CI, 2.566–4.280; p < 0.001), higher number of removed nodes (OR, 1.024; 95% CI, 1.004–1.044; p = 0.017) and higher number of positive nodes (p < 0.001) were predictors of BCR, while SNB was negatively correlated to BCR (OR, 0.682; 95% CI, 0.479–0.969; p = 0.033). Based upon the results from multivariate analysis, higher PSA (OR, 1.013; 95% CI, 1.008–1.018; p < 0.001), primary pathological Gleason grade > 3 (OR, 2.352; 95% CI, 1.793–3.085; p < 0.001), positive surgical margin (OR, 1.361; 95% CI, 1.048–1.768; p = 0.021), seminal vesicle invasion (OR, 1.744; 95% CI, 1.263–2.408; p = 0.001), higher number of removed nodes (OR, 1.025; 95% CI, 1.002–1.048; p = 0.032), and higher number of positive nodes (p < 0.001) were independent predictors of BCR, while SNB remained inversely correlated to BCR (OR, 0.535; 95% CI, 0.368–0.777; p = 0.001).

The univariate analysis in ePLND group showed the same predictors of BCR as the entire cohort (Table 3). The results of multivariate analysis were also similar with the exception of positive surgical margin, which was not identified as an independent predictor of BCR in this group. In the ePLND+SNB group the predictors in univariate analysis were again the same as in the overall cohort, with the exception of the number of removed nodes. However, in the multivariate analysis only a higher number of positive nodes remained independent predictor of BCR (Table 4).

Table 2. Univariate and multivariate pre- and postoperative factors for biochemical recurrence in overall cohort.						
Variables	Univariate			Multivariate		
	Odds	95% CI	p	Odds	95% CI	P
Preoperative serum PSA	1.014	1.010-1.017	**0.000**	1.013	1.008-1.018	**0.000**
Ct			**0.000**			0.559
T2 vs T1	1.07	0.731-1.567	0.728	0.859	0.583-1.266	0.443
T3 vs T1	2.359	1.607-3.463	**0.000**	0.983	0.651-1.486	0.937
Primary pathologic Gleason Grade > 3	3.746	2.923-4.801	**0.000**	2.352	1.793-3.085	**0.000**
Secondary pathologic Gleason Grade > 3	0.859	0.67-1.103	0.234			
SN biopsy	0.682	0.479-0.969	**0.033**	0.535	0.368-0.777	**0.001**
Positive surgical margin	2.111	1.657-2.688	**0.000**	1.361	1.048-1.768	**0.021**
Extracapsular extension	3.314	2.566-4.280	**0.000**	1.302	0.921-1.841	0.135
Seminal vesicle invasion	4.097	3.213-5.224	**0.000**	1.744	1.263-2.408	**0.001**
Number of removed nodes	1.024	1.004-1.044	**0.017**	1.025	1.002-1.048	**0.032**
Number of positive nodes	-	-	**0.000**	-	-	**0.000**

1-2 vs 0 positive nodes	3.783	2.843-5.034	**0.000**	2.266	1.654-3.106	**0.000**
>2 vs 0 positive nodes	8.447	5.713-12.489	**0.000**	3.555	2.269-5.570	**0.000**

Table 3. Univariate and multivariate pre- and postoperative factors for biochemical recurrence in ePLND group.

Variables	Univariate			Multivariate		
	Odds	95% CI	p	Odds	95% CI	P
Preoperative serum PSA	1.013	1.009-1.017	**0.000**	1.013	1.008-1.018	**0.000**
cT			**0.000**			0.741
T2 vs T1	1.129	0.753-1.694	0.557	0.85	0.562-1.285	0.440
T3 vs T1	2.506	1.659-3.785	**0.000**	0.884	0.562-1.391	0.595
Primary pathologic Gleason Grade > 3	3.843	2.943-5.019	**0.000**	2.51	1.875-3.36	**0.000**
Secondary pathologic Gleason Grade > 3	0.817	0.627-1.066	0.136			
Positive surgical margin	1.999	1.541-2.592	**0.000**	1.304	0.981-1.732	0.067
Extracapsular extension	3.186	2.417-4.199	**0.000**	1.289	0.887-1.874	0.183
Seminal vesicle invasion	3.850	2.966-4.999	**0.000**	1.772	1.255-2.503	**0.001**

Number of removed nodes	1.043	1.021-1.067	**0.000**	1.034	1.009-1.059	**0.007**
Number of positive nodes	-	-	**0.000**	-	-	**0.000**
1-2 vs 0 positive nodes	3.993	2.914-5.471	**0.000**	2.237	1.578-3.173	**0.000**
>2 vs 0 positive nodes	11.346	7.334-17.552	**0.000**	3.746	2.257-6.217	**0.000**

Table 4. Univariate and multivariate pre- and postoperative factors for biochemical recurrence in ePLND+SNB group.

Variables	Univariate			Multivariate		
	Odds	95% CI	p	Odds	95% CI	P
Preoperative serum PSA	1.038	1.018-1.059	**0.000**	1.013	0.989-1.039	0.290
cT	-	-	**0.021**			0.171
T2 vs T1	0.800	0.261-2.454	0.696	0.785	0.223-2.761	0.706
T3 vs T1	2.113	0.718-6.216	0.174	1.584	0.469-5.345	0.459
Primary pathologic Gleason Grade > 3	3.598	1.822-7.106	**0.000**	1.622	0.729-3.610	0.236
Secondary pathologic Gleason Grade > 3	1.430	0.651-3.140	0.372			
Positive surgical margin	2.731	1.419-5.254	**0.003**	1.703	0.852-3.405	0.132

Extracapsular extension	3.918	1.983-7.741	**0.000**	1.240	0.475-3.235	0.660
Seminal vesicle invasion	6.025	3.094-11.731	**0.000**	2.159	0.788-5.917	0.134
Number of removed nodes	0.992	0.941-1.045	0.750			
Number of positive nodes	-	-	**0.000**	-	-	**0.025**
1-2 vs 0 positive nodes	4.218	2.055-8.661	**0.000**	2.521	1.155-5.505	**0.020**
>2 vs 0 positive nodes	6.060	2.358-15.572	**0.000**	3.319	1.094-10.065	**0.034**

Observed Outcome vs Nomogram Prediction

Based on the AUC, the performance of MSKCC nomogram was better in the ePLND+SNB group than in the ePLND group (AUC, 0.804; 95% CI, 0.725-0.884 and AUC, 0.789; 95% CI, 0.753-0.826, respectively). In the calibration plots (Fig. 2A and 2B), the nomogram was underestimating the probability of BCR-free status in the ePLND+SNB group (mean absolute error = 0.021) while the ePLND group was performing almost as predicted (mean absolute error = 0.009). The decision curve analyses indicated that in the ePLND+SNB group the MSKCC nomogram resulted in higher net benefit compared to the ePLND group, for most of the examined BCR probabilities (Fig. 3A and 3B).

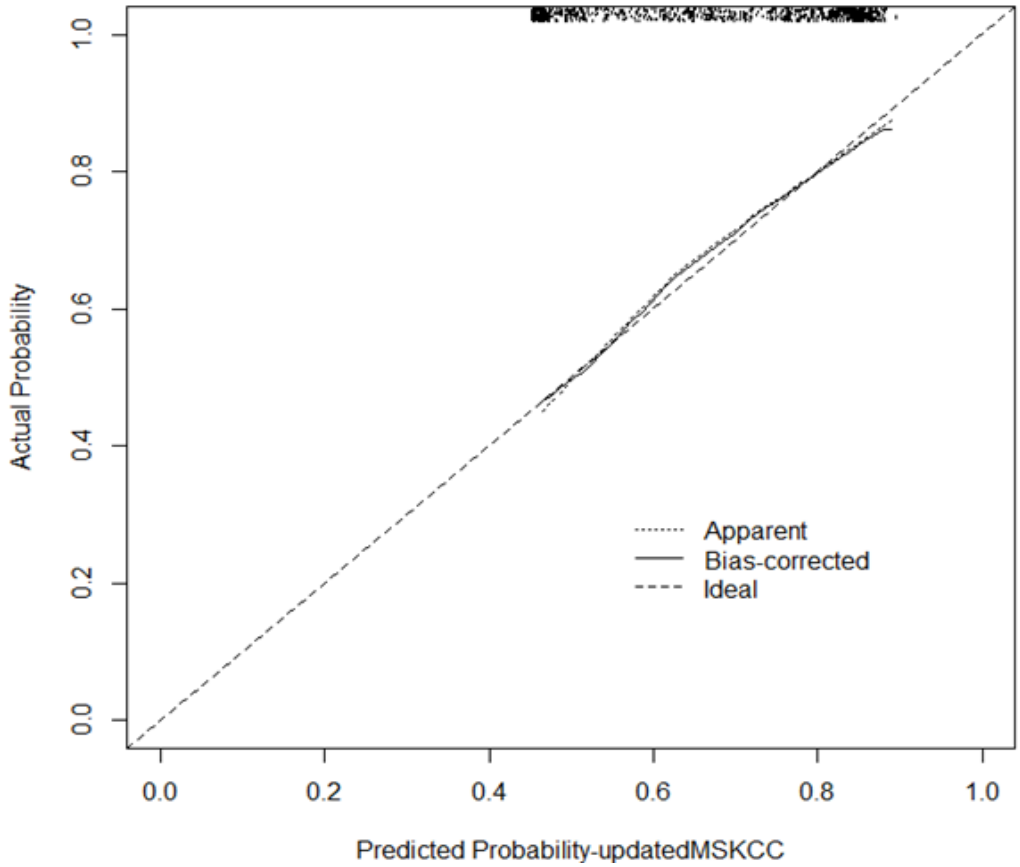

FIGURE 2A. Nomograms calibration plot for ePLND group. The dotted plot indicates the location of the ideal nomogram, in which actual and predicted probabilities are identical. Expected performance on future data represented through the solid line.

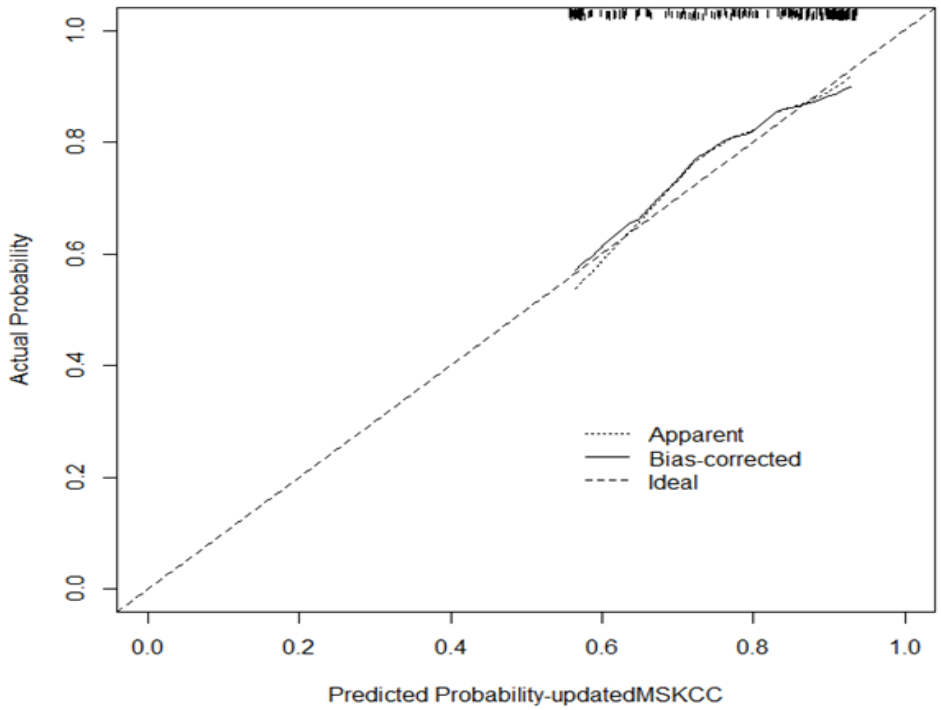

FIGURE 2B. Nomograms calibration plot for ePLND+SNB group. The dotted plot indicates the location of the ideal nomogram, in which actual and predicted probabilities are identical. Expected performance on future data represented through the solid line.

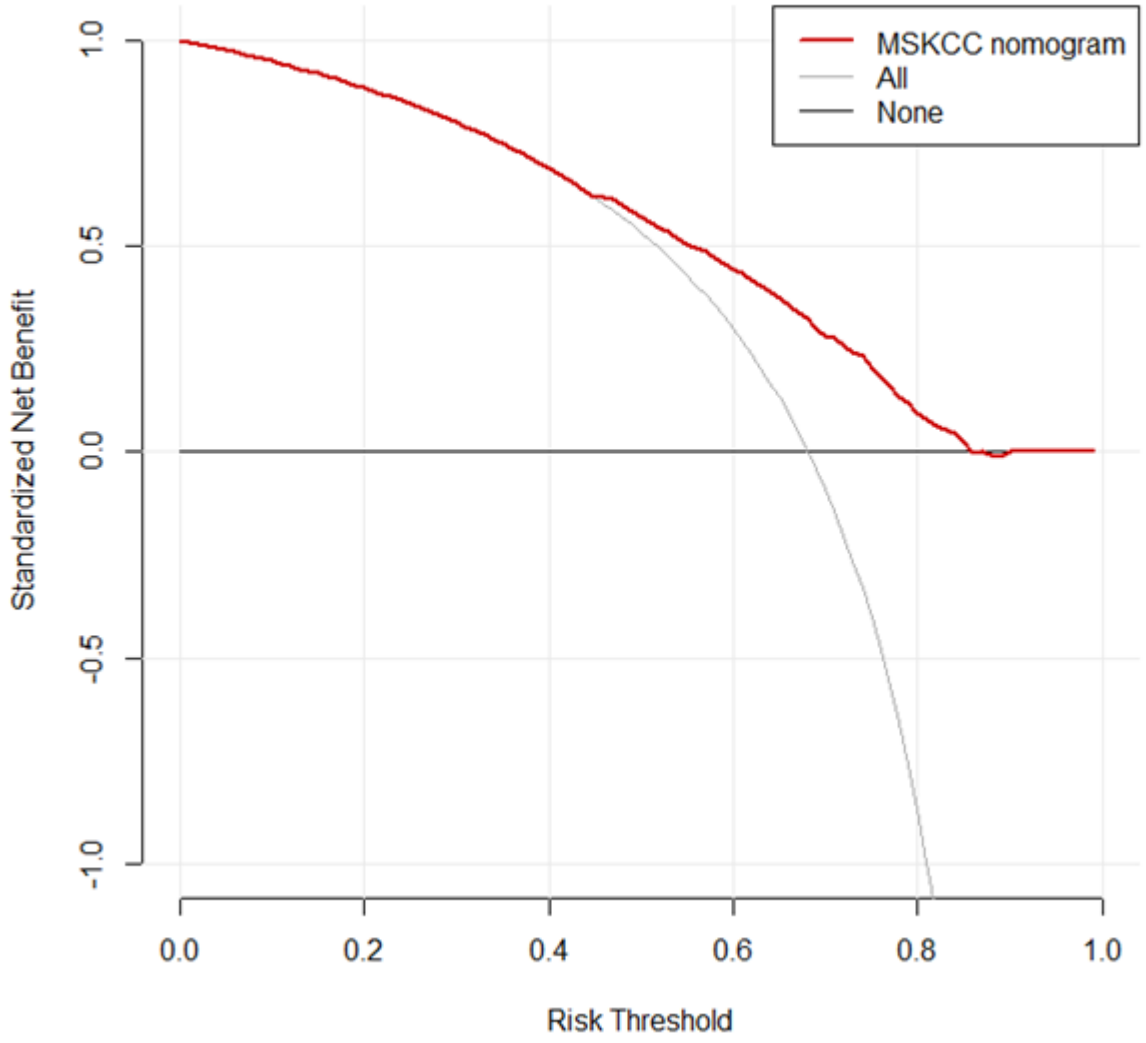

FIGURE 3A. Decision curve analyses for biochemical recurrence predictions in ePLND group. The red line indicates the net benefit of using the updated MSKCC nomogram. The assumption that all patients will recur (grey line). The assumption that no patients will recur (black line).

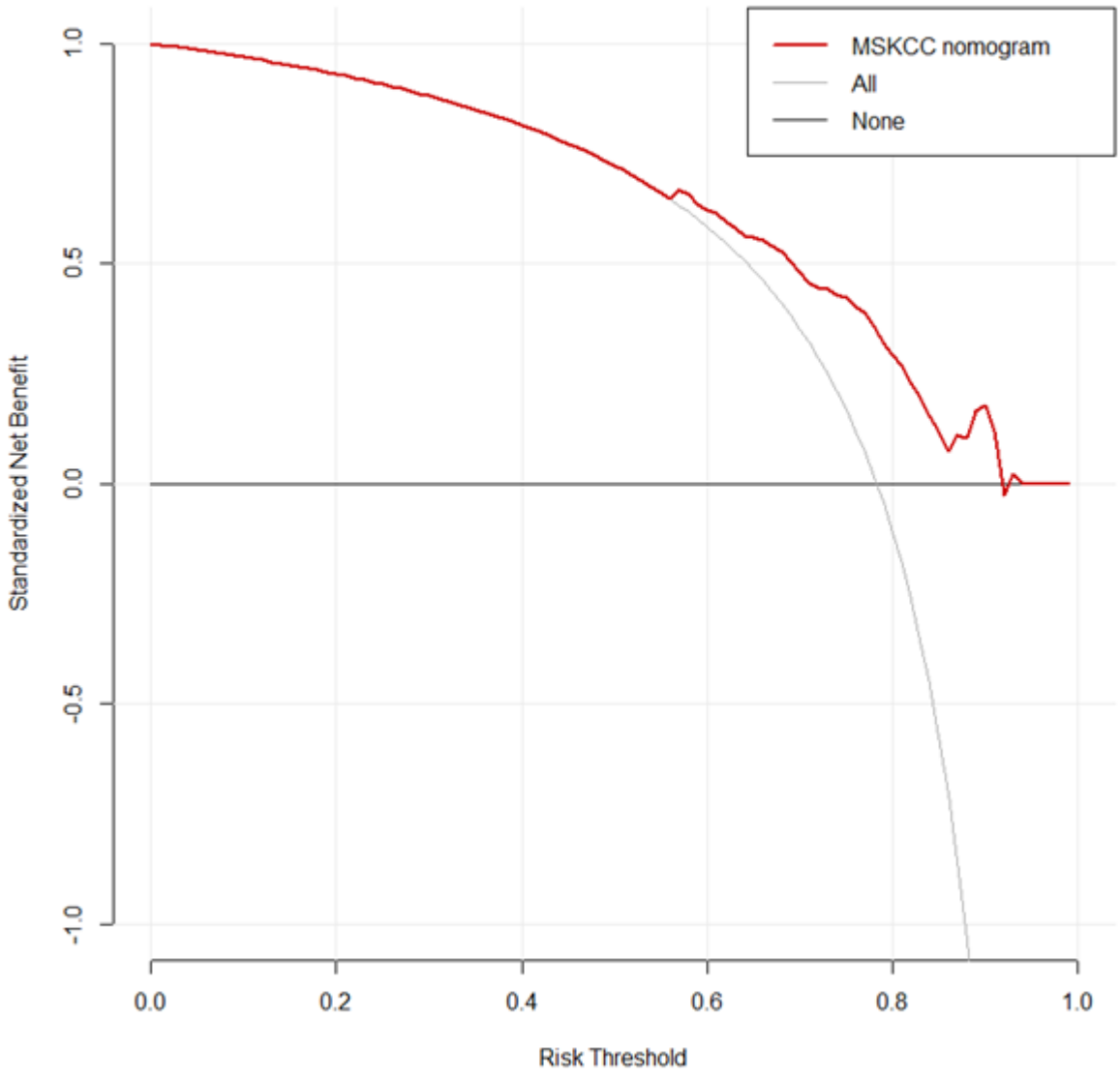

FIGURE 3B. Decision curve analyses for biochemical recurrence predictions in ePLND+SNB group. The red line indicates the net benefit of using the updated MSKCC nomogram. The assumption that all patients will recur (grey line). The assumption that no patients will recur (black line).

Discussion

To the best of our knowledge, our study is the first to explore the BCR outcome of men treated by RARP and ePLND compared to a cohort of men additionally treated with ePLND+SNB. Based on our results, when SNB was applied, there

was a 17% increase on the number of patients who achieved a 5-year BCR-free status. This improved outcome was independent of LN status. In the subgroup of patients where more than 14 LNs where removed, a 29.4% increase in the percentage of 5-year BCR-free patients was observed compared to the ePLND-only patients. The decision to perform a subgroup analysis for men with ≥ 14 LNs removed was based on previous reports demonstrating favorable survival outcomes in patients treated with ePLND and more than 14 nodes removed (17-19).

To increase the power of our analysis we compared the observed BCR outcomes with the predictions of the recently updated post-operative MSKCC nomogram (9), performing in that way the first external validation of this nomogram. Our study has demonstrated a reasonably accurate predictive accuracy of the nomogram for the entire cohort (AUC, 0.789; 95% CI, 0.754-0.824). Moreover, the prediction was better in the ePLND+SNB (AUC, 0.804) compared to the ePLND group (AUC, 0.789). The favorable outcome observed in the calibration analysis of the ePLND+SNB group strengthens our observation of the improved BCR-free outcome when SNB is performed. It also suggests that the improved outcome of men after SNB is independent of clinical characteristics such as Gleason, PSA, and tumor stage. the decision curve analyses indicated that the net benefit of the MSKCC nomogram was higher in the ePLND+SNB group compared to the ePLND group in almost the entire range of threshold probabilities.

The explanation for the improved BCR-free survival in the ePLND+SNB group compared to the ePLND group is a matter of speculation. Fossati et al. in their recent systematic review reported that the therapeutic role of ePLND itself is still not evident from the current literature (20). We observed a higher number of removed and histologically positive nodes when SNB was performed. In line with these findings a diagnostic and therapeutic effect of combining ePLND+SNB has been suggested in the systematic review from Wit et al. (15). This review indicates that the SNs were the only metastatic site in 73% of LN-positive patients while in 1 in 20 patients who underwent ePLND, metastatic LNs would have been missed without SNB. In an alternative study, Winter et al. also detected more LN-positive patients compared to the prediction of the

Briganti nomogram when sentinel lymphadenectomy was performed (21). Recently, the detection rate of SNs has shown also further improvement with the application of new detection techniques e.g by combining indocyanine green-99mTechnetium-nanocolloid with fluorescein (22). A recent SN consensus panel suggested that SNB could identify metastatic nodes outside the extended lymphadenectomy template but it should be combined with ePLND especially in intermediate- and high-risk patients since often positive non-SNs were found besides the SNB (23,24). In addition to the improved detection rate, targeted SN dissection allows for a separate and thus more accurate histopathological examination, thereby increasing the detection especially of small LN metastases (25). Muck et al. have shown improved clinical outcomes in patients treated with radical prostatectomy combined with ePLND+SNB when they have a low nodal tumor burden (micro-metastases) (26).

In accordance to other studies (27) our Cox regression analysis showed that adverse pathology characteristics such as primary pathology Gleason grade > 3, positive surgical margin, seminal vesicle invasion and extracapsular extension were independent predictors of BCR. Fischer et al. (28) in a sample of 459 men demonstrated a 2-year BCR risk of ≥50% in patients with positive surgical margin, extracapsular extension or seminal vesicle invasion. In our Cox analysis the number of positive nodes was also an independent predictor of BCR in the overall cohort and in both groups. Moreover, the initial Stephenson nomogram (6) performed worse than the updated nomogram (AUC: 0.789 vs 0.681 in the overall cohort) confirming the value of replacing the positive LN status in the initial nomogram with the number of positive nodes in the updated nomogram (9).

Limitations

Limitations of our study include the retrospective setting, the relatively short median follow-up and the selection bias due to a single institution case series. Finally, the data depend on factors such as the extent of LN dissection and

complexities regarding tissue handling and the accuracy of histologic detection and reporting of nodal metastases.

Conclusion

Adding SNB to ePLND resulted in improved BCR-free outcome compared to ePLND-only in men after RARP. This observation was strengthened by the improved prediction outcome as compared to the MSKCC nomogram. SNB also resulted in favorable nodal staging through the detection of more positive nodes than ePLND. SNB remains an attractive and promising staging intervention that may expand surgical options in managing men with localized PCa. Further research and randomized studies to assess the effect of SNB on LN detection rate and the relationship between SNB and BCR are warranted.

References

1. Stephenson AJ, Scardino PT, Eastham JA, et al. Preoperative nomogram predicting the 10-year probability of prostate cancer recurrence after radical prostatectomy. J Natl Cancer Inst. 2006;98:715-717.
2. Freedland SJ, Humphreys EB, Mangold LA, et al. Risk of prostate cancer-specific mortality following biochemical recurrence after radical prostatectomy. JAMA. 2005;294:433-439.
3. Zhang YD, Wu CJ, Bao ML, et al. MR-based prognostic nomogram for prostate cancer after radical prostatectomy. J Magn Reson Imaging. 2017;45:586-596.
4. D'Amico AV, Whittington R, Malkowicz SB, et al. Biochemical outcome after radical prostatectomy, external beam radiation therapy, or interstitial radiation therapy for clinically localized prostate cancer. JAMA. 1998;280:969-974.
5. Cooperberg MR, Pasta DJ, Elkin EP, et al. The University of California, San Francisco Cancer of the prostate risk assessment score: a straightforward and reliable preoperative predictor of disease recurrence after radical prostatectomy. J Urol. 2005;173:1938-1342.
6. Stephenson AJ, Scardino PT, Eastham JA, et al. Postoperative nomogram predicting the 10-year probability of prostate cancer recurrence after radical prostatectomy. J Clin Oncol. 2005;23:7005-7012.
7. Lughezzani G, Budäus L, Isbarn H, et al. Head-to-head comparison of the three most commonly used preoperative models for prediction of biochemical recurrence after radical prostatectomy. Eur Urol. 2010;57:562-5688.
8. Walz J, Chun FK, Klein EA, et al. Nomogram predicting the probability of early recurrence after radical prostatectomy for prostate cancer. J Urol. 2009;181:601-607.

9. Nguyen DP, Kent M, Vilaseca A, et al. Updated postoperative nomogram incorporating the number of positive lymph nodes to predict disease recurrence following radical prostatectomy. Prostate Cancer Prostatic Dis. 2017;20:105-109.

10. Budäus L, Leyh-Bannurah SR, Salomon G, et al. Initial experience of (68)Ga-PSMA PET/CT imaging in high-risk prostate cancer patients prior to radical prostatectomy. Eur Urol. 2016;69:393-396.

11. Mottet N, Bellmunt J, Bolla M, et al. EAU-ESTRO-SIOG guidelines on prostate cancer. Part 1: screening, diagnosis, and local treatment with curative intent. Eur Urol. 2017;71:618-629.

12. Rouzier R, Uzan C, Rousseau A, et al. Multicenter prospective evaluation of the reliability of the combined use of two models to predict non-sentinel lymph node status in breast cancer patients with metastatic sentinel lymph nodes: the MSKCC nomogram and the Tenon score. Results of the NOTEGS study. Br J Cancer. 2017;116:1135-1140.

13. Schubert T, Uphoff J, Henke RP, Wawroschek F, Winter A. Reliability of radioisotope-guided sentinel lymph node biopsy in penile cancer: verification in consideration of the european guidelines. BMC Urol. 2015;15:98.

14. van der Poel HG, Meershoek P, Grivas N, KleinJan G, van Leeuwen FW, Horenblas S. Sentinel node biopsy and lymphatic mapping in penile and prostate cancer. Urologe A. 2017;56:13-17.

15. Wit EM, Acar C, Grivas N, et al. Sentinel Node Procedure in Prostate Cancer: A systematic review to assess diagnostic accuracy. Eur Urol. 2017;71:596-605.

16. KleinJan GH, van den Berg NS, Brouwer OR, et al. Optimisation of fluorescence guidance during robot-assisted laparoscopic sentinel node biopsy for prostate cancer. Eur Urol. 2014;66:991-998.

17. Abdollah F, Gandaglia G, Suardi N, et al. More extensive pelvic lymph node dissection improves survival in patients with node-positive prostate cancer. Eur Urol. 2015;67:212-219.

18. Briganti A, Blute ML, Eastham JH, et al. Pelvic lymph node dissection in prostate cancer. Eur Urol. 2009;55:1251-1265.

19. Kluth LA, Abdollah F, Xylinas E, et al. Clinical nodal staging scores for prostate cancer: a proposal for preoperative risk assessment. Br J Cancer. 2014;111:213-219.

20. Fossati N, Willemse PM, Van den Broeck T, et al. The benefits and harms of different extents of lymph node dissection during radical prostatectomy for prostate cancer: a systematic review. Eur Urol. January 24, 2017 [Epub ahead of print].

21. Winter A, Kneib T, Henke RP, Wawroschek F. Sentinel lymph node dissection in more than 1200 prostate cancer cases: rate and prediction of lymph node involvement depending on preoperative tumor characteristics. Int J Urol. 2014;21:58-63.

22. van den Berg NS, Buckle T, KleinJan GH, van der Poel HG, van Leeuwen FW. Multispectral fluorescence imaging during robot-assisted laparoscopic sentinel node biopsy: a first step towards a fluorescence-based anatomic roadmap. Eur Urol. June 23, 2016 [Epub ahead of print].

23. van der Poel HG, Wit EM, Acar C, et al. Sentinel node biopsy for prostate cancer: report from a consensus panel meeting. BJU Int. February 10, 2017 [Epub ahead of print].

24. Holl G, Dorn R, Wengenmair H, Weckermann D, Sciuk J. Validation of sentinel lymph node dissection in prostate cancer: experience in more than 2,000 patients. Eur J Nucl Med Mol Imaging. 2009;36:1377-1382.

25. Acar C, Kleinjan GH, van den Berg NS, Wit EM, van Leeuwen FW, van der Poel HG. Advances in sentinel node dissection in prostate cancer from a technical perspective. Int J Urol. 2015;22:898-909.

26. Muck A, Langesberg C, Mugler M, Rahnenführer J, Wullich B, Schafhauser W. Clinical outcome of patients with lymph node-positive prostate cancer following radical prostatectomy and extended sentinel lymph node dissection. Urol Int. 2015;94:296-306.

27. Karl A, Buchner A, Tympner C, et al. Risk and timing of biochemical recurrence in pT3aN0/Nx prostate cancer with positive surgical margin - A multicenter study. Radiother Oncol. 2015;116:119-124.

28. Fischer S, Lin D, Simon RM, et al. Do all men with pathological Gleason score 8-10 prostate cancer have poor outcomes? Results from the SEARCH database. BJU Int. 2016;118:250-257.

4

Validation and head-to-head comparison of three nomograms predicting probability of lymph node invasion of prostate cancer in patients undergoing extended and/or sentinel lymph node dissection.

Grivas N, Wit E, Tillier C, van Muilekom E, Pos F, Winter A, van der Poel H.

Eur J Nucl Med Mol Imaging. 2017 Dec;44(13):2213-2226.

Abstract

Purpose - The updated Winter nomogram is the only nomogram predicting lymph node invasion (LNI) in prostate cancer (PCa) patients based on sentinel node (SN) dissection (sLND). The aim of the study was to externally validate the Winter nomogram and examine its performance in patients undergoing extended pelvic lymph node dissection (ePLND), ePLND combined with SN biopsy (SNB) and sLND only. The results were compared with the Memorial Sloan Kettering Cancer Center (MSKCC) and updated Briganti nomograms.

Methods - This retrospective study included 1183 patients with localized PCa undergoing robot-assisted laparoscopic radical prostatectomy (RARP) combined with pelvic lymphadenectomy and 224 patients treated with sLND and external beam radiotherapy (EBRT), aiming to offer pelvic radiotherapy only in case of histologically positive SNs. In the RARP population, ePLND was applied in 956 (80.8%) patients while 227 (19.2%) patients were offered ePLND combined with additional SNB.

Results - The median numbers of removed nodes were 10 (interquartile range, IQR=6-14), 15 (IQR=10-20) and 7 (IQR=4-10) in the ePLND, ePLND+SNB, and sLND groups, respectively. Corresponding LNI rates were 16.6%, 25.5% and 42%. Based on the AUC, the performance of Briganti nomogram (0.756) in the ePLND group was superior to both the MSKCC (0.744) and Winter nomogram (0.746). The Winter nomogram, however was the best predictor of LNI in both the ePLND+SNB (0.735) and sLND (0.709) populations. In the calibration analysis, all nomograms showed better accuracy in the low/intermediate risk patients while in the high risk population an overestimation of the risk for LNI was observed.

Conclusion - The SN based updated nomogram showed better prediction in the SN population. The results were also comparable, relative to predictive tools developed with (e)PLND, suggesting a difference in sampling accuracy between SNB and non-SNB. Patients who benefit most from the nomogram would be those with a low/intermediate risk of LN metastasis.

Introduction

The local lymph node (LN) status is a major prognostic factor in prostate cancer (PCa). Even the newest imaging methods, like 68gallium prostate-specific membrane antigen (PSMA) positron emission tomography (PET)/CT have a low sensitivity (49–66%) in detection of LN metastases and metastases smaller than 4mm are likely to be missed (1). Prevalence of lymph node invasion (LNI) ranges from 1.1% to 26% in contemporary patients with a significantly greater rate in patients undergoing extended pelvic lymph node dissection (ePLND) relative to patients undergoing only limited PLND (2-3). For these reasons ePLND is considered the gold standard method for LN staging of intermediate and high-risk (>5%) PCa patients (4). However, the oncological benefit of ePLND was not proven in recent systematic review of the literature (5). Moreover, the extended template may not include all lymphatic drainage sites and it is additionally correlated with increased morbidity and surgical complications (6).

In the era of widely applied prostate cancer screening and the resulting stage migration, the risk of LNI has gradually decreased (7). Aiming to identify low risk patients, in whom ePLND could be omitted, several nomograms based on preoperative clinico-pathological variables and ePLND outcomes, were developed (7-11). Despite the fact that all of these ePLND-derived nomograms have demonstrated high accuracy when externally validated, their performance characteristics still requires periodic reappraisals in contemporary cohorts to ensure validity (12-17).

In order to avoid the morbidity of ePLND and avoid under-sampling, the concept of selective sentinel node (SN) biopsy (SNB) has been developed. SNB is a standard procedure in melanoma, breast and penile cancer while it is increasingly applied also in PCa (18-20). Recent studies have demonstrated that sentinel lymph node dissection (sLND) combined with ePLND could provide better lymph node staging in localized PCa (21-22). However, European Association of Urology (EAU) Guidelines suggest the application of SNB as an experimental method, mainly due to the lack of large comparative studies and the lack of consensus on the definition, technique and outcome reporting in PCa (4, 20).

In 2015, Winter et al. reported the first sLND-based nomogram, including the preoperative prostate specific antigen (PSA), the clinical stage and the sum Gleason score as LNI predictors (23). The nomogram showed a high staging accuracy with an area under the receiver operating characteristics curve (AUC) of 82%. The recently updated nomogram added the variables of the primary and secondary Gleason grade as well as the percentage of positive cores, demonstrating again a high bootstrap-corrected predictive accuracy (AUC: 83.5%) (24). PSA, clinical stage, primary, secondary Gleason grade and the percentage of positive cores are also included in the two most widely used LNI nomograms i.e. the updated Briganti nomogram and the Memorial Sloan Kettering Cancer Center (MSKCC)-LNI-cores nomogram (11, 25).

The aim of the study was to externally validate the updated Winter nomogram and examine its ability in predicting LNI in patients undergoing extended and/or sentinel pelvic lymph node dissection. The results were compared with the validation outcomes of the updated Briganti and MSKCC nomograms.

Materials and Methods

Patients

Between January 2006 and November 2016, 1183 consecutive patients with localized PCa underwent robot-assisted laparoscopic radical prostatectomy (RARP), along with pelvic lymphadenectomy while 224 patients were treated with sLND and external beam radiotherapy (EBRT), aiming to offer primary pelvic radiotherapy including the prostate only in case of histologically positive SNs. Men with a negative sLND would receive prostate-only EBRT. In both cases of radiotherapy additional androgen ablation was applied. In the RARP population, ePLND was applied in 956 (80.8%) patients while 227 (19.2%) patients were offered ePLND combined with additional SNB (ePLND+SNB) within the scope of a clinical study. Patients who declined participation were offered only ePLND. The indication for LND was based on guidelines' recommendations at the year of diagnosis. The primary tumor was staged by digital rectal examination, trans-rectal ultrasound or magnetic resonance

imaging (MRI) and classified per the 2009 TNM staging system. PSA was measured using standard assays. All patients were subjected to trans-rectal ultrasound-guided prostate biopsy and the total number of cores taken as well as the number and the percentage of positive cores, the Gleason sum, the primary and secondary Gleason grade, the number of removed and positive LNs were prospectively recorded.

Our cohort was used to perform an external validation and comparison of the 3 different nomograms i.e. updated Winter, updated Briganti nomogram and MSKCC nomogram, in three groups of patients i.e. patients who were submitted to RARP and ePLND, those who were offered RARP+ePLND+SNB and those who were submitted to EBRT and sLND.

ePLND and SNB Technique

The RARP, the ePLND, the SNB technique and the pathology examination were performed as described earlier (26). In brief, surgery was performed by a urologist experienced in laparoscopic or robotic-assisted surgery using either a standard laparoscopic set-up or the da Vinci S(i) Surgical system (Intuitive Surgical Inc., Sunnyvale, CA, USA). The ePLND consisted of excision of the nodes along the external iliac artery and vein, the obturator nodes, the internal iliac nodes, and the nodes overlying the common iliac vessels up to the ureteral crossing.

All SNs were identified using a combination of 99mTc-nanocolloid technetium and indocyanine green (ICG) at a dose of 240 MBq, trans-rectally injected on the morning of surgery into the peripheral zone of the prostate under ultrasound guidance. Planar imaging of the pelvic area from anterior and a lateral position was performed at 15-30 min and 2 hours after injection followed by Single-Photon Emission Computed Tomography and low-dose CT (SPECT-CT) images in order to generate a roadmap for the intraoperative localization of the individual SNs. In case of non-visualization of SNs, an ePLND up to the ureter-vessel crossing was performed.

Statistical analysis

Univariate and multivariate logistic regression models predicting the presence of LNI were applied for the three groups. Covariates consisted of preoperative PSA (coded as continuous variable), clinical stage, primary and secondary biopsy Gleason grade (categorized as ≤3 vs ≥4) and percentage of positive cores (defined as the number of positive cores over the total number of cores taken). The performance of the three nomograms was quantified with respect to discrimination and calibration. Discrimination was quantified with the AUC and the P-value of Hosmer–Lemeshow (HL) goodness-of-fit test. Calibration was studied with graphic representations of the relationship between the observed outcome frequencies and the predicted probabilities (calibration curves) and the two informative parameters: Intercept (calibration-in-the-large) and Slope, which evaluate the correspondence between the predicted and the actual probabilities. A decision curve analysis was performed to evaluate and compare the net benefit for different threshold probabilities. Finally, we calculated the nomogram cutoffs associated with optimal negative predictive value (NPV) in order to identify patients with a low risk of LNI where ePLND could be spared. Values of $P < .05$ were considered statistically significant. SPSS software ver. 22.0 (SPSS Inc., Chicago, IL) and the R statistical package (R Foundation for Statistical Computing, Vienna, Austria) were used to perform the statistical analysis.

Results

Subgroups comparisons

i. ePLND versus ePLND+SNB

Descriptive patient characteristics and comparison between the two groups according to LN status are shown in Table 1. Mean number of removed LNs was 10 (interquartile range, IQR= 6-14) and 15 (IQR=10-20) in the ePLND and EPLND+SNB groups, respectively ($p< 0.001$). Correspondingly, LNI was found in 16.6% and 25.5% of the patients. Moreover, the ePLND group had higher

mean PSA (15.1 vs 11.2, P< 0.02). No difference was observed in the mean number of positive LNs (2.1 vs 2.6, p = 0.7) in men with LNI.

Table 1. ePLND versus ePLND+SNB. Characteristics of patients according to lymph node invasion.						
	pN0			pN1		
	ePLND (n = 797)	ePLND+SNB (n=169)	P Value	ePLND (n = 159)	ePLND+SNB (n = 58)	P Value
Age, years						
Mean (median)	63.5 (64)	63.9 (64)	.513	63.9 (65)	64.1 (64)	.883
IQR	60-68	61-68		60-68	59.7-68.2	
PSA level, ng/ml						
Mean (median)	12.6 (9.1)	10.8 (8)	.004	17.5 (12)	12 (8.6)	.002
IQR	6.5-15	5.6-12.3		7.5-18.8	6.2-12	
Clinical stage, no. (%)	.581			.058		
T1c	138 (17.1)	33 (19.8)		16 (10.1)	6 (10.3)	
T2a	108 (13.6)	18 (10.8)		9 (5.7)	4 (6.9)	
T2b	161 (20.2)	28 (16.8)		26 (16.4)	13 (22.4)	
T2c	210 (26.3)	47 (28.1)		32 (20.1)	12 (20.7)	
T3	180 (22.8)	41 (24.5)		76 (47.7)	23 (39.6)	
Primary Gleason	.55			.449		

grade, no. (%)						
≤ 3	514 (64.5)	116 (68.6)		77 (48.4)	23 (39.7)	
≥ 4	283 (35.5)	53 (31.4)		82 (51.6)	35 (60.3)	
Secondary Gleason grade, no. (%)	.141			.621		
≤ 3	309 (38.8)	49 (29)		55 (34.6)	23 (39.7)	
≥ 4	488 (61.2)	120 (71)		104 (65.4)	35 (60.3)	
Overall Gleason score, no. (%)	.349			.886		
2-6	172 (21.6)	16 (9.5)		20 (12.6)	3 (5.2)	
7	434 (54.5)	123 (72.8)		81 (50.9)	34 (58.6)	
8-10	191 (23.9)	30 (17.8)		58 (36.5)	21 (36.2)	
Biopsy cores taken, no.						
Mean (median)	9.4 (10)	9.5 (10)	.29	9.2 (10)	8.8 (9)	.682
IQR	8-12	8-12		8-12	7.7-12	
% of positive biopsy cores						
Mean (median)	46.4 (42.8)	44.6 (37.5)	.255	64.7 (62.5)	59.8 (50)	.255
IQR	25-62.5	25-59.1		41.6-100	30.5-89.2	

Removed and examined LNs, no.						
Mean (median)	9.93 (9)	15.3 (14)	<.001	13.2 (13)	16.8 (17)	<.001
IQR	6-13.2	10-20		9-17	12-22	
Positives LNs, no.						
Mean (median)	N/A	N/A	N/A	2.1 (1)	2.6 (1)	0.703
IQR				1-3	1-3	

ii. ePLND versus sLND

Descriptive patient characteristics and comparison between the two groups according to LN status are shown in Table 2. Mean number of removed LNs was lower in sLND group (7.9 vs 10, $p < 0.001$) but significantly more patients had positive LNs (42.0% vs 16.6%). Moreover the sLND group had a higher mean PSA (28.0 vs 15.1, $p < 0.01$), more advanced clinical stage (cT3-4) ($p < 0.001$), higher Gleason score ($p < 0.01$) and higher percentage of positive cores (69.4 vs 55.5, $p \leq 0.002$). However, no difference was observed in the mean number of positive LNs (2.1 vs 2.1, $p = 0.92$) in men with LNI.

Table 2. ePLND versus sLND. Characteristics of patients according lymph node invasion.

	pN0			pN1		
	ePLND (n = 797)	sLND (n=133)	P Value	ePLND (n = 159)	sLND (n = 91)	P Value
Age, years						
Mean (median)	63.5 (64)	64.6 (65)	.062	63.9 (65)	63.92 (64)	.442
IQR	60-68	61-69		60-68	62-67	
PSA level, ng/ml						
Mean (median)	12.6 (9.1)	25.1(15.2)	<.001	17.5 (12)	31.22 (16)	.009
IQR	6.5-15	9-29		7.5-18.8	8.5-31	

Clinical stage, no. (%)	<.001			<.001		
T1c	138 (17.1)	6 (4.6)		16 (10.1)	2 (2.1)	
T2a	108 (13.6)	10 (7.5)		9 (5.7)	4 (4.3)	
T2b	161 (20.2)	10 (7.5)		26 (16.4)	4 (4.3)	
T2c	210 (26.3)	19 (14.3)		32 (20.1)	12 (13.2)	
T3	180 (22.8)	88 (66.1)		76 (47.7)	69 (76.1)	
Primary Gleason grade, no. (%)	.102			.125		
≤ 3	514 (64.5)	70 (52.6)		77 (48.4)	37 (40.7)	
≥ 4	283 (35.5)	63 (47.4)		82 (51.6)	54 (59.3)	
Secondary Gleason grade, no. (%)	<.001			.066		
≤ 3	309 (38.8)	35 (26.3)		55 (34.6)	18 (19.8)	
≥ 4	488 (61.2)	98 (73.7)		104 (65.4)	73 (80.2)	
Overall Gleason score, no. (%)				.013		

2-6	172 (21.6)	18 (13.5)		20 (12.6)	4 (4.3)	
7	434 (54.5)	61 (45.9)		81 (50.9)	34 (37.4)	
8-10	191 (23.9)	54 (40.6)		58 (36.5)	53 (58.3)	
Biopsy cores taken, no.						
Mean (median)	9.4 (10)	8.85 (9)	.185	9.2 (10)	9.16 (10)	.563
IQR	8-12	8-12		8-12	8-12	
% of positive biopsy cores						
Mean (median)	46.4 (42.8)	62.16 (62.5)	<.001	64.7 (62.5)	76.78 (86.6)	.002
IQR	25-62.5	41.6-87.5		41.6-100	50-100	
Removed and examined LNs, no.						
Mean (median)	9.93 (9)	8.05 (7)	<.001	13.2 (13)	7.76 (7)	<.001
IQR	6-13.2	4-10		9-17	5-10	
Positives LNs, no.						
Mean (median)	N/A	N/A	N/A	2.1 (1)	2.1 (1)	0.922
IQR				1-3	1-2	

iii. ePLND+SNB versus sLND

Descriptive patient characteristics and comparison between the two groups according to LN status are shown in Table 3. Mean number of removed lymph nodes was lower in sLND group (7.9 vs 15.0, $p < 0.001$) but significantly more patients had positive LNs (42.0% vs 25.5%). Moreover the sLND group had higher mean PSA (28 vs 11.2, $p< 0.001$), more advanced clinical stage ($p<0.001$), higher Gleason score ($p<0.02$) and higher percentage of positive cores (69.4% vs 51.5 %, $p<0.001$). However no significant difference was

observed in the mean number of positive LNs (2.6 vs 2.1, p =0.67) in men with LNI.

Table 3. ePLND+SNB versus sLND. Characteristics of patients according to lymph node invasion.						
	pN0			pN1		
	ePLND+SNB (n = 169)	sLND (n=133)	P Value	ePLND+SNB (n = 58)	sLND (n = 91)	P Value
Age, years						
Mean (median)	63.9 (64)	64.6 (65)	.257	64.1 (64)	63.92 (64)	.771
IQR	61-68	61-69		59.7-68.2	62-67	
PSA level, ng/ml						
Mean (median)	10.8 (8)	25.1(15.2)	<.001	12 (8.6)	31.22 (16)	<.001
IQR	5.6-12.3	9-29		6.2-12	8.5-31	
Clinical stage, no. (%)	<.001			<.001		
T1c	33 (19.8)	6 (4.6)		6 (10.3)	2 (2.1)	
T2a	18 (10.8)	10 (7.5)		4 (6.9)	4 (4.3)	
T2b	28 (16.8)	10 (7.5)		13 (22.4)	4 (4.3)	
T2c	47 (28.1)	19 (14.3)		12 (20.7)	12 (13.2)	
T3	41 (24.5)	88 (66.1)		23 (39.6)	69 (76.1)	
Primary Gleason grade, no. (%)	.077			0.554		
≤ 3	116 (68.6)	70 (52.6)		23 (39.7)	37 (40.7)	

≥ 4	53 (31.4)	63 (47.4)		35 (60.3)	54 (59.3)	
Secondary Gleason grade, no. (%)	.002			.071		
≤ 3	49 (29)	35 (26.3)		23 (39.7)	18 (19.8)	
≥ 4	120 (71)	98 (73.7)		35 (60.3)	73 (80.2)	
Overall Gleason score, no. (%)	.001			.019		
2-6	16 (9.5)	18 (13.5)		3 (5.2)	4 (4.3)	
7	123 (72.8)	61 (45.9)		34 (58.6)	34 (37.4)	
8-10	30 (17.8)	54 (40.6)		21 (36.2)	53 (58.3)	
Biopsy cores taken, no.						
Mean (median)	9.5 (10)	8.85 (9)	.478	8.8 (9)	9.16 (10)	.456.
IQR	8-12	8-12		7.7-12	8-12	
% of positive biopsy cores						
Mean (median)	44.6 (37.5)	62.16 (62.5)	<.001	59.8 (50)	76.78 (86.6)	.001
IQR	25-59.1	41.6-87.5		30.5-89.2	50-100	
Removed and examined LNs, no.						
Mean (median)	15.3 (14)	8.05 (7)	<.001	16.8 (17)	7.76 (7)	<.001
IQR	10-20	4-10		12-22	5-10	
Positives LNs, no.						

Mean (median)	N/A	N/A	N/A	2.6 (1)	2.1 (1)	0.676
IQR				1-3	1-2	

Predictors of LNI

Clinical stage, primary Gleason grade and percentage of positive cores were significant predictors of LNI in the univariate analysis of all groups. In all groups, secondary Gleason grade was not a significant predictor, while PSA was not correlated with LNI only in ePLND+SNB group. Tables 4, 5 and 6 report the univariate and multivariate regression analysis of the association between predictors and presence of LNI for ePLND, ePLND+SNB and sLND groups, respectively. In the predictive accuracy analyses (AUC), percentage of positive cores was the most accurate predictor of LNI in all groups. At multivariate analysis, primary biopsy Gleason grade and percentage of positive cores were independent-predictors of LNI in all groups, while PSA and clinical stage were additional predictors in the ePLND group.

Table 4. Univariate and multivariate logistic regression analyses predicting the presence of lymph node invasion in ePLND group.

Covariates	Univariate analysis			Multivariate analysis	
	Odds ratio (95% CI)	p value	AUC (%)	Odds ratio (95% CI)	p value
Prostate-specific antigen level, ng/ml	1.02 (1.007–1.03)	0.001	59.7	1.02 (1–1.03)	0.005
Clinical stage	–	<0.001	67.9	–	<0.001
T2 vs T1	1.61 (0.79–3.24)	0.182		1.53 (0.69–3.35)	0.29
T3 vs T1	5.93 (2.94–11.94)	<0.001		4.36 (1.97–9.64)	<0.001
Primary Gleason grade					

≥4 vs ≤3	2.11 (1.46–3.04)	<0.001	61	1.72 (1.14–2.6)	0.009
Secondary Gleason grade					
≥4 vs ≤3	1.24 (0.84–1.82)	0.265	54.2		
Percentage of positive cores, %	1.02 (1.01–1.03)	<0.001	68.6	1.02 (1.01-1.03)	<0.001

Table 5. Univariate and multivariate logistic regression analyses predicting the presence of lymph node invasion in ePLND+SNB group .

Covariates	Univariate analysis			Multivariate analysis	
	Odds ratio (95% CI)	p value	AUC (%)	Odds ratio (95% CI)	p value
Prostate-specific antigen level, ng/ml	1.01 (0.984–1.03)	0.442	53	-	-
Clinical stage	–	0.022	61	–	0.08
T2 vs T1	1.59 (0.60–4.21)	0.182		1.39 (0.49–3.94)	0.53
T3 vs T1	3.35 (1.23–9.13)	0.018		2.75 (0.93–8.09)	0.066
Primary Gleason grade					
≥4 vs ≤3	3.22 (1.74–6.02)	<0.001	64.2	3.5 (1.8–6.7)	<0.001
Secondary Gleason grade					
≥4 vs ≤3	0.58 (0.31–1.09)	0.092	49.9	-	-
Percentage of positive cores, %	1.02 (1–1.03)	0.001	64.4	1.02 (1-1.03)	0.001

Table 6. Univariate and multivariate logistic regression analyses predicting the presence of lymph node invasion in sLND group.					
Covariates	Univariate analysis			Multivariate analysis	
	Odds ratio (95% CI)	p value	AUC (%)	Odds ratio (95% CI)	p value
Prostate-specific antigen level, ng/ml	1.02 (1.002–1.028)	0.022	54.9	1.002 (0.986–1.02)	0.837
Clinical stage	–	0.017	58.8	–	0.064
T2 vs T1	1.61 (0.26–15.49)	0.679		1.45 (0.78–2.66)	0.809
T3 vs T1	4.51 (0.51–39.55)	0.033		3.55 (1.9–6.62)	0.248
Primary Gleason grade					
≥4 vs ≤3	2.39 (1.38–4.13)	0.002	60.7	2.10 (1.09–4.30)	0.025
Secondary Gleason grade					
≥4 vs ≤3	1.10 (0.57–2.1)	0.651	51.3		
Percentage of positive cores, %	1.02 (1.01–1.03)	<0.001	66.9	1.02 (1.008-1.033)	0.001

Nomograms performance

It is interesting that although the Briganti and Winter nomograms use the same parameters, Briganti stresses more on PSA and clinical stage while Winter more on Gleason score, in particular secondary Gleason score. The performance of the Winter nomogram (Fig. 1) was reasonably accurate in ePLND group (AUC: 0.746) and comparable to Briganti and MSKSCC

nomogram (AUC: 0.756 and 0.744, respectively). In this group, the HL test showed good fit for Winter (P: 0.86) that was better than for the Briganti (P: 0.169) and MSKCC (P: 0.065) nomograms. In both the ePLND+SNB and sLND group (Fig. 2-3) the Winter nomogram also had better predictive ability (AUC: 0.735 and 0.709, respectively) compared to Briganti (AUC: 0.725 and 0.707, respectively) and MSKCC nomogram (AUC: 0.73 and 0.676, respectively). In the ePLND+SNB group, the HL test showed good fit for the Winter nomogram (P: 0.808), which was better than for Briganti (P: 0.705) and MSKCC (P: 0.619). In sLND patients, the result of the HL test was not significant only for Winter nomogram (P: 0.076) while Briganti and MSKCC didn't fit well in this population (P: 0.007 and P: 0.030, respectively). Based on AUC, the Winter nomogram was performing better in low grade tumors (Gleason score ≤ 7) in both the ePLND+SNB and sLND groups compared to high grade (Gleason score ≥ 8) tumors (0.706 vs 0.698 and 0.756 vs 0.607) while in ePLND similar results were shown (0.742 vs 0.743).

In the calibration plots, all nomograms showed good performance in the low/intermediate risk patients while in the high risk population an overestimation of the risk for LNI was observed in all groups (Fig. 4A-C). Similar to the results of ROC analysis, Slope and intercept values of Winter nomogram were better for ePLND+SNB and sLND groups (0.66/1.22 and 0.63/1.37, respectively) compared to ePLND (0.44/-0.45). Compared to the Briganti and MSKCC nomograms, the Winter nomogram had a lower absolute error in all groups. In the decision curve analysis Winter nomogram showed a better clinical net benefit in the higher thresholds in sLND group, while it performed similar to the other two nomograms in the ePLND and ePLND+SNB groups (Fig. 5A-C).

We also calculated the cutoffs for the nomograms to help the clinician with the decision of when to spare ePLND. The cutoff with the best tradeoff between ePLND omission and missing LNI for the Winter nomogram was 15%, leaving 9 patients (6.6% of all LNI positive) with LNI undetected and avoiding LND in 23 % of all patients. For the Briganti nomogram, the best cutoff was 4%, leaving 6 patients (4.4%) with LNI undetected and avoiding LND in 22% of all patients. For the MSKCC the best cut-off was 6%, leaving 12 patients (8.8%) with LNI undetected and avoiding LND in 28 % of all patients.

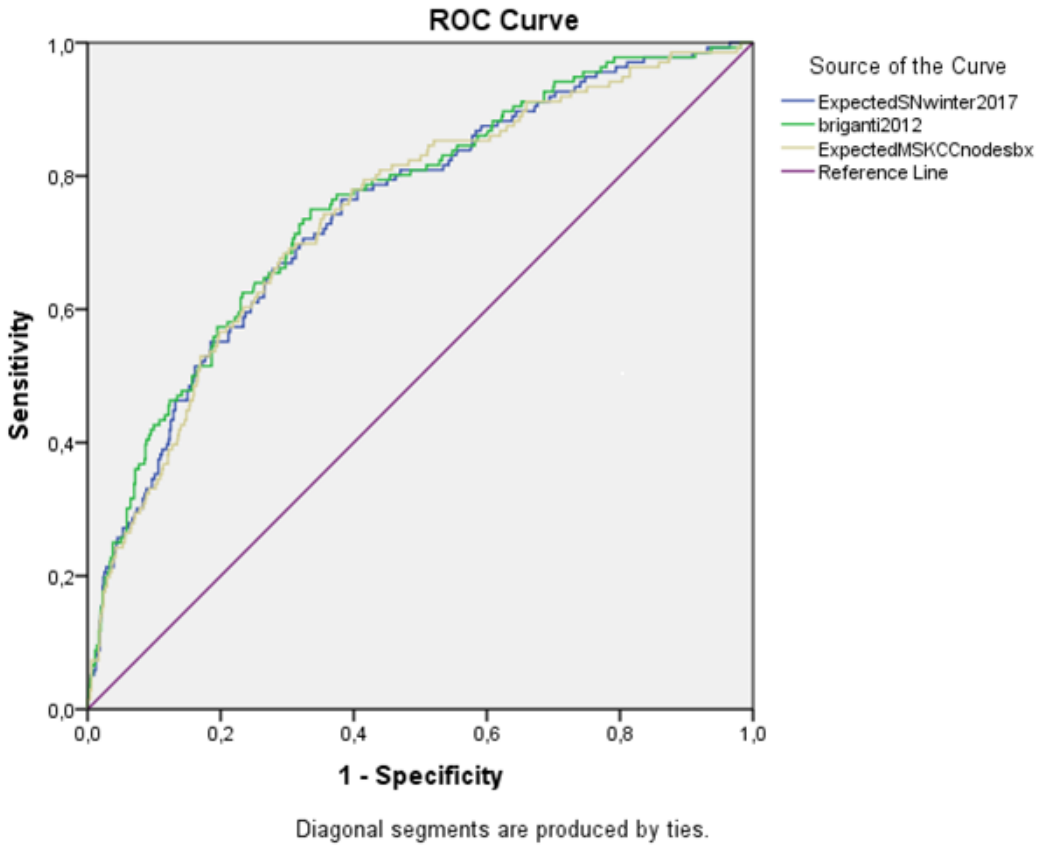

Fig. 1. Validation of the three nomograms for ePLND group using the receiver operating characteristic (ROC) curve. The area under the ROC curve (AUC) was 0.746 (95% CI, 0.70–0.791), 0.756 (95% CI, 0.71-0.80) and 0.744 (95% CI, 0.69-0.79) for Winter, Briganti and MSKCC nomogram, respectively.

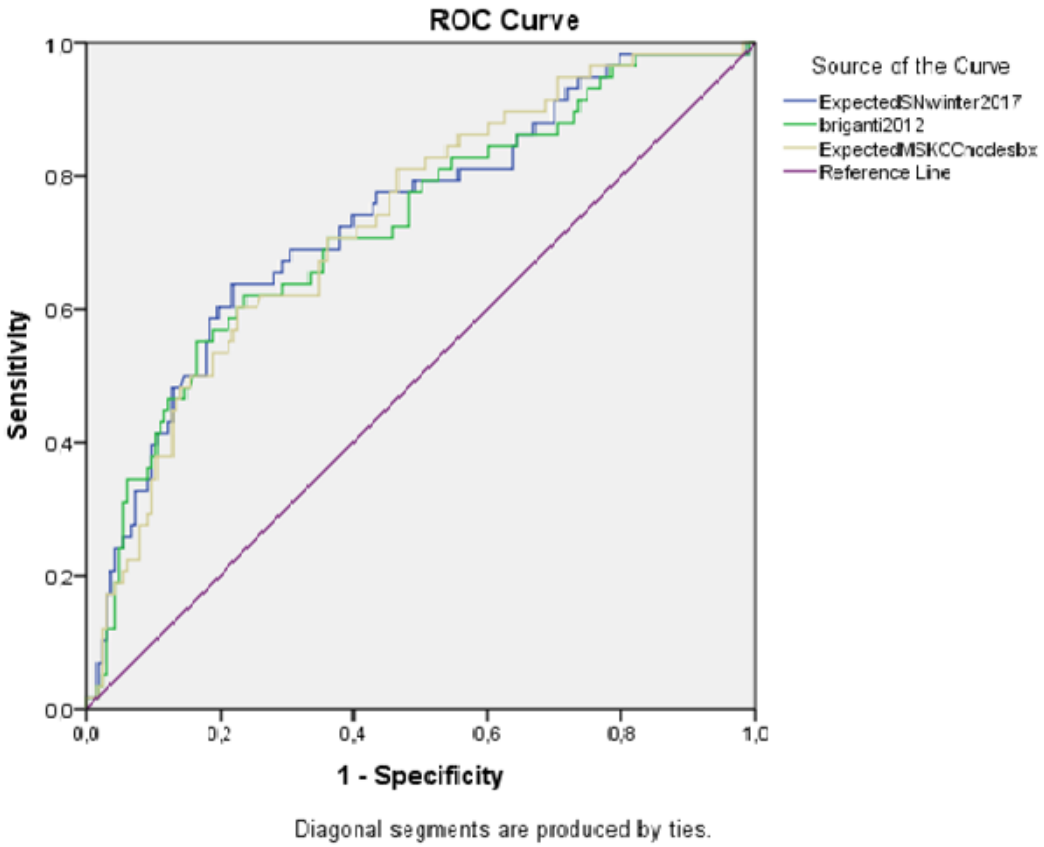

Fig. 2. Validation of the three nomograms for ePLND+SNB group using the receiver operating characteristic (ROC) curve. The area under the ROC curve (AUC) was 0.735 (95% CI, 0.65–0.81), 0.725 (95% CI, 0.64-0.80) and 0.730 (95% CI, 0.65-0.80) for Winter, Briganti and MSKCC nomogram, respectively.

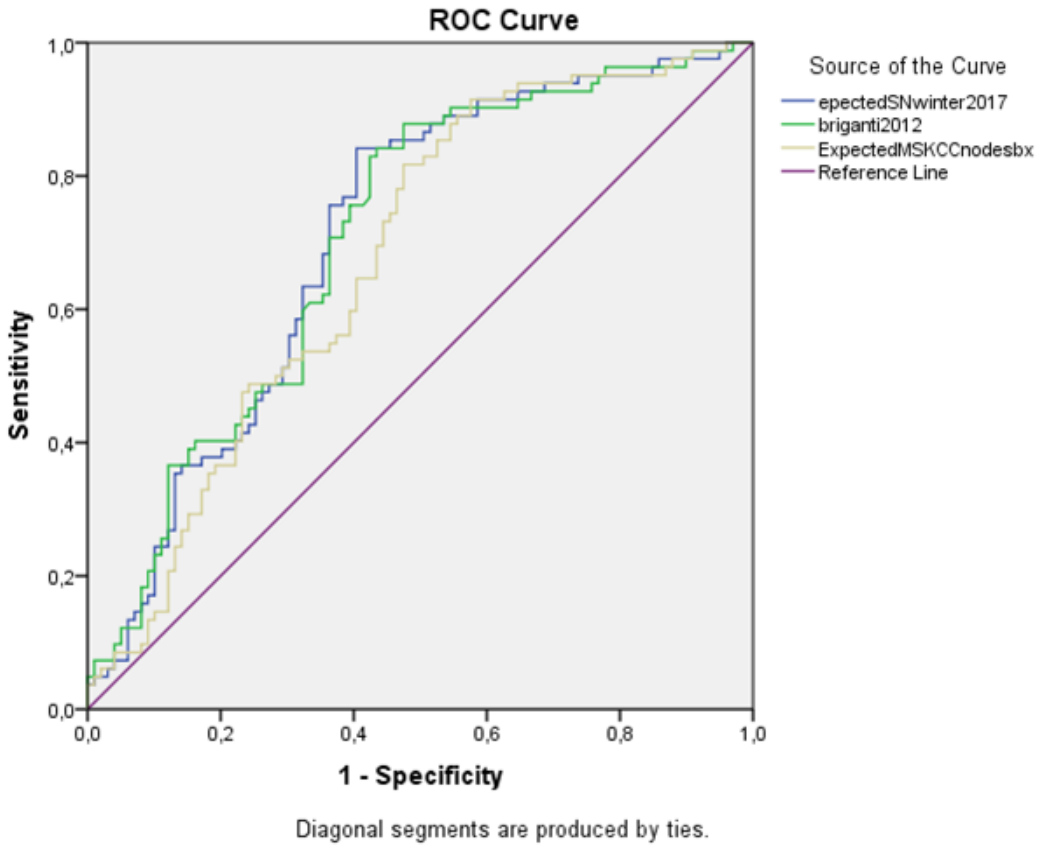

Fig. 3. Validation of the three nomograms for sLND group using the receiver operating characteristic (ROC) curve. The area under the ROC curve (AUC) was 0.709 (95% CI, 0.63–0.78), 0.707 (95% CI, 0.63-0.78) and 0.676 (95% CI, 0.59-0.75) for Winter, Briganti and MSKCC nomogram, respectively.

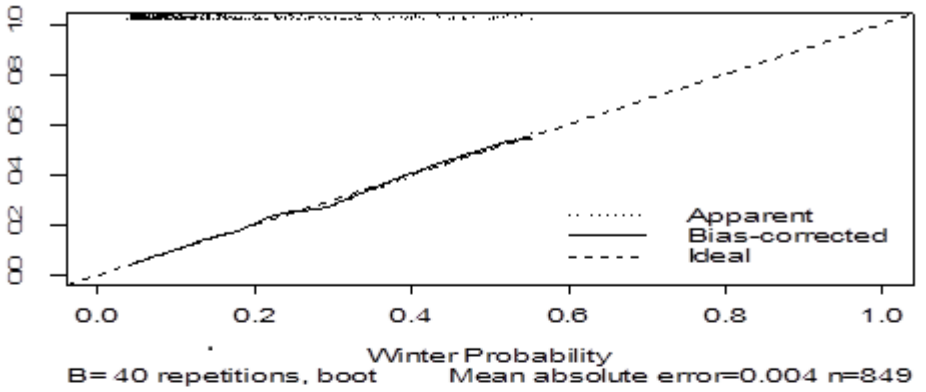

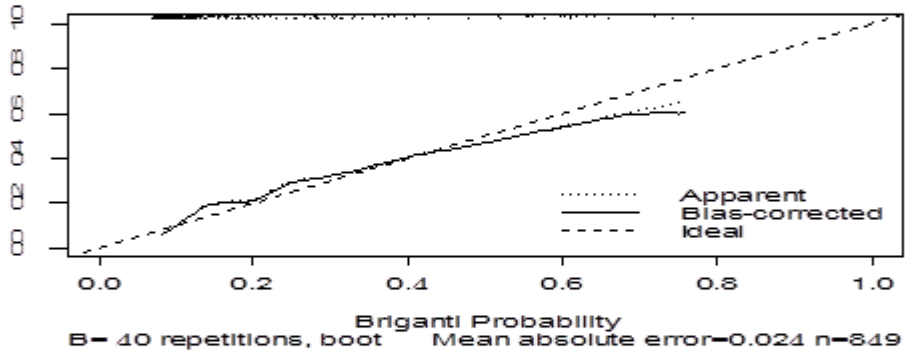

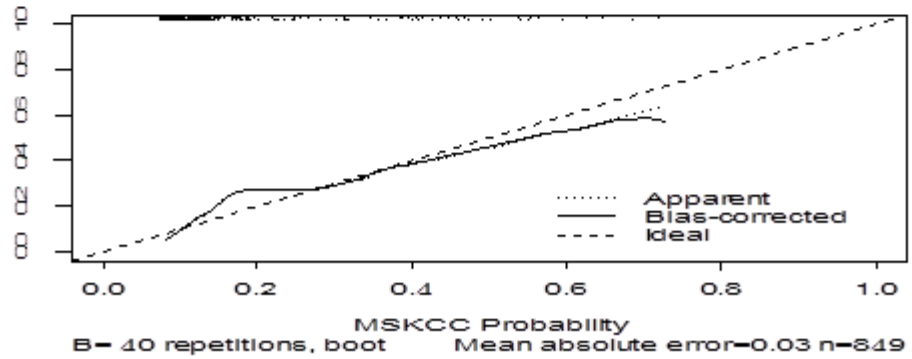

Fig. 4A. Nomograms calibration plot for ePLND group. The dotted plot indicates the location of the ideal nomogram, in which actual and predicted probabilities are identical. Expected performance on future data represented through the solid line.

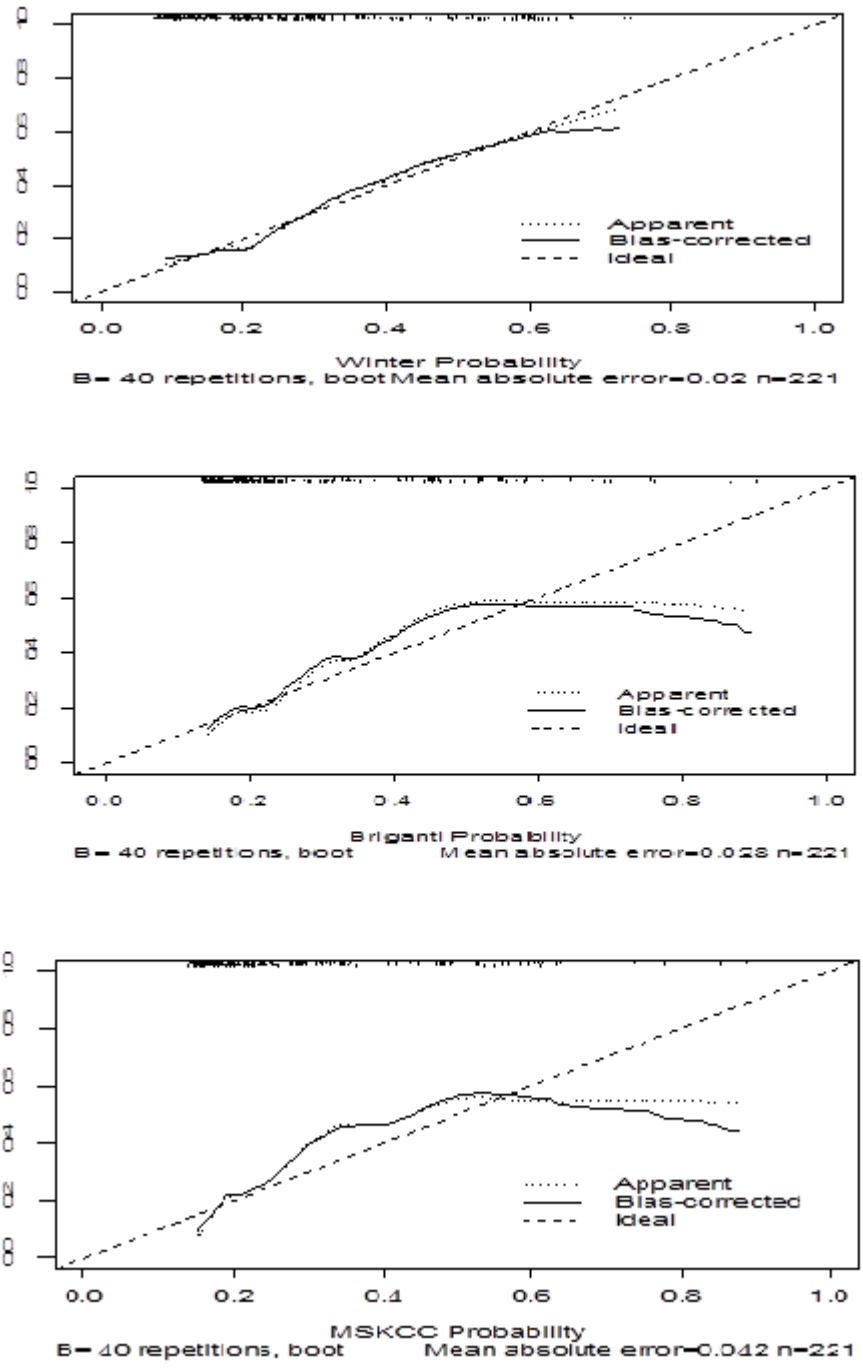

Fig. 4B. Nomograms calibration plot for ePLND+SNB group. The dotted plot indicates the location of the ideal nomogram, in which actual and predicted probabilities are identical. Expected performance on future data represented through the solid line.

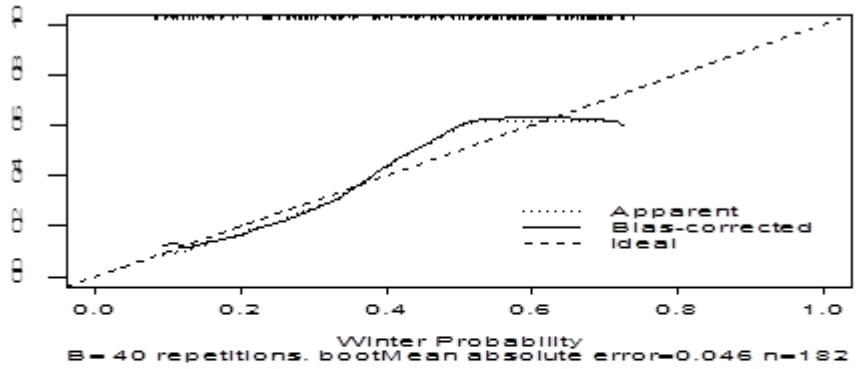

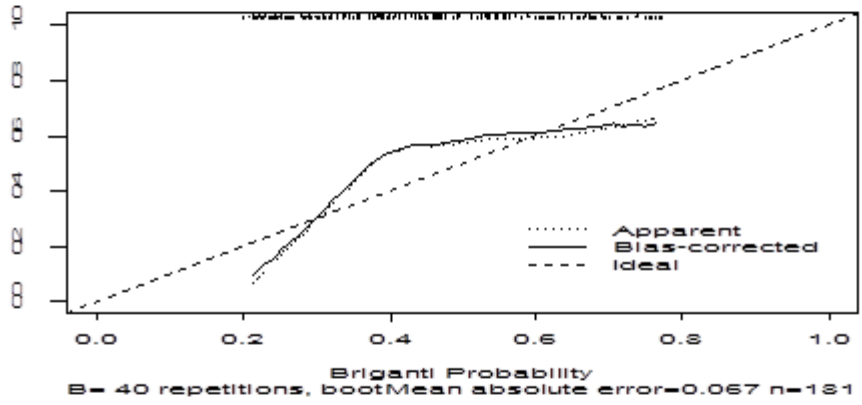

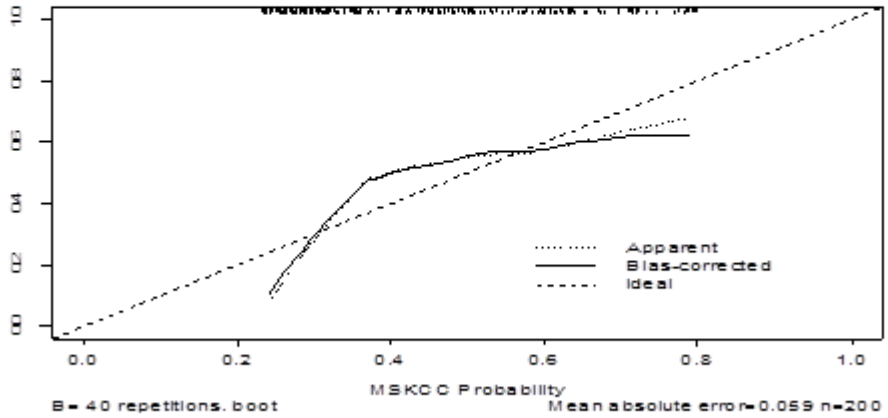

Fig. 4C. Nomograms calibration plot for sLND group. The dotted plot indicates the location of the ideal nomogram, in which actual and predicted probabilities

are identical. Expected performance on future data represented through the solid line.

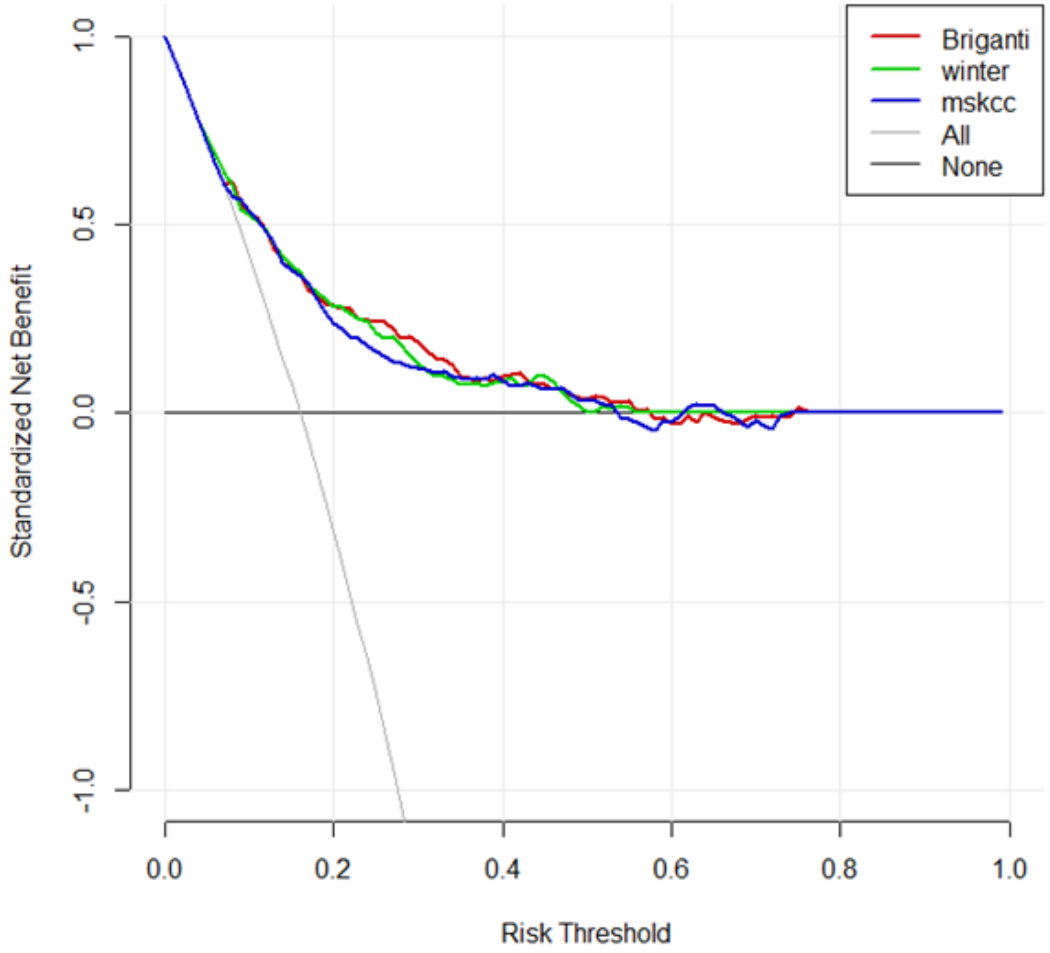

Fig. 5A. Decision curve analyses demonstrating the net benefit associated with the use of the three nomograms in ePLND group.

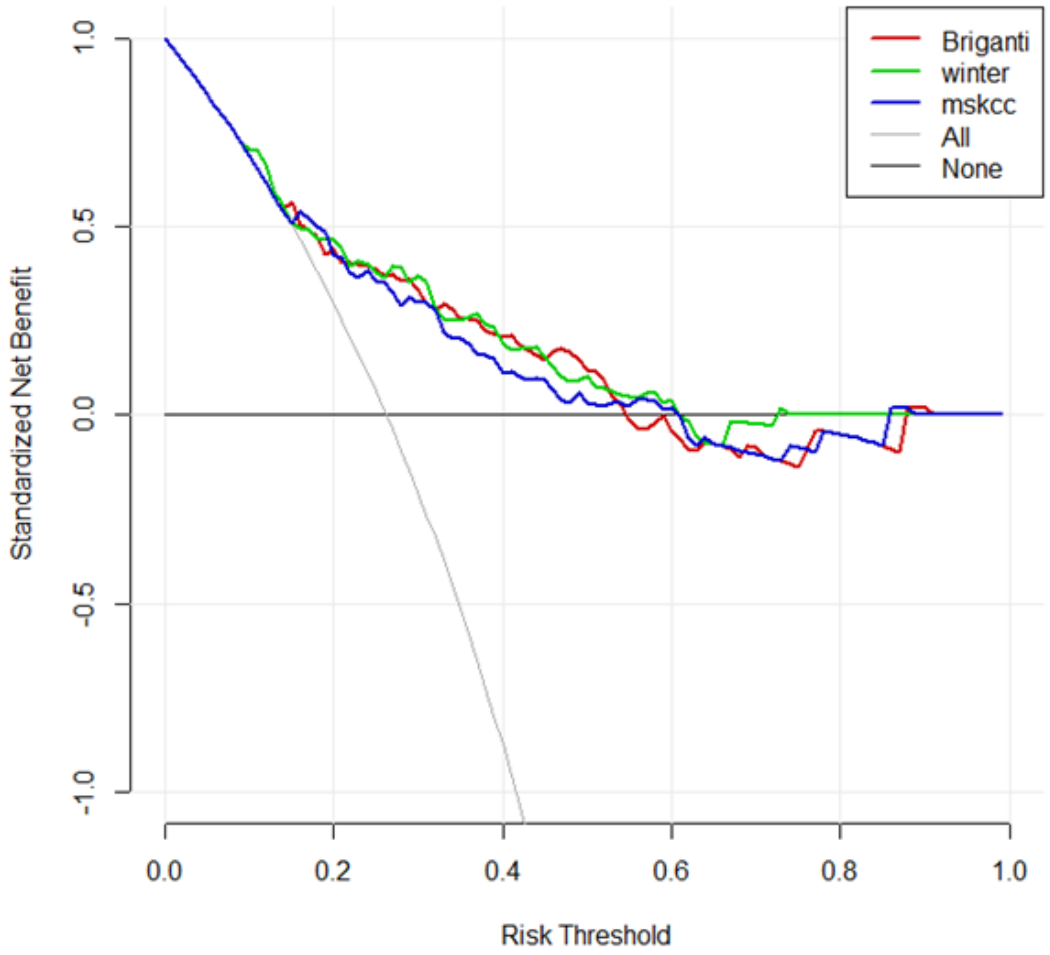

Fig. 5B. Decision curve analyses demonstrating the net benefit associated with the use of the three nomograms in ePLND+SNB group.

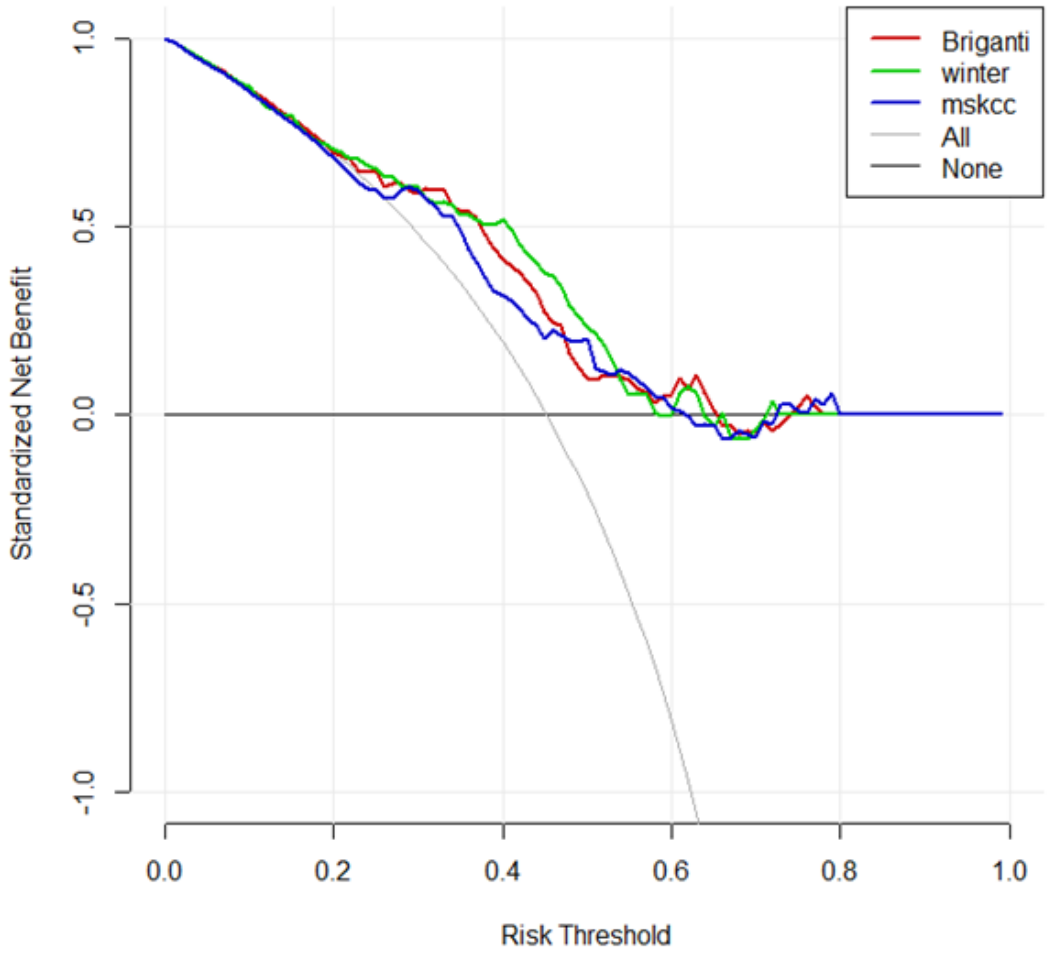

Fig. 5C. Decision curve analyses demonstrating the net benefit associated with the use of the three nomograms in sLND group.

Discussion

Prior to suggesting the use of a nomogram in the everyday clinical practice, a formal external validation is required in the local population, even in the presence of previous external validations in other populations (12, 27).

Therefore, we decided to perform the first external validation of the updated version of the only existing SN based nomogram and compare its performance with the Briganti and MSKCC nomogram, using accuracy and calibration tests. To address this topic, we used a large contemporary cohort of men treated with RARP and ePLND±SNB and a cohort of men treated with EBRT+sLND.

Although Briganti et al. (11) in their updated publication have reported that all LNI prediction models should be based on ePLND series, a recent meta-analysis has shown that SNB has diagnostic accuracy comparable to ePLND, with high sensitivity (95.2%), specificity (100%), positive (100%) and negative (98%) predictive value and low false positive (0%) and negative rate (4.8%) (20). In addition an increase in nodal yield was shown when combining ePLND with SNB by increasing the detection rate of affected nodes. Joniau et al. have also suggested that the sentinel approach allows an individualized extension of LN dissection outside the boarders of ePLND (6). Our discrimination results showed that the updated Winter nomogram performed as well as the Briganti and MSKCC nomogram in ePLND group while it outperformed both nomograms in the two SN groups. This is a significant observation because it's the first time shown that a SN based nomogram is as accurate or even better than nomograms based on ePLND. The value of the inclusion of the percentage of positive core in the updated nomogram was also confirmed from the regression analysis in our cohort, in accordance with previous studies supporting the role of percentage of positive cores as the foremost predictor of LNI (8, 27).

Our RARP-based study has demonstrated a high predictive accuracy for the Briganti nomogram (AUC=0.756) in ePLND group, in accordance to the original publication (AUC=0.76) of the updated nomogram (11). Dell'Oglio et al. were the only who reported a validation of Briganti nomogram based also on robot-assisted ePLND, reporting also a good accuracy (AUC= 0.818) (17). All other studies validated the updated Briganti nomogram performing open ePLND, showing also high predictive ability (AUC: 0.76-0.82) (13-16).

There is no consensus on the ideal cut-off level for the avoidance of ePLND in PCa. The National Comprehensive Cancer Network suggests the cut-off of 2%

which avoids 47.7% of the ePLNDs at the expense of 12.1% of the cases remaining with LNI (28). The use of the 5% cutoff for Briganti nomogram would allow the avoidance of ePLND in about 65% at the cost of missing 12% of patients with LNI (11). In our cohort, the optimal cutoff for the Briganti nomogram was relatively similar (6%) resulting though in the avoidance of ePLND in a smaller number (33%) of patients at the cost of missing 10% of patients with LNI. However, such differences have been observed also in other validation studies, especially the one which was based on robot-assisted lymphadenectomy (17), and could be attributed to the different baseline characteristics of the included populations and especially to the lower mean number of LNs removed in our ePLND group (10 versus 20.8 in the updated Briganti publication). A lower number (median: 6) of removed LNs were also reported from Abdollah et al. in their recent nomogram for predicting LNI after RARP (29). Moreover, variability in surgical technique and expertise as well as in the pathologic evaluation may contribute to differences in the number of lymph nodes removed and examined (11, 30). In addition, there are publications suggesting that RARP is considered to negatively influence the extent of lymph node dissection (31).

Winter et al. in their original nomogram suggested a 7% cutoff, avoiding sLND in 31.3% of the patients and missing 3% of all LNI. In our cohort the optimal cutoff for the updated Winter nomogram with the best trade-off between ePLND omission and missing LNI was 15%, leaving 6.6% of all LNI patients with LNI undetected and avoiding LND in 23% of all patients. Godoy et al. from MSKCC (9) proposed a 6% cut-off in their nomogram based on clinical stage, PSA and sum Gleason score. Our cut-off for the MSKCC-LNI-cores nomogram (including PSA, clinical stage, primary and secondary Gleason grade and the percentage of positive cores) was also 6%, leaving 12 patients (8.8%) with LNI undetected and avoiding LNI in 28 % of all patients.

An interesting observation is that Winter nomogram is performing worse in high grade tumors (Gleason score ≥ 8), in accordance to previous reports showing poorer outcomes of SNB in highly aggressive tumors (32). An overestimation of LNI risk was also observed in the prediction of Winter nomogram in our high risk patients. This could be attributed to differences between the two validation

cohorts, indicated also from the observation that primary Gleason grade and the percentage of positive cores were the only independent predictors of LNI in all of our groups, while in Winters' cohort PSA, clinical stage and secondary Gleason grade were additional predictors. Another explanation could be the different SN technique applied; open vs robot assisted, and the additional usage of ICG in our population. On the other hand, our calibration analysis demonstrated also that the SN based nomogram performed better in low/intermediate risk patients. This observation is in accordance to the results from the meta-analysis from Wit et al (20). It is suggested that in these patient groups, the SN is often the only tumor-bearing node, and therefore the application of SNB is encouraged mostly in these lower risk patients (12). On the other hand, an overestimation was observed in the prediction of Winter nomogram in high risk patients. Winters nomogram was based on open lymphadenectomy which could affect the SN detection/removal rate. Moreover, patients with high-risk disease could be false-negative or could have both positive SNs and positive non-SNs (33). In conclusion, in high-risk disease SNB should be combined with ePLND. The addition of the percentage of cancer involvement in the prostate cores as well as the percentage of high-grade disease, and the presence of perineural invasion could increase the accuracy of LNI predictions in future nomograms (12).

Limitations

The limitations of this study include those inherent to a retrospective review of prospectively collected data and the selection bias associated with a surgical series from a single institution. The data depend on factors such as the extent of thorough lymph node dissection within the template and complexities of tissue handling and threshold capabilities for histologic detection of nodal metastases. Moreover, the number of dissected SNs were not available. The favorable discrimination of Winter nomogram observed with HL test is limited from the low statistical power of this test, since HL does not properly take into account overfitting and it is arbitrary to bins choice and computing method (34). Finally, all patients underwent robot assisted laparoscopic ePLND and sLND,

while the patients in the nomogram-developing studies underwent open lymph node dissection (either extended or SN guided) which, as previously explained, could have an impact on the number of removed and histologically positive LNs.

Conclusions

Our study gives evidence that the concept of a SN based nomogram is successful, because it provides comparative predictions relative to the ePLND models and superior predictions when SNB is performed. Probably, patients who benefit most from the nomogram would be those with a low/intermediate risk of LN metastasis. In high-risk patients SNB should be combined with ePLND. Future studies are needed to explore if potential benefits result also in equivalent or improved oncologic outcomes.

References

1. Budäus L, Leyh-Bannurah SR, Salomon G, Michl U, Heinzer H, Huland H, et al. Initial Experience of (68)Ga-PSMA PET/CT Imaging in High-risk Prostate Cancer Patients Prior to Radical Prostatectomy. Eur Urol. 2016;69(3):393-6.
2. Briganti A, Chun FK, Salonia A, Zanni G, Scattoni V, Valiquette L, et al. Validation of a nomogram predicting the probability of lymph node invasion among patients undergoing radical prostatectomy and an extended pelvic lymphadenectomy. Eur Urol. 2006;49(6):1019-26; discussion 1026-7.
3. Touijer K, Rabbani F, Otero JR, Secin FP, Eastham JA, Scardino PT, et al. Standard versus limited pelvic lymph node dissection for prostate cancer in patients with a predicted probability of nodal metastasis greater than 1%. J Urol. 2007;178(1):120-4.
4. Mottet N, Bellmunt J, Bolla M, Briers E, Cumberbatch MG, De Santis M, et al. EAU-ESTRO-SIOG Guidelines on Prostate Cancer. Part 1: Screening, Diagnosis, and Local Treatment with Curative Intent. Eur Urol. 2017;71(4):618-629.
5. Fossati N, Willemse PM, Van den Broeck T, van den Bergh RC, Yuan CY, Briers E, et al. The Benefits and Harms of Different Extents of Lymph Node Dissection During Radical Prostatectomy for Prostate Cancer: A Systematic Review. Eur Urol. 2017;72(1):84-109.
6. Joniau S, Van den Bergh L, Lerut E, Deroose CM, Haustermans K, Oyen R, et al. Mapping of pelvic lymph node metastases in prostate cancer. Eur Urol. 2013;63(3):450-8.
7. Briganti A, Blute ML, Eastham JH, Graefen M, Heidenreich A, Karnes JR, et al. Pelvic lymph node dissection in prostate cancer. Eur Urol. 2009;55(6):1251-65.
8. Briganti A, Karakiewicz PI, Chun FK, Gallina A, Salonia A, Zanni G, et al. Percentage of positive biopsy cores can improve the ability to predict lymph node invasion in patients undergoing radical prostatectomy and extended pelvic lymph node dissection. Eur Urol. 2007;51(6):1573-81.

9. Godoy G, Chong KT, Cronin A, Vickers A, Laudone V, Touijer K, et al. Extent of pelvic lymph node dissection and the impact of standard template dissection on nomogram prediction of lymph node involvement. Eur Urol. 2011;60(2):195-201.
10. Heidenreich A, Pfister D, Thüer D, Brehmer B. Percentage of positive biopsies predicts lymph node involvement in men with low-risk prostate cancer undergoing radical prostatectomy and extended pelvic lymphadenectomy. BJU Int. 2011;107(2):220-5.
11. Briganti A, Larcher A, Abdollah F, Capitanio U, Gallina A, Suardi N, et al. Updated nomogram predicting lymph node invasion in patients with prostate cancer undergoing extended pelvic lymph node dissection: the essential importance of percentage of positive cores. Eur Urol. 2012;61(3):480-7.
12. Shariat SF, Karakiewicz PI, Suardi N, Kattan MW. Comparison of nomograms with other methods for predicting outcomes in prostate cancer: a critical analysis of the literature. Clin Cancer Res. 2008;14(14):4400-7.
13. Schmitges J, Karakiewicz PI, Sun M, Abdollah F, Budäus L, Isbarn H, et al. Predicting the risk of lymph node invasion during radical prostatectomy using the European Association of Urology guideline nomogram: a validation study. Eur J Surg Oncol. 2012;38(7):624-9.
14. Hansen J, Rink M, Bianchi M, Kluth LA, Tian Z, Ahyai SA, et al. External validation of the updated Briganti nomogram to predict lymph node invasion in prostate cancer patients undergoing extended lymph node dissection. Prostate. 2013;73(2):211-8.
15. Gacci M, Schiavina R, Lanciotti M, Masieri L, Serni S, Vagnoni V, et al. External validation of the updated nomogram predicting lymph node invasion in patients with prostate cancer undergoing extended pelvic lymph node dissection. Urol Int. 2013;90(3):277-82.
16. Winter A, Kneib T, Henke RP, Wawroschek F. Sentinel lymph node dissection in more than 1200 prostate cancer cases: rate and prediction of lymph node involvement depending on preoperative tumor characteristics. Int J Urol. 2014;21(1):58-63.

17. Dell'Oglio P, Abdollah F, Suardi N, Gallina A, Cucchiara V, Vizziello D, et al. External validation of the European association of urology recommendations for pelvic lymph node dissection in patients treated with robot-assisted radical prostatectomy. J Endourol. 2014;28(4):416-23.
18. Schubert T, Uphoff J, Henke RP, Wawroschek F, Winter A. Reliability of radioisotope-guided sentinel lymph node biopsy in penile cancer: verification in consideration of the European guidelines. BMC Urol. 2015;15:98.
19. van der Poel HG, Meershoek P, Grivas N, KleinJan G, van Leeuwen FW, Horenblas S. Sentinel node biopsy and lymphatic mapping in penile and prostate cancer. Urologe A. 2017;56(1):13-17.
20. Wit EM, Acar C, Grivas N, Yuan C, Horenblas S, Liedberg F, et al. Sentinel Node Procedure in Prostate Cancer: A Systematic Review to Assess Diagnostic Accuracy. Eur Urol. 2017;71(4):596-605.
21. KleinJan GH, van den Berg NS, Brouwer OR, de Jong J, Acar C, Wit EM, et al. Optimisation of fluorescence guidance during robot-assisted laparoscopic sentinel node biopsy for prostate cancer. Eur Urol. 2014;66(6):991-8.
22. Acar C, Kleinjan GH, van den Berg NS, Wit EM, van Leeuwen FW, van der Poel HG. Advances in sentinel node dissection in prostate cancer from a technical perspective. Int J Urol. 2015;22(10):898-909.
23. Winter A, Kneib T, Rohde M, Henke RP, Wawroschek F. First Nomogram Predicting the Probability of Lymph Node Involvement in Prostate Cancer Patients Undergoing Radioisotope Guided Sentinel Lymph Node Dissection. Urol Int. 2015;95(4):422-8.
24. Winter A, Kneib T, Rohde M, Henke R, Wawroschek F. Updated nomogram predicting lymph node involvement in prostate cancer patients undergoing radioisotope guided sentinel lymphadenectomy: Percentage of positive cores represents the leading predictor. Submitted in Journal of Cancer.
25. Memorial Sloan Kettering Cancer Center. Prostate Cancer Nomograms Pre-Radical Prostatectomy. Available at:

https://www.mskcc.org/nomograms/prostate/pre-op/coefficients. Accessed December 20, 2016.

26. Grivas N, Wit E, Pos F, de Jong J, Vegt E, Bex A, et al. Sentinel Lymph Node Dissection to Select Clinically Node-negative Prostate Cancer Patients for Pelvic Radiation Therapy: Effect on Biochemical Recurrence and Systemic Progression. Int J Radiat Oncol Biol Phys. 2017;97(2):347-354.
27. Kattan MW. Factors affecting the accuracy of prediction models limit the comparison of rival prediction models when applied to separate data sets. Eur Urol. 2011;59(4):566-7.
28. Mohler J, Bahnson RR, Boston B, Busby JE, D'Amico A, Eastham JA, et al. NCCN clinical practice guidelines in oncology: prostate cancer. J Natl Compr Canc Netw. 2010;8(2):162-200.
29. Abdollah F, Klett DE, Sammon JD, Dalela D, Sood A, Hsu L, et al. Predicting lymph node invasion in patients treated with robot-assisted radical prostatectomy. Can J Urol. 2016;23(1):8141-50.
30. Briganti A, Capitanio U, Chun FK, Gallina A, Suardi N, Salonia A, et al. Impact of surgical volume on the rate of lymph node metastases in patients undergoing radical prostatectomy and extended pelvic lymph node dissection for clinically localized prostate cancer. Eur Urol. 2008;54(4):794-802.
31. Briganti A, Bianchi M, Sun M, Suardi N, Gallina A, Abdollah F, et al. Impact of the introduction of a robotic training programme on prostate cancer stage migration at a single tertiary referral centre. BJU Int. 2013;111(8):1222-30.
32. Holl G, Dorn R, Wengenmair H, Weckermann D, Sciuk J. Validation of sentinel lymph node dissection in prostate cancer: experience in more than 2,000 patients. Eur J Nucl Med Mol Imaging. 2009;36(9):1377-82.
33. Weckermann D, Dorn R, Holl G, Wagner T, Harzmann R. Limitations of radioguided surgery in high-risk prostate cancer. Eur Urol. 2007;51(6):1549-56.
34. Bertolini G, D'Amico R, Nardi D, Tinazzi A, Apolone G. One model, several results: the paradox of the Hosmer-Lemeshow goodness-of-fit

test for the logistic regression model. J Epidemiol Biostat. 2000;5(4):251-3.

Part II

MRI and primary diagnosis of prostate cancer, "more than detecting extracapsular growth"

5

Seminal vesicle invasion on multi-parametric magnetic resonance imaging: Correlation with histopathology.

Grivas N, Hinnen K, de Jong J, Heemsbergen W, Moonen L, Witteveen T, van der Poel H, Heijmink S.

Eur J Radiol. 2018 Jan;98:107-112.

Abstract

Objectives: The pre-treatment risk of seminal vesicle (SV) invasion (SVI) from prostate cancer is currently based on nomograms which include clinical stage (cT), Gleason score (GS) and prostate-specific antigen (PSA). The aim of our study was to evaluate the staging accuracy of 3tesla (3T) multi-parametric (mp) Magnetic Resonance Imaging (MRI) by comparing the imaging report of SVI with the tissue histopathology. The additional value in the existing prediction models and the role of radiologists' experience were also examined.

Methods: After obtaining institutional review board approval, we retrospectively reviewed clinico-pathological data from 527 patients who underwent a robot-assisted radical prostatectomy (RARP) between January 2012 and March 2015. Preoperative prostate imaging with an endorectal 3T-mp-MRI was performed in all patients. Sequences consisted of an axial pre-contrast T1 sequence, three orthogonally-oriented T2 sequences, axial diffusion weighted and dynamic contrast-enhanced sequences. We considered SVI in case of low-signal intensity in the SV on T2-weighted sequences or apparent mass while diffusion-weighted and DCE sequences were used to confirm findings on T2. Whole-mount section pathology was performed in all patients. The sensitivity, specificity, positive predictive value (PPV) and negative predictive value (NPV) of MRI (index test) for the prediction of histological SVI (reference standard) were calculated. We developed logistic multivariable regression models including: clinical variables (PSA, cT, percentage of involved cores/total cores, primary GS 4–5) and Partin table estimates. MRI results (negative/positive exam) were then added in the models and the multivariate modeling was reassessed. In order to assess the extent of SVI and the reason for mismatch with pathology an MRI-review from an expert genitourinary radiologist was performed in a subgroup of 379 patients.

Results: A total of 54 patients (10%) were found to have SVI on RARP-histopathology. In the overall cohort sensitivity, specificity, PPV and NPV for SVI detection on MRI were 75.9%, 94.7%, 62% and 97% respectively. Based on our sub-analysis, the radiologist's expertise improved the accuracy demonstrating a sensitivity, specificity, PPV and NPV of 85.4%, 95.6%, 70.0%

and 98.2%, respectively. In the multivariate analysis PSA (odds ratio [OR] 1.07, p = 0.008), primary GS 4 or 5 (OR 3.671, p = 0.007) and Partin estimates (OR 1.07, p = 0.023) were significant predictors of SVI. When MRI results were added to the analysis, a highly significant prediction of SVI was observed (OR 45.9, p < 0.0001). Comparing Partin, MRI and Partin with MRI predictive models, the areas under the curve were 0.837, 0.884 and 0.929, respectively.

Conclusions: MRI had high diagnostic accuracy for SVI on histopathology. It provided added diagnostic value to clinical/Partin based SVI-prediction models alone. A key factor is radiologist's experience, though no inter-observer variability could be examined due to the availability of a single expert radiologist.

Introduction

Accurate prostate cancer (PCa) staging is critical in guiding a patient's treatment decision and it could prevent both under- and overtreatment. In case of suspected extracapsular extension (ECE) or seminal vesicle (SV) invasion (SVI) patients are usually not offered a radical prostatectomy due to the risk of irradical resection while brachytherapy is not an option due to the risk of under-dosage to the SV. In patients with suspected SVI who are treated with external beam radiotherapy (EBRT) the radiation field is recommended to include the base of the seminal vesicles (1). However, this extended field will also increase the irradiated volume of rectal and bladder wall, affecting the complication rate as well.

Pre-treatment risk of SVI is currently based on prediction models, such as the Kattan nomogram (2) and the Partin tables (3). In addition, patients are stratified into risk-groups (4), according to the clinical T stage (cT), Gleason score (GS) and prostate-specific antigen (PSA). Local staging with multiparametric (mp)-Magnetic Resonance Imaging (MRI) has become widely available and provides new diagnostic means to assess the local extent of prostate tumours. In the literature a wide range of sensitivity and specificity (5) for the detection of SVI is reported, mainly attributed to differences in technique, such as MR field-strength, coil-type and variation in radiologist's' experience (6).

We hypothesized that with contemporary, state of the art, high-quality mp-MRI and an experienced, dedicated genito-urinary (GU) radiologist, SVI can be detected accurately. The aim of our study was to evaluate the staging accuracy of 3 tesla (3T) multi-parametric (mp) magnetic resonance imaging (MRI) by comparing the imaging report of SVI with the tissue histopathology. The additional value in the existing prediction models and the role of radiologists' experience were also examined.

Materials and Methods

Patient population

We performed a retrospective, single-institution cohort study. Institutional Review Board approval was obtained for the study, while the requirement for

informed consent was waived. Between January 2012 and March 2015, a total of 688 patients with biopsy-proven primary prostate PCa were treated with a Robot Assisted Radical Prostatectomy (RARP) using the da Vinci S(i) Surgical system (Intuitive Surgical Inc., Sunnyvale, CA,USA). After excluding 37 patients who did not have a preoperative MRI and 123 patients with MRIs performed in other hospitals, the final study population consisted of 527 patients. Information on pathology and radiology were retrospectively collected from the electronic patient information system (Ezis, Chipsoft, Amsterdam, the Netherlands). Patient clinical and pathological data were entered into a prospective database at the time of diagnosis.

MRI technique

All patients were pre-operatively staged with an endorectal coil mp- 3T MRI (Achieva, Philips). Sequences (Table 1) consisted of an axial pre-contrast T1 sequence, three orthogonally-oriented T2 sequences, axial diffusion weighted and dynamic contrast-enhanced (DCE) sequences (using Dotarem, Guebet, France). We considered SVI in case of low-signal intensity in the SV on T2-weighted sequences or apparent mass while diffusion-weighted and DCE sequences were used to confirm findings on T2 (Fig.1). Pre-contrast T1 images were used to exclude hematoma.

Table 1. MRI sequences.

	Axial T2	DWI	3D T1	DCE
TE (ms)	120	various	1.79	1.9
TR (ms)	4252	4931	3.6	4
FOV (mm)	200 x 281	256 x 256	280 x 445	260 x 260
Matrix	288 x 391	112 x 110	280 x 299	144 x 144
Slice thickness (mm)	3	3	0.84	3

B values	-	0, 200, 800	-	-
Duration	3min58s	3min12s	5min23s	4min56s

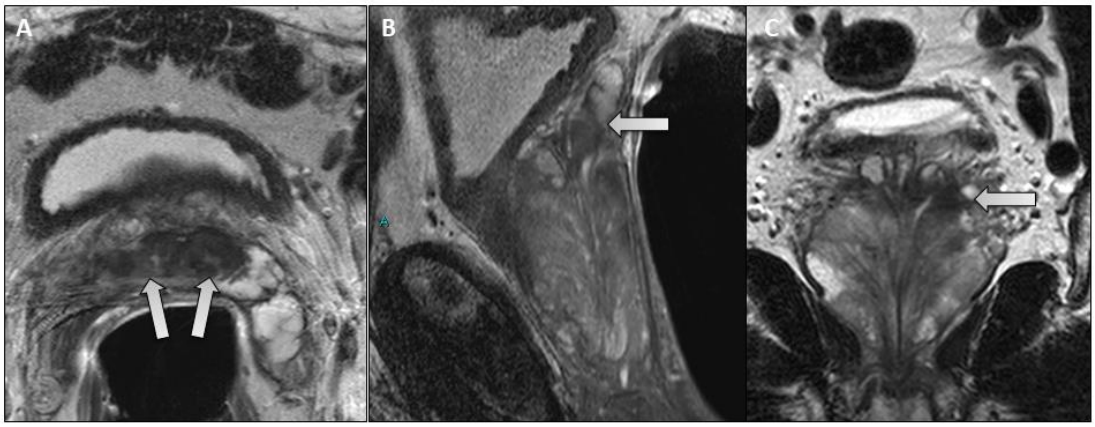

Fig. 1. Example of a true positive SVI MRI finding. A 63-year-old patient with PSA 29 ng/ml and 5/5 biopsies positive on the left side showing Gleason score 5+4 prostate cancer. On the preoperative 3T endorectal coil (ERC) MRI (A axial slice, B sagittal slice, C coronal slice) a hypointense lesion in the peripheral zone on the left side at the base of the prostate was observed invading both seminal vesicles (arrows, mT3b). Histopathology of the prostate specimen revealed a Gleason score 5+3 pT3bN0R0 prostate cancer.

At the time of inclusion, MRIs were reported by a number of different radiologists, with varying experience in GU imaging. However, the majority of

all scans (72%) were reported by one expert GU radiologist (SWH) with >10 years of experience in reporting prostate MRI.

Pathology analysis and staging

Whole-mount section pathology was performed in all patients. The base of the SV was available in all specimens. Staging was done according to the 2009 TNM classification for staging of prostate cancer (7) based on the cT, GS and PSA. SVI was defined as cancer invasion into the extraprostatic portion of the seminal vesicles (8). Risk group stratification was performed according to Ash et al. (4) into low risk (≤cT2a, GS: 6, PSA <10ng/ml), intermediate risk (cT2b–T2c, GS: 7, PSA 10–20ng/ml) and high risk (two or three intermediate risk-criteria and any combination of cT3, GS ≥8 or PSA >20ng/ml). Clinical characteristics were additionally entered into the most recent version of the Partin nomogram [9], based on patients treated from 2006 -2011.

Subgroup analyses

In order to assess the extent of SVI and the reason for mismatch with pathology, a subgroup analysis was performed based solely on the MRI-reports from an expert GU radiologist (SH). Another analysis was done based on the revision results of 77 pathology specimens from an expert GU pathologist (JdeJ). The extent of SVI on pathology revision was scored ranging from small to large based on an extension length of 1 cm as cut-off. Finally, we examined whether the seminal vesicle lesion showed continuous growth, originating from the prostate tumour.

Statistical analysis

Baseline descriptive statistics were used to present demographics, tumor and MRI data. Only patients with complete data were included in the analysis. Sensitivity, specificity, positive predictive value (PPV) and negative predictive value (NPV) of MRI (index test) for the diagnosis of histological SVI (reference standard) were calculated. We additionally developed logistic multivariable regression models including: clinical variables (PSA, cT, percentage of involved cores/total cores, primary GS 4–5) and Partin Table estimates. MRI results (negative/positive exam) were then added to the model and the multivariate modeling was reassessed. The predictive ability of each model was compared by receiver operating characteristic (ROC) curves based on the area under the curve (AUC) before and after the addition of MRI information to each model. In addition, a decision curve analysis was performed to evaluate and compare the net benefit for each model. A p value <0.05 was considered significant. Statistical analysis was performed using the statistical package of social sciences (SPSS) version 22.0 (SPSS, Chicago, IL) and the R statistical package (R Foundation for Statistical Computing, Vienna, Austria).

Results

Overall cohort

Patient's baseline clinical and pathological characteristics are presented in Table 2. 54 patients (10%) had SVI on pathology, whereas 67 patients (13%) were diagnosed with suspected SVI based on MRI. Based on the correlation of pre-operative MRI with pathology the sensitivity, specificity, PPV and NPV of MRI was 75.9%, 94.7%, 62% and 97%, respectively (Table 3).

Table 2. Patient's characteristics.	
Age, yr, median (IQR)	64(60-68)
PSA, ng/ml, median (IQR)	7.4 (5.3-12)
Biopsy Gleason Score, n (%)	
6	230 (43.6)

7	222 (42.1)
≥8	75 (14.3)
Percentage of positive/total cores, median (IQR)	25 (10-40)
Clinical stage (not based on MRI), n (%)	
≤T2	421 (79.9)
T3a	68 (12.9)
T3b	38 (7.2)
Risk classification, n (%)	
Low	79 (15)
Intermediate	139 (26.4)
High	309 (58.6)
Partin score, median (IQR)	9 (3-23)
MRI SVI, n (%)	
No	461 (87.5)
Yes	66 (12.5)
Pathological stage, n (%)	
≤T2	397 (75.3)
T3a	70 (13.3)
T3b	60 (11.4)
Pathological Gleason Score, n (%)	
6	139 (26.4)
7	313 (59.4)
≥8	75 (14.2)
Histological SVI, n (%)	
No	473 (89.8)
Yes	54 (10.2)

Table 3. Correlation of SVI on MRI with pathology.				
		Histological-SVI		Total
		Yes	No	
MRI-SVI	Yes	41	25	66
	No	13	448	461
Total		54	473	527

When stratifying patients into risk groups (Table 4), according to the MRI-cT stage, a strong correlation ($p < 0.0001$) was found between high risk prostate cancer and SVI, with only 3 (0.05%) patients in the low and intermediate risk groups having SVI. However, the high risk group consisted of 67% of all patients and therefore high risk as a diagnostic criterion would have a PPV of only 14.6%. Based on Partin risk stratification with a 15% cut-off risk of SVI, as most often used in clinical practice, 34.7% of all patients would have been included in the increased SVI risk group with a sensitivity, specificity, NPV and PPV of 83.3%, 70.8%, 24,6% and 97.4% for the clinical prediction.

Table 4. Histological SVI by risk group.				
		Histological-SVI		Total
		Yes	No	
Risk group	Low risk	1	23	24
	Intermediate risk	2	146	148
	High risk	51	299	350
Total		54	468	522

As shown in Table 5, in the multivariate analysis PSA, primary Gleason 4 or 5 and Partin estimates were significant predictors of SVI, with primary Gleason 4 or 5 being the strongest factor (odds ratio [OR] 3.671, $p = 0.007$). When MRI results were added in the analysis, they showed a significant association with the outcome (OR 45.9, 95% CI: 11.864-177.788, $p < 0.0001$). The combined MRI and Partin model outperformed individual models in the receiver-operating characteristic analysis (Fig. 2). Comparing Partin, MRI and Partin with MRI predictive models, the areas under the curve were 0.837, 0.884 and 0.929,

respectively (Table 6). In the decision curve analysis the combined Partin/MRI model showed a better clinical net benefit across all thresholds of probabilities (Fig. 3).

Table 5. Multivariate modeling analysis for predictors of histological SVI.

	Without MRI				With MRI			
Clinical variables	OR	95% CI		*p* value	OR	95% CI		*p* value
PSA	1.070	1.020	1.142	0.008	1.088	1.017	1.163	0.014
% core involvement	1.011	0.992	1.030	0.271	1.003	0.979	1.028	0.804
Age at surgery	1.064	0.982	1.154	0.129	1.062	0.963	1.172	0.226
cT	2.862	0.730	11.222	0.132	3.062	0.543	17.261	0.205
Primary GS 4/5	3.671	1.429	9.430	0.007	4.807	1.419	16.276	0.012
Partin SVI	1.070	1.009	1.134	0.023	1.114	1.041	1.194	0.002
MRI SVI result	—	—	—	—	45.925	11.864	177.778	<.0001

Table 6. AUCs for the prediction models of seminal vesical invasion.			
Model	AUC	95% CI	
Partin only	0.837	0.775	0.899
MRI only	0.884	0.82	0.947
Partin with MRI	0.929	0.876	0.981

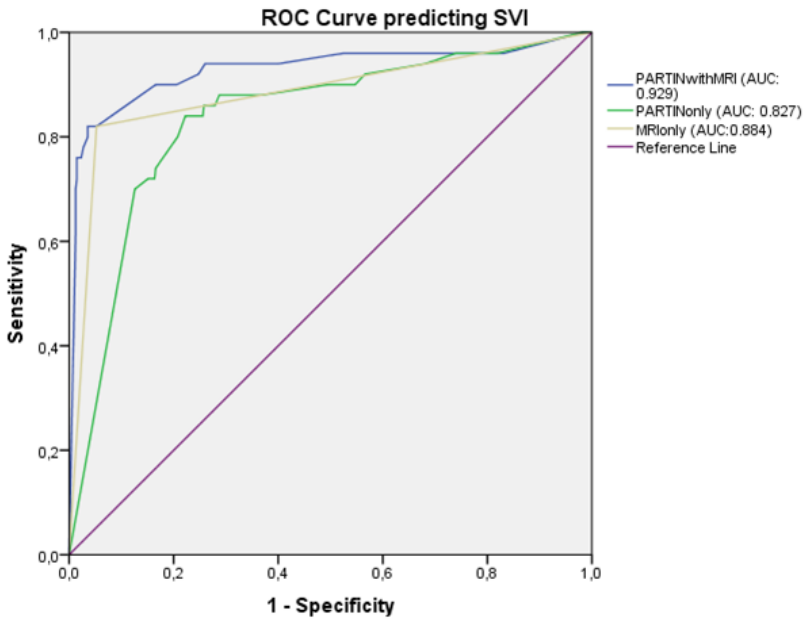

Fig.2. Receiver operating characteristic (ROC) curves for seminal vesicle invasion (SVI) prediction.

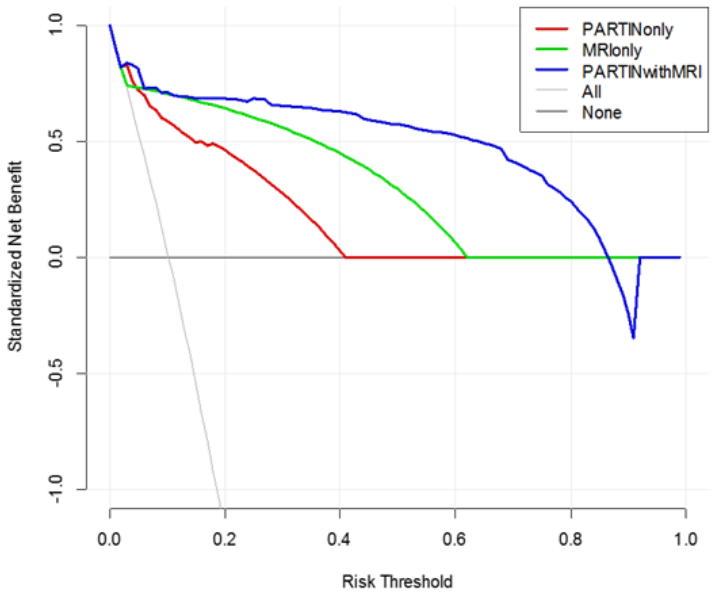

Fig. 3. Decision curve analyses demonstrating the net benefit associated with the use of the three predicting models.

Subgroup analyses

In 379 patients (72% of all patients) the MRI's results were assessed by our expert GU radiologist only. This increased the sensitivity, specificity, PPV and NPV to 84.4%, 95.6%, 70% and 98% respectively (Table 7). In the 6 patients in whom SVI was missed, 4 patients had a cT3a stage on MRI (6.4% of total cT3a patients) and again PSA and GS were not predictive of SVI. The pathology revision for these six patients further improved the sensitivity of MRI to 89.7%: two patients had invasion only in the intraprostatic region of the seminal vesicle while in one patient SVI consisted only of microscopic angioinvasive SVI growth (in absence of tumour mass). In two patients SVI was confined only to the base of the seminal vesicles and in one patient it extended beyond the base.

Table 7. Correlation of SVI on MRI with pathology based on a subanalysis from an expert radiologist.				
		Histological-SVI		
		Yes	No	Total
MRI-SVI	Yes	35	15	50
	No	6	323	329
Total		41	338	379

In 4/77 (5.2%) revised radical prostatectomy specimens the pathology report was modified: in 3 cases, initially considered SVI-positive, there was only marginal SVI in the intraprostatic region of the vesicles while in one case SVI was missed in the original examination. Revision showed that SVI follows a continuous spreading pattern originating from the prostate tumour into the vesicles in 94% of SVI cases. In only 38% of patients SVI was unilateral, and the extension score was high in 76% of the patients.

Discussion

To our knowledge, this is the largest study, comparing contemporary pre-operative state of the art mpMRI with SVI at histopathology. In our institution, patients treated with prostate EBRT undergo a routine prostate MRI prior to EBRT. In case of radiologic signs of SVI, the SVs are included in the target volume. In the absence of SVI signs, still most patients receive standard elective irradiation of the seminal vesicles because of the suggested risk of occult SVI, based on data mainly from the Partin Tables (9). In these patients the first 2 cm of the SVs are typically included into the clinical target volume as advised by Boehmer et al. (1). However, in the original Partin tables, no MRI was performed and therefore there was an increased risk of understaging. In our population the majority of SVI cases was diagnosed on MRI. Therefore, the Partin tables would overestimate the SVI risk for the remaining patients, who have no radiologic signs of SVI. Moreover, in the more recent updates of the Partin tables, only 3% of patients had proven pathologic SVI and the vast

majority of these patients had a T1c disease with GS=6 or GS=3+4 and PSA <10 ng/ml [9,10]. Therefore it is arguable whether these relatively low-risk patients can be used to model SVI risk in patients with a high to intermediate risk prostate tumour.

Part of the high accuracy may lie in the fact that the MRI was performed at a high field strength of 3T using an endorectal coil. Literature shows a broad range of accuracy for pre-operative mp 3T prostate MRI as reported by Otto et al (5), with sensitivities ranging between 50% and 100%. Furthermore, in a previous study by Gupta et al. the superiority of mp 3T MRI for the diagnosis of organ confinement compared to the Partin Tables was shown, with an area under the curve of 0.82 versus 0.62, respectively (11). However, this study didn't report specific predictive values for SVI.

The added value of MRI on Partin, CAPRA and clinical prediction models have been also shown by Morlacco et al. (12) reporting AUC values of 0.75 versus 0.82 for Partin and Partin + MRI predictive models, respectively while for CAPRA and CAPRA + MRI models, the AUC were 0.75 versus 0.83. In low risk cases the sensitivity of Partin tables for detecting SVI is comparable to that with MRI, although our expert radiologist attained a slightly better sensitivity. According to our analysis, if we would fully rely on Partin+MRI prediction we could spare SV irradiation in 84% of the patients while the corresponding percentage using Partin-only model is 27% (with a cut-off risk of SVI >15% in both models).

The strong relationship between SVI and other pre-operative clinical characteristics, such as ECE, has been reported from Wheeler et al. (13). This may be explained by similar pathologic mechanisms, showing tumor progression to invasive growth, whether in the form of SVI or ECE. A favorable diagnostic accuracy of MRI for ECE has been reported from recent studies (14, 15). In accordance to others we found that an experienced GU radiologist has a favorable impact on the diagnostic accuracy of SVI diagnosis (16-18). Tay et al. (15) has also reported that a dedicated radiologist can significantly improve the ECE prediction compared to a non-specialized radiologist (AUC: 0.91 vs 0.72]. Finally, a recent meta-analysis of 34 studies have showed that the use

of endorectal coil can improve the sensitivity (0.59 vs 0.51) and specificity (0.97 vs 0.94) of MRI for SVI detection (19).

For future investigations**,** it might be interesting to see whether mapping of the ECE location in respect to SVI, may improve this relationship. For instance, it seems plausible that ECE near the base of the prostate has a much stronger relationship with SVI than ECE at the apex. If this might be the case, perhaps a margin concept around the tumor, as seen on MRI, may further decrease the risk of undertreatment of occult SVI (20).

Limitations

Some limitations should be considered. We showed results from a single-center, retrospective cohort. Our study had a small sample size compared to the original Partin tables that consisted of more than 1000 patients and the updated versions that consisted of even more than 5000 patients (3,9). Moreover a selection bias is the fact that the pathology and MRI revisions were not available for our entire cohort.

EBRT treated patients were excluded in our analysis, due to lack of pathology confirmation. In order to apply our prediction model for EBRT patients management we should consider potential differences between EBRT and prostatectomy populations. There are distinct differences between patients that undergo a prostatectomy and patients that undergo EBRT, with generally higher stages and higher ages for the EBRT patients. Nonetheless, our cohort did contain a relatively large number of patients in the intermediate and high prostate cancer risk groups, most suitable for comparison with an EBRT population. It is known that the diagnostic accuracy of MRI for the detection of extraprostatic extension is higher for intermediate and high risk cases (21) while a sensitivity of 50% has been reported in low risk disease (22). Also, it is expected that mainly low-volume SVI is difficult to diagnose on MRI, because of only microscopic SVI and this type of SVI will be found more frequently in prostatectomy patients. In addition, the pathology specimen evaluation was limited to the first part of the seminal vesicles only. Therefore, we can’t formally

exclude invasion further up the seminal vesicles. However, SVI was seen in a continuous spreading pattern in 94% of our patients, with tumor originating from the prostate gland and extending into the seminal vesicles. In only 1 patient, SVI consisted of microscopic angioinvasive growth in the absence of tumor mass, in which case a non-continuous spreading pattern was seen. In a pathologic analysis by Kestin et al., SVI was limited to the first 2 cm's in 90% of patients with any SVI invasion, with only 1% risk of SVI beyond 2 cm in the total population (23).

Finally, due to the availability of a single expert GU radiologist, no interobserver variability could be examined. For these purposes a second validation in a comparable cohort with both mp 3T MRI and dedicated GU radiologists is warranted.

Conclusions

Endorectal mp-3T-MRI shows excellent prediction of SVI, especially when it is interpreted by an experienced GU radiologist. MRI information can provide an added value when compared with clinical-based, Partin Table models alone for the prediction of SVI.

References

1. D.Boehmer, P. Maingon, P. Poortmans, et al., Guidelines for primary radiotherapy of patients with prostate cancer, Radiother. Oncol. 79 (3) (2006) 259-269.

2. L. Wang, H. Hricak, M.W. Kattan, et al., Prediction of seminal vesicle invasion in prostate cancer: incremental value of adding endorectal MR imaging to the Kattan nomogram, Radiology. 242 (1) (2007) 182-188.

3. A.W. Partin, J. Yoo, H.B. Carter, et al., The use of prostate specific antigen, clinical stage and Gleason score to predict pathological stage in men with localized prostate cancer, J. Urol. 150 (1) (1993) 110-114.

4. D. Ash, A.Flynn, J. Battermann, et al., ESTRO/EAU/EORTC recommendations on permanent seed implantation for localized prostate cancer, Radiother. Oncol. 57 (3) (2000) 315-321.

5. J. Otto, G. Thörmer, M. Seiwerts, et al., Value of endorectal magnetic resonance imaging at 3T for the local staging of prostate cancer, Rofo. 186 (8) (2014) 795-802.

6. C.M. Hoeks, J.O. Barentsz, T. Hambrock, et al., Prostate cancer: multiparametric MR imaging for detection, localization, and staging, Radiology. 261 (1) (2011) 46-66.

7. L.H. Sobin, M. Gospodariwicz, C. Wittekind C, 7th Edition., TNM classification of malignant tumors. UICC International Union Against Cancer, Wiley-Blackwell, 2009, pp. 243-248.

8. D.M. Berney, T.M. Wheeler, D.J Grignon, et al. International Society of Urological Pathology (ISUP) Consensus Conference on Handling and Staging of Radical Prostatectomy Specimens. Working group 4: seminal vesicles and lymph nodes. Mod. Pathol. 24 (1) (2011) 39-47.

9. J.B. Eifler, Z. Feng, B.M. Lin, et al., An updated prostate cancer staging nomogram (Partin tables) based on cases from 2006 to 2011, BJU. Int. 111 (1) (2013) 22-29.

10. D.V. Makarov, B.J Trock, E.B. Humphreys, et al., Updated nomogram to predict pathologic stage of prostate cancer given prostate-specific antigen level, clinical stage, and biopsy Gleason score (Partin tables) based on cases from 2000 to 2005, Urology. 69 (6) (2007) 1095-1101.

11. R.T. Gupta, K.F. Faridi, A.A. Singh, et al., Comparing 3-T multiparametric MRI and the Partin tables to predict organ-confined prostate cancer after radical prostatectomy, Urol. Oncol. 32 (8) (2014) 1292-1299.

12. A. Morlacco, V. Sharma, B.R Viers, et al., The Incremental Role of Magnetic Resonance Imaging for Prostate Cancer Staging before Radical Prostatectomy, Eur. Urol. 71 (5) (2017) 701-704.

13. T.M. Wheeler, O. Dillioglugil, M.W. Kattan, et al., Clinical and pathological significance of the level and extent of capsular invasion in clinical stage T1-2 prostate cancer, Hum. Pathol. 29 (8) (1998) 856-862.

14. T.S. Feng, A.R. Sharif-Afshar, J. Wu, et al., Multiparametric MRI Improves Accuracy of Clinical Nomograms for Predicting Extracapsular Extension of Prostate Cancer, Urology. 86 (2) (2015) 332-337.

15. K.J. Tay, R.T. Gupta, A.F. Brown, et al., Defining the Incremental Utility of Prostate Multiparametric Magnetic Resonance Imaging at Standard and Specialized Read in Predicting Extracapsular Extension of Prostate Cancer, Eur. Urol. 70 (2) (2016) 211-213.

16. E. Sala, O. Akin, C.S. Moskowitz, et al., Endorectal MR imaging in the evaluation of seminal vesicle invasion: diagnostic accuracy and multivariate feature analysis, Radiology. 238 (3) (2006) 929-937

17. F.N. Soylu, Y. Peng, Y. Jiang, et al., Seminal vesicle invasion in prostate cancer: evaluation by using multiparametric endorectal MR imaging, Radiology. 267 (3) (2013) 797-806.

18. M. Mullerad, H. Hricak, L. Wang, et al., Prostate cancer: detection of extracapsular extension by genitourinary and general body radiologists at MR imaging, Radiology. 232 (1) (2004) 140-146.

19. M. de Rooij, E.H. Hamoen, J.A Witjes, J.O. Barentsz, M.M. Rovers. Accuracy of Magnetic Resonance Imaging for Local Staging of Prostate Cancer: A Diagnostic Meta-analysis. Eur Urol. 70 (2) (2016) 233-245.

20. B.S. Teh, M.D. Bastasch, T.M. Wheeler, et al., IMRT for prostate cancer: defining target volume based on correlated pathologic volume of disease, Int. J. Radiat. Oncol. Biol. Phys. 56 (1) (2003) 184-191.

21. J.P. Radtke, B.A. Hadaschik, M.B. Wolf, et al., The Impact of Magnetic Resonance Imaging on Prediction of Extraprostatic Extension and Prostatectomy Outcome in Patients with Low-, Intermediate- and High-Risk Prostate Cancer: Try to Find a Standard, J. Endourol. 29 (12) (2015) 1396-1405.

22. F. Cornud, T. Flam, L. Chauveinc, et al., Extraprostatic spread of clinically localized prostate cancer: factors predictive of pT3 tumor and of positive endorectal MR imaging examination results, Radiology. 224 (1) (2002) 203-210.

23. L. Kestin, N. Goldstein, F. Vicini, et al., Treatment of prostate cancer with radiotherapy: should the entire seminal vesicles be included in the clinical target volume?, Int. J. Radiat. Oncol. Biol. Phys. 54 (3) (2002) 686-97.

6

Patterns of Benign Prostate Hyperplasia Based on Magnetic Resonance Imaging Are Correlated With Lower Urinary Tract Symptoms and Continence in Men Undergoing a Robot-assisted Radical Prostatectomy for Prostate Cancer.

Grivas N, van der Roest R, Tillier C, Schouten D, van Muilekom E, Schoots I, van der Poel H, Heijmink S.

Urology. 2017 Sep;107:196-201.

Abstract

Objective: To investigate the association between benign prostatic hyperplasia (BPH) patterns, classified by magnetic resonance imaging (MRI), with lower urinary tract symptoms (LUTS) or continence, preoperatively and after robot-assisted laparoscopic radical prostatectomy (RARP).

Materials and Methods: This retrospective study included 49 prostate cancer patients, with prostate size >47 cm^3, who underwent an endorectal MRI followed by RARP. Five BPH patterns were identified according to Wasserman and additional prostate measurements were recorded. LUTS were assessed using the International Prostate Symptom Score (IPSS) and the PR25-LUTS-Questionnaire score. Continence was assessed using the International Consultation of Incontinence Questionnaire-Short Form.

Results: BPH pattern 3 (44.9%) was identified most common, followed by pattern 5 (26.6%), 1 (24.5%), 2 and 4 (both 2%). BPH patterns were significant predictors of preoperative LUTS, with pedunculated with bilateral transition zone (TZ) and/or retrourethral enlargement (pattern 5) causing more severe symptoms compared to bilateral TZ and retro-urethral enlargement (pattern 3) and bilateral TZ enlargement (pattern 1), while pattern 3 was additionally associated with more voiding symptoms compared to pattern 1. None of the BPH patterns was predictive of postoperative LUTS and continence. Independent predictors of continence at 12 months were lower preoperative PR25-LUTS score (P = .022) and longer membranous urethral length (P = .025).

Conclusions: MRI is useful for classifying patients in BPH patterns which are strongly associated with preoperative LUTS. However, BPH patterns did not predict remnant LUTS or postoperative incontinence. Postoperative continence status was only associated with preoperative LUTS and MUL.

Introduction

Benign prostatic hyperplasia (BPH) is the pathological process of periurethral transition zone (TZ) enlargement of the prostate, often resulting in lower urinary tract symptoms (LUTS) (1). The incidence of BPH and the severity of LUTS increase with age, approaching 40% in men aged over 50 years old (2). LUTS have a negative impact on the quality of life (QoL) causing also a significant healthcare cost, which is expected to increase in the next decades (3).

Imaging has a significant role in the evaluation of BPH patients. Transrectal ultrasound (TRUS) is the most common imaging tool which can depict the prostate and TZ volume, the presence of enlarged middle lobe and areas suspicious of prostate cancer (PCa) (4). However, the accuracy of TRUS is user dependent, it could under- or overestimate prostate volumes larger than 50 cm^3 or smaller than 30 cm^3, respectively, while the mixed echo pattern of BPH may mask central and anterior located tumors (5). These limitations have led to the increased use of multiparametric Magnetic Resonance Imaging (MRI) especially for PCa recently showing a diagnostic sensitivity of 95% for significant tumors (6). In BPH, prostate segmentation with MRI is also an accurate technique for determining prostate and TZ volume, while it has been additionally used for choosing the optimal medical therapy, based on the stromal/glandular ratio and for the assessment of interventional procedures, including ablation and prostatic artery embolization (7,8). A new MRI classification of BPH patterns was recently published by Wasserman et al (9). This classification is of significant interest since it could be associated with patients' reported LUTS and determine treatment options (10).

Since in clinical practice LUTS often lead to serum PSA measurement with a subsequent possible diagnosis of PCa, many men with early, localized PCa suffer from LUTS caused by BPH. Since a prostatectomy provides treatment of both BPH and PCa, many men opt for radical surgical removal of the prostate. However, there is limited knowledge on the effects of Robot-assisted laparoscopic Radical Prostatectomy (RARP) on LUTS especially in men with BPH and PCa.

Aim of our study was to investigate the association between MRI-based BPH patterns and LUTS as these were assessed from two questionnaires, filled out pre- and post-RARP. In addition, we evaluated the predictive role of BPH patterns and preoperative LUTS on continence status after RARP.

Materials and Methods

Patients

We retrospectively identified 49 PCa patients who underwent pelvic staging MRI followed by RARP between September 2014 and October 2015. All men had prostate volume above our institutional median volume (47 cm^3). Further selection criteria were: at least one follow up visit after RARP, normal preoperative continence, no contraindication for MRI, no tumor in the TZ, no prior treatment for PCa, no previous transurethral resection of the prostate and no medical therapy for incontinence, whereas medical treatment of LUTS was allowed. RARP was performed using the da Vinci S(i) surgical robot (Intuitive Surgical, Inc., Sunnyvale, CA, USA) as described earlier (11). Age, Body Mass Index (BMI), prostate-specific antigen (PSA), Gleason sum score and clinical stage were recorded.

MRI Measurements and BPH patterns

Multiparametric MRI was performed using a 3 Tesla system (Philips, Best, The Netherlands) with an endorectal coil. The prostate and TZ volume, the length of retro-urethral enlargement, the length of intravesical prostatic protrusion (IPP), the anterior fibromuscular stroma (AFMS) distance, the inner levator distance (ILD) and the membranous urethra length (MUL), were measured on T2-weighted images (Fig. 1). The TZ index was calculated by dividing the TZ volume by prostate volume (12). BPH patterns according to the MRI classification of Wasserman et al (9). were determined on the axial and sagittal MRI images (Fig. 2). Images were analyzed with a DICOM viewer PACS

(Carestream Health, Inc., Rochester, NY). All measurements were done by two raters blinded to outcome.

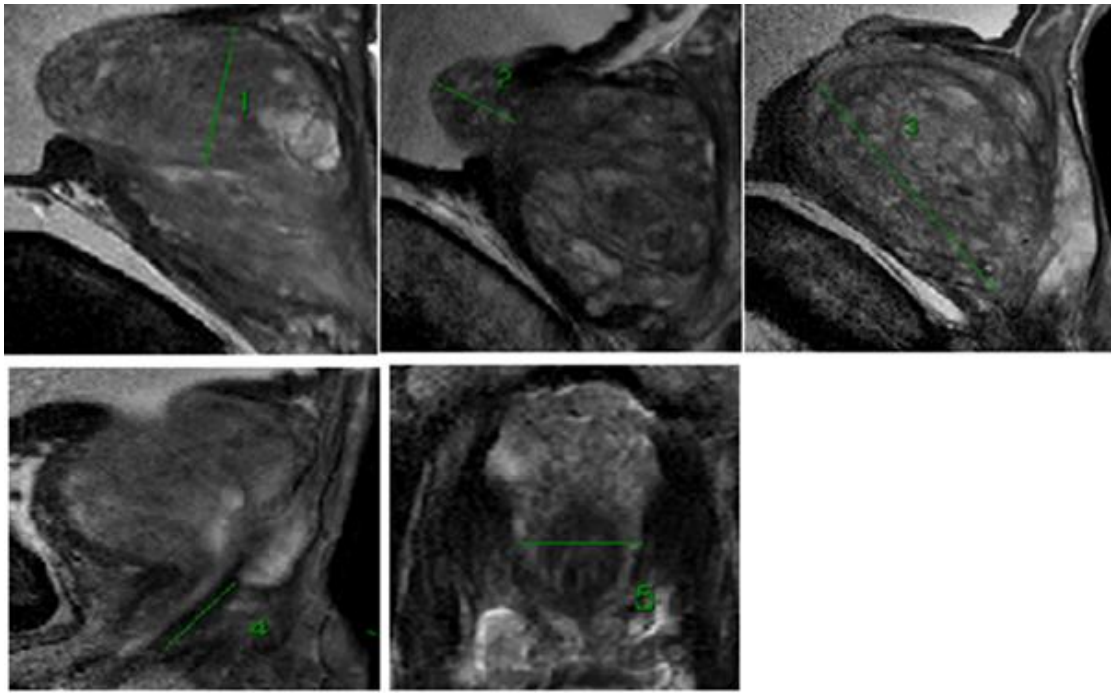

Figure 1. Magnetic Resonance Imaging (MRI) length measurements: 1, retro-urethral enlargement; 2, intravesical prostatic protrusion; 3, anterior fibromuscular stroma; 4, membranous urethra length; 5, inner levator distance.

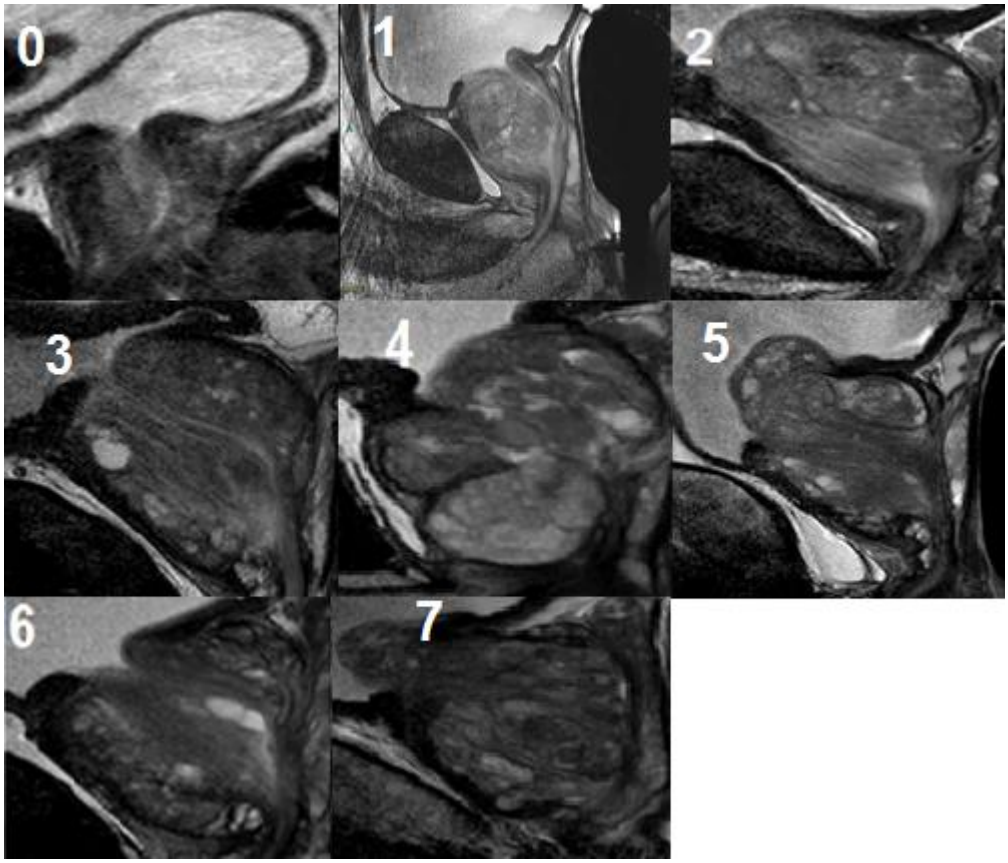

Figure 2. Benign prostatic hyperplasia (BPH) patterns, according to Wasserman et al (9): Pattern 0, prostate volume≤25 cm^3 showing little or no zonal enlargements; Pattern 1, bilateral transition zone enlargement; Pattern 2, retro-urethral enlargement; Pattern 3, bilateral transition zone and retro-urethral enlargement; Pattern 4, pedunculated enlargement; Pattern 5, pedunculated with bilateral transition zone and/or retrourethral enlargement; Pattern 6, subtrigonal or ectopic enlargement; Pattern 7, other combinations of enlargements.

Outcome Assessment

The primary outcome was the change from baseline in postoperative vs. preoperative LUTS. The association between pre/postoperative LUTS and BPH patterns, prostate MRI-measurements or clinical parameters were investigated. LUTS were evaluated by two widely used questionnaires; the International Prostate Symptom Score (IPSS) and the European Organization for Research and Treatment of Cancer Quality of Life Questionnaire (EORTC-QLQ)-PR25-

LUTS domain. The IPSS questionnaire includes seven questions about LUTS (incomplete emptying, frequency, intermittency, urgency, weak stream, straining, nocturia). A sum of the scores of these questions is the total IPSS score ranging from 0 to 35. The IPSS-storage symptoms (IPSS-ss) score is the sum of the scores from the questions 2, 4, and 7, while the IPSS-voiding symptoms (IPSS-vs) score is the sum of the scores from the questions 1, 3, 5, and 6 (13). The PR25-LUTS questionnaire is developed to evaluate LUTS in men with PCa based on 8 questions (frequency, nocturia, urgency, sleep disturbance, dysuria, incontinence, limitation of daily activities, need to stay close to the toilet) with a total score ranging from 8 to 32 (14). The two questionnaires were completed by the patient preoperatively and at 6 and 12 months follow up.

The secondary outcome was the prevalence of postoperative continence at 12 months, which was assessed using the International Consultation on Incontinence Questionnaire-Short Form (ICIQ-SF) questionnaire (15). Total score ranged from 0 to 21 while continent patients were considered those who answered that they never leak urine (question 4a). The association of the continence status with preoperative total IPSS, IPSS-ss, IPSS-vs and PR25-LUTS scores was also investigated, together with the BPH patterns and the MRI/clinical parameters.

Statistical Analysis

The Spearman's rho correlation coefficient (r) and the linear regression analysis (r^2) were used to calculate possible associations between the questionnaires scores and the clinical and MRI parameters. The Kruskal-Wallis and the Hodges-Lehmann tests were used to determine the differences and estimate the 95% confidence interval (CI) of the median differences among the BPH patterns, respectively. A binary logistic regression analysis of each variable for the prediction of continence after RARP was also performed. The 95% CI was calculated for all odds ratios (ORs). Values of $P<.05$ were considered statistically significant. SPSS software version 22.0 (SPSS Inc., Chicago, IL) was used to perform the statistical analysis.

Results

Patient characteristics, MRI measurements, BPH patterns and questionnaires scores are presented in Table 1. In our patient cohort, isolated subtrigonal or ectopic enlargement (pattern 6) or other combinations of enlargements (pattern 7) were not identified. Rarely isolated retro-urethral enlargement (pattern 2) (2%) or isolated pedunculated enlargement (pattern 4) (2%) were identified. These patterns were excluded from further analysis.

Table 1. Summary of patients characteristics	
Median age at surgery (IQR)	66 (62-70)
Median kg/m^2 BMI (IQR)	25.7 (23.2-28.5)
Median ng/ml PSA (IQR)	9.6 (7-13)
No. biopsy Gleason score (%):	
6 or Less	21 (42.9)
7	22 (44.9)
8 or Greater	6 (12.2)
No. clinical stage (%):	
cT1	11 (22.5)
cT2	32 (65.3)
cT3	6 (12.2)
Median MRI variables (IQR):	
Prostate volume (cm^3)	62 (55-78)
TZ volume (cm^3)	46.7 (50.9-78.1)
TZ index	0.74 (0.65-0.80)
Retro-urethral enlargement length (mm)	10.9 (8.7-13.9)
IPP (mm)	7.9 (5.2-11.1)
AFMS distance (mm)	42.5 (38.1-46.8)
ILD (mm)	18.2 (16-19.7)
MUL (mm)	16.2 (14.1-18.4)
Patterns of BPH (%)	
Pattern 1	12 (24.5)
Pattern 2	1 (2)
Pattern 3	22 (44.9)
Pattern 4	1 (2)
Pattern 5	13 (26.6)
Median preoperative total IPSS score (IQR)	11 (6.7-15.5)

Median total IPSS score, 6 months (IQR)	5 (3-7.5)
Median total IPSS score, 12 months (IQR)	5 (3.7-7.2)
Median preoperative IPSS-ss score (IQR)	5 (2.2-7)
Median IPSS-ss score, 6 months (IQR)	3 (2-6)
Median IPSS-ss score, 12 months (IQR)	3 (2-5)
Median preoperative IPSS-vs score (IQR)	5 (2-9)
Median IPSS-vs score, 6 months (IQR)	1 (0-3)
Median IPSS-vs score, 12 months (IQR)	1 (0-2.8)
Median preoperative PR25-LUTS score (IQR)	13 (10-15)
Median PR25-LUTS score, 6 months (IQR)	12 (10-13)
Median PR25-LUTS score, 12 months (IQR)	11 (9-13)
Median ICQ-SF score, 12 months (IQR)	3 (0-5)

Bilateral TZ and retro-urethral enlargement (pattern 3) was the most common BPH pattern (44.9%), followed by pedunculated with bilateral TZ and/or retrourethral enlargement (pattern 5) (26.6%), and bilateral TZ enlargement (pattern 1) (24.5%),

Preoperative associations

Compared to pattern 1, patients with pattern 3 BPH had higher median preoperative total IPSS (11 vs 7, CI 1-8, *P*=.021), bigger retro-urethral enlargement (12.6 vs 9.2 mm, CI 1.18-5.26, *P*=.004) and longer ILD (18.6 vs 16 mm, CI 0.28-3.75, *P*=.037). In pattern 5 a longer ILD was observed compared to pattern 1 (18 vs 16 mm, CI 0.3-3.99, *P*=.041) as well as a higher preoperative total IPSS and a longer IPP compared to pattern 1 (21 vs 7, CI 6-17, *P*=.002 and 12.3 vs 6 mm, CI 3.6-10.1, *P*<.001) and pattern 3 (21 vs 11

mm, 2-12 CI, *P*=.004 and 12.3 vs 7.5 mm, CI 2.4-8.7, *P*=0.002). In the linear regression analysis (Table 2) higher preoperative total IPSS score was only associated with longer IPP (*P*=.025) (Fig. 3). Total preoperative IPSS and PR25-LUTS scores were significantly associated (*P*<.001). However, the differences among BPH patterns regarding the PR25-LUTS score were not significant (pattern 5 vs 1: *P*=.07; pattern 3 vs 1: *P*=.13; pattern 5 vs 3: *P*=.16). PR25-LUTS score was marginally associated with IPP (*P*=.064).

Table 2. Linear regression analysis between preoperative IPSS and clinical-MRI parameters.

Predictors	Linear regression analysis	
	Regression coefficient (95% CI)	*P* value
Age	-0.208 (-0.601, 0.121)	.186
BMI	-0.089 (-0.857, 0.481)	.573
PSA	-0.067 (-0.342, 0.223)	.672
Gleason score	-0.102 (-1.804, 3.515)	.519
Clinical stage	-0.077 (-1.640, 1.005)	.63
Prostate volume (cm^3)	-0.085 (-0.117, 0.068)	.591
TZ volume (cm^3)	-0.266 (-0.2, 0.017)	.097
TZ index	-0.084 (-22.7, 13.5)	.608
Retro-urethral enlargement length (mm)	-0.075 (-0.697, 0.431)	.637
IPP (mm)	0.347 (0.058, 0.807)	.025
AFMS distance (mm)	-0.292 (-0.68, 0.025)	.068
ILD (mm)	0.224 (-0.159, 1.274)	.124

MUL (mm)	-0.221 (-0.749-0.307)	.403

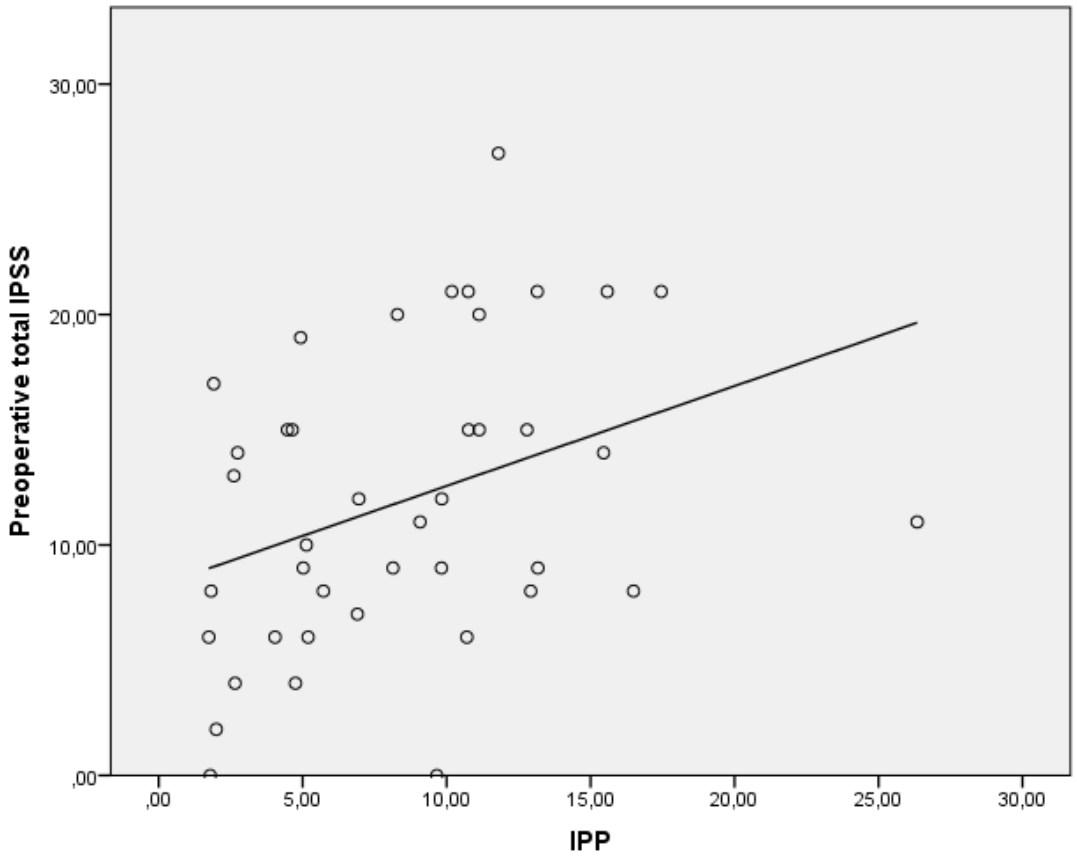

Figure 3. Association between preoperative total international prostate symptom score (IPSS) and intravesical prostatic protrusion (IPP) (r^2=.120; *P*=.025).

Patients with pattern 5 BPH had higher median IPSS-ss score compared to pattern 1 (8 vs 4, CI 1-7, *P*=.013) and pattern 3 (8 vs 4.5, CI 1-6, *P*=.011). Similarly, a higher IPSS-vs score was observed in pattern 5 compared to pattern 1 (9.5 vs 3.5, CI 3-10, *P*=.001) and pattern 3 (9.5 vs 5.5, CI 1-7, *P*=.031). Significant difference was also observed in IPSS-vs score between patterns 3 and 1 (5.5 vs 3.5, CI 1-5, *P*=.04). In the linear regression analysis higher IPSS-ss was only associated with longer IPP (r^2=.119, *P*=.022) while the association was not significant with IPSS-vs score (r^2=.074, *P*=.074).

Postoperative associations

Individual BPH patterns were not associated with postoperative LUTS (as expressed by total IPSS, IPSS-ss, IPSS-vs, PR25-LUTS scores) at 6 and 12 months postoperatively. Furthermore, clinical and MRI measurements were not associated with postoperative LUTS at any time point. Only PR25-LUTS at 12 months was significantly associated with preoperative PR25-LUTS score (*P*=.004), total preoperative IPSS score (*P*=.037) and 12 months total IPSS (*P*=0.02).

Median total IPSS score was significantly lower at 6 months and 12 months compared to preoperative total IPSS (both 5 vs 11, *P*<.001), mainly due to a significant reduction in median IPSS-vs score (both 1 vs 5, *P*<.001). The improvement in LUTS was more prominent in patterns 5 and 3 (Fig. 4). The median IPPS-ss score was not significantly reduced at 6 months (3 vs 5, *P*=.117) and 12 months (3.5 vs 5, *P*=.144), while median PR25-LUTS score was significantly lower at 12 months (11 vs 13.00, *P*=.048) but not at 6 months (12 vs 13, *P*=.239).

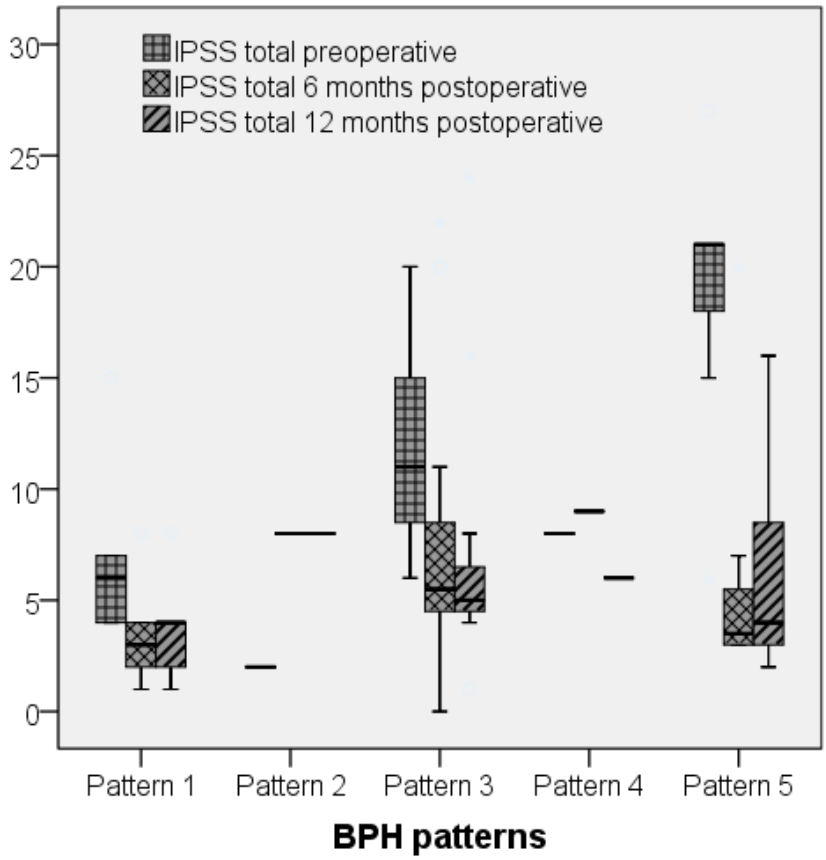

Figure 4. Total international prostate symptom score (IPSS) distribution among the five benign prostatic hyperplasia (BPH) patterns preoperatively and at 6 and 12 months, follow up.

Based on the question 4a of ICIQ-SF score, the continence rate at 12 months was 49%. No association between BPH patterns and ICIQ-SF score at 12 months was observed. ICIQ-SF score was significantly associated with preoperative total IPSS score (r=.365, *P*=.022), PR25-LUTS score (r=.633, *P*<.001) and IPSS-ss score (r=.538, *P*<.001) but not with IPSS-vs score (r=.277, *P*=.083). In the univariate binary logistic regression (Table 4) analysis, the only factors found to be predictors of continence were lower preoperative total IPSS (OR .896, CI .803-.998, *P*=.047), IPSS-ss (OR 0.731, CI 0.573-0.934, *P*=.012) and PR25-LUTS scores (OR 0.726, CI 0.562-0.938, *P*=.014) and longer MUL (OR 1.263, CI 1.008-1.582, *P*=.042). In the multivariate analysis only preoperative PR25-LUTS score and MUL remained significantly associated with continence status.

Table 4. Univariate and multivariate binary logistic regression analysis of postoperative continence.						
Covariates	Univariate analysis			Multivariate analysis*		
	OR	95% CI	*P*	OR	95% CI	*P*
Age	0.975	0.874-1.087	.648			
BMI	0.918	0.763-1.106	.367			
PSA	1.031	0.947-1.123	.477			
Gleason score	1.327	0.598-2.945	.487			
Clinical stage	1.495	0.926-2.414	.1			
Prostate volume (cm3)	1.017	0.987-1.047	.272			
TZ volume (cm3)	1.015	0.967-1.065	.557			
TZ index	2.250	0.033-15.51	.706			
Retro-urethral enlargement length (mm)	0.975	0.827-1.15	.766			
IPP (mm)	0.967	0.858-1.091	.589			
AFMS distance (mm)	1.029	0.923-1.147	.608			
ILD (mm)	0.843	0.664-1.071	.161			

BPH patterns 5 vs 1 5 vs 3	 1.500 0.955	 0.275-8.189 0.196-4.638	.821 .640 .954			
Preoperative total IPSS score	0.896	0.803-0.998	**.047**	1.032	0.884-1.206	.687
Preoperative PR25-LUTS score	0.726	0.562-0.938	**.014**	0.674	0.481-0.495	**.022**
MUL (mm)	1.263	1.008-1.582	**.042**	1.352	1.038-1.760	**.025**
Preoperative IPSS-ss score	0.731	0.573-0.934	**.012**			

Discussion

Functional parameters after radical prostatectomy (RP) have been the subject of extensive studies (16). Most of these studies have used validated questionnaires to objectively assess continence, erectile function and QoL (16). To our knowledge, our study is the first which additionally focused on the association of preoperative BPH patterns and LUTS with postoperative LUTS and continence rates at 6 and 12 months.

Our results have shown a strong association of the MRI-based BPH patterns with preoperative total IPSS, IPSS-ss and IPSS-vs, demonstrating the significant role of MRI in the evaluation of BPH. The total IPSS score was stronger associated with BPH patterns compared to PR25-LUTS score, suggesting that the IPSS score is a better measure of BPH related complaints, while PR25-LUTS may perform better in PCa taking also into account that its development was based on PCa patients (14). Older studies based on histological types and the stromal component of BPH have also shown association with LUTS severity (17). However, Guneyli et al. did not show an association between preoperative total IPSS and BPH patterns, while TZ volume was the only significant predictor in their multivariate analysis (13).

LUTS were most severe in patients with BPH pattern 5, followed by men with pattern 3 and pattern 1. This should be attributed to the higher IPP of pattern 5 related also to the pedunculated imaging of the adenoma in this specific pattern. IPP itself was found to be a significant predictor of preoperative LUTS while no association with PSA and prostate volume was found. This observation is in accordance with Lim et al. and Franco et al. who reported that IPP is a more powerful predictor of bladder outlet obstruction than either PSA or prostate volume (18,19). Matsukawa et al. found IPP as the most significant predictor of the total IPSS improvement in patients treated with dutasteride while Cumpanas et al. reported that an IPP length of more than 10 mm could be a predicting factor of treatment failure in patients treated with tamsulosin (20,21). Thus the value of IPP could extend in the medical treatment of LUTS/BPH.

Compared to the amount of data on urinary incontinence, there is a relative paucity of data on the impact of RP on LUTS, especially in the context of RARP (22). Based on our results a significant improvement in postoperative LUTS was observed which was more prominent in patterns 5 and 3. The improvement in IPSS was better in voiding symptoms compared to storage symptoms. Moreover, postoperative LUTS were strongly associated with baseline LUTS. A recent study in RARP treated patients showed that LUTS improved over 10 years of follow-up, with greater improvements observed among patients with baseline clinically significant LUTS (23). Long-term improvements of LUTS have been also reported after open RP, especially in men with more severe symptoms preoperatively (24). Johnson et al. have additionally shown that RP results in a greater decrease of IPSS compared to radiotherapy and brachytherapy (25). This improvement in LUTS is likely because of immediate and definitive relief of bladder outlet obstruction by the removal of the prostate gland. On the other hand, RP may also cause bladder denervation and ischemic changes which could provoke detrusor under- or overactivity (26).

The only factors found to be predictors of incontinence after RARP were higher preoperative total IPSS/IPSS-ss/PR25-LUTS scores and a shorter MUL. Lavigueur-Blouin et al. have also shown that a lower preoperative IPSS score was an independent predictor of early continence after RARP (27). A systematic review has also demonstrated that pre-existing LUTS have a

negative impact on continence (28). Regarding MUL, a recent meta-analysis has shown that every extra millimeter of MUL is associated with a 9% greater odd for continence recovery, confirming the role of MUL as one of the strongest predictive factors of post radical prostatectomy incontinence (29).

In our analysis, age, BMI and prostate size were not predictors of postoperative incontinence. A possible explanation may be the fact that patients selected for surgery were relatively fit with a median age of 66 years old and they had relatively low preoperative BMI and prostate size. Our observations are in accordance with Kadono et al. who have also shown that age, BMI and prostate volume were not associated with post-RARP incontinence in a cohort of 111 patients (30).

Limitations

Our study is an observational, single institutional study with retrospective analysis of prospectively collected data. The sample size was relatively small and a selection bias could exist since we selected patients with prostate volumes above our median institutional value. This seems justified, however, since no size definition of BPH is present in the literature, other than any prostate enlargement in men over 50 years. Finally, we did not perform urodynamic studies while the use of the endorectal probe might have had an impact on the measurements.

Conclusions

Our data provide an insight into the BPH component of preoperative LUTS. MRI is useful for assessing IPP and classifying patients in BPH patterns which were found to be associated with preoperative LUTS. However, BPH patterns did not predict remnant LUTS or postoperative incontinence but men with elevated preoperative IPSS had improvement of LUTS. The questionnaires can predict postoperative LUTS and along with MUL, the continence status after prostatectomy.

References

1. Gacci M, Corona G, Sebastianelli A, et al. Male Lower Urinary Tract Symptoms and Cardiovascular Events: A Systematic Review and Meta-analysis. Eur Urol. 2016; 70: 788-796.

2. Verhamme KM, Dieleman JP, Bleumink GS, et al. Incidence and prevalence of lower urinary tract symptoms suggestive of benign prostatic hyperplasia in primary care--the Triumph project. Eur Urol. 2002; 42: 323-328.

3. Speakman M, Kirby R, Doyle S, et al. Burden of male lower urinary tract symptoms (LUTS) suggestive of benign prostatic hyperplasia (BPH) - focus on the UK. BJU Int. 2015; 115: 508-519.

4. Loch AC, Bannowsky A, Baeurle L, et al. Technical and anatomical essentials for transrectal ultrasound of the prostate. World J Urol. 2007; 25: 361-366.

5. Matthews GJ, Motta J and Fracehia JA. The accuracy of transrectal ultrasound prostate volume estimation: clinical correlations. J Clin Ultrasound. 1996; 24: 501-505.

6. Ahmed HU, El-Shater Bosaily A, Brown LC, et al. Diagnostic accuracy of multi-parametric MRI and TRUS biopsy in prostate cancer (PROMIS): a paired validating confirmatory study. Lancet. 2017 Feb 25;389(10071):815-822. doi: 10.1016/S0140-6736(16)32401-1. Epub 2017 Jan 20.

7. Turkbey B, Fotin SV, Huang RJ, et al. Fully automated prostate segmentation on MRI: comparison with manual segmentation methods and specimen volumes. AJR Am J Roentgenol. 2013; 201: W720-729.

8. Kisilevzky N and Faintuch S. MRI assessment of prostatic ischaemia: best predictor of clinical success after prostatic artery embolisation for benign prostatic hyperplasia. Clin Radiol. 2016; 71: 876-882.

9. Wasserman NF, Spilseth B, Golzarian J, et al. Use of MRI for Lobar Classification of Benign Prostatic Hyperplasia: Potential Phenotypic Biomarkers for Research on Treatment Strategies. AJR Am J Roentgenol. 2015; 205: 564-571.

10. Guneyli S, Ward E, Thomas S, et al. Magnetic resonance imaging of benign prostatic hyperplasia. Diagn Interv Radiol. 2016; 22: 215-219.

11. van der Poel HG, de Blok W, Joshi N, et al. Preservation of lateral prostatic fascia is associated with urine continence after robotic-assisted prostatectomy. Eur Urol. 2009; 55: 892-900.

12. Kaplan SA, Te AE, Pressler LB, et al. Transition zone index as a method of assessing benign prostatic hyperplasia: correlation with symptoms, urine flow and detrusor pressure. J Urol. 1995; 154: 1764-1769.

13. Guneyli S, Ward E, Peng Y, et al. MRI evaluation of benign prostatic hyperplasia: Correlation with international prostate symptom score. J Magn Reson Imaging. 2017; 45: 917-925.

14. van Andel G, Bottomley A, Fosså SD, et al. An international field study of the EORTC QLQ-PR25: a questionnaire for assessing the health-related quality of life of patients with prostate cancer. Eur J Cancer. 2008; 44: 2418-2424.

15. Avery K, Donovan J, Peters TJ, et al. ICIQ: a brief and robust measure for evaluating the symptoms and impact of urinary incontinence. Neurourol Urodyn. 2004; 23: 322-330.

16. van der Poel HG, Tillier C, de Blok WM, et al. Interview-based versus questionnaire-based quality of life outcomes before and after prostatectomy. J Endourol. 2013; 27: 1411-1416.

17. Ichiyanagi O, Sasagawa I, Ishigooka M, et al. Relationship between urodynamic type of obstruction and histological component of the prostate in patients with benign prostatic hyperplasia. Eur Urol. 1999; 36: 203-206.

18. Lim KB, Ho H, Foo KT, et al. Comparison of intravesical prostatic protrusion, prostate volume and serum prostatic-specific antigen in the evaluation of bladder outlet obstruction. Int J Urol. 2006; 13: 1509-1513.

19. Franco G, De Nunzio C, Leonardo C, et al. Ultrasound assessment of intravesical prostatic protrusion and detrusor wall thickness--new standards for noninvasive bladder outlet obstruction diagnosis? J Urol. 2010; 183: 2270-2274.

20. Matsukawa Y, Kato M, Funahashi Y, et al. What are the predicting factors for the therapeutic effects of dutasteride in male patients with lower urinary tract symptoms? Investigation using a urodynamic study. Neurourol Urodyn. 2017 Jan 19. doi: 10.1002/nau.23185. [Epub ahead of print].

21. Cumpanas AA, Botoca M, Minciu R, et al. Intravesical prostatic protrusion can be a predicting factor for the treatment outcome in patients with lower urinary tract symptoms due to benign prostatic obstruction treated with tamsulosin. Urology. 2013; 81: 859-863.

22. Honda M, Kawamoto B, Morizane S, et al. Impact of postoperative phosphodiesterase type 5 inhibitor treatment on lower urinary tract symptoms after robot-assisted radical prostatectomy: a longitudinal study. Scand J Urol. 2017; 51: 33-37.

23. Gordon A, Skarecky DW and Ahlering T. Long-term outcomes in severe lower urinary tract symptoms in men undergoing robotic-assisted radical prostatectomy. Urology. 2014; 84: 826-831.

24. Prabhu V, Taksler GB, Sivarajan G, et al. Radical prostatectomy improves and prevents age dependent progression of lower urinary tract symptoms. J Urol. 2014; 191: 412-417.

25. Johnson ME, Zaorsky NG, Martin JM, et al. Patient reported outcomes among treatment modalities for prostate cancer. Can J Urol. 2016; 23: 8535-8545.

26. Matsukawa Y, Hattori R, Komatsu T, et al. De novo detrusor underactivity after laparoscopic radical prostatectomy. Int J Urol. 2010; 17: 643-648.

27. Lavigueur-Blouin H, Noriega AC, Valdivieso R, et al. Predictors of early continence following robot-assisted radical prostatectomy. Can Urol Assoc J. 2015; 9: e93-97.

28. Heesakkers J, Farag F, Bauer RM, et al. Pathophysiology and Contributing Factors in Postprostatectomy Incontinence: A Review. Eur Urol. 2016 Oct 6. pii: S0302-2838(16)30666-2. doi: 10.1016/j.eururo.2016.09.031. [Epub ahead of print]

29. Mungovan SF, Sandhu JS, Akin O, et al. Preoperative Membranous Urethral Length Measurement and Continence Recovery Following Radical Prostatectomy: A Systematic Review and Meta-analysis. Eur Urol 2017; 71: 368-378.

30. Kadono Y, Ueno S, Kadomoto S, et al. Use of preoperative factors including urodynamic evaluations and nerve-sparing status for predicting urinary continence recovery after robot-assisted radical prostatectomy: Nerve-sparing technique contributes to the reduction of postprostatectomy incontinence. Neurourol Urodyn. 2016; 35: 1034-1039.

7

The value of periprostatic fascia thickness and fascia preservation as prognostic factors of erectile function after nerve sparing robot-assisted radical prostatectomy

Nikolaos Grivas, Rosanne C. van der Roest, Clarize M. Korne, Gijs H. KleinJan, Karolina Sikorska, Ivo G. Schoots, Corinne Tillier, Bram van den Broek, Kees Jalink, Stijn W.T.J.P. Heijmink, Tessa Buckle, Fijs W.B. van Leeuwen, Henk G. van der Poel

World J Urol. 2018 Jun 23. doi: 10.1007/s00345-018-2387-3. [Epub ahead of print]

Abstract

Objectives: To determine the correlation of preoperative fascia thickness (FT) and intraoperative fascia preservation (FP) with erectile function (EF) after nerve-sparing robot-assisted radical prostatectomy (RARP).

Methods: Our analysis included 106 patients, with localized prostate cancer and no erectile dysfunction (ED) before RARP, assessed with preoperative 3tesla (3T) multiparametric magnetic resonance imaging (MRI). FP score was defined as the extent of FP from the base to the apex of the prostate, quantitatively assessed by the surgeon. The median fascia thickness (MFT) per patient was defined as the sum of the median FT of 12 MRI regions. The preserved MFT (pMFT) was the sum of the saved MFT. The percentage of pFMT (ppMFT) was also calculated. Fascia surface (FS) was measured on MRI and it was combined with FP score resulting in preserved FS (pFS) and percentage of pFS (ppFS).

Results: FP score, pMFT, ppMFT, pFS and ppFS were significantly lower ($p < 0.0001$) in patients with ED. In the multivariate regression analysis lower FP score (odds ratio [OR] 0.721, $p = 0.03$) and lower ppMFT (OR 0.001, $p = 0.027$) were independent predictors of ED. ROC analysis showed the highest area under the curve for ppMFT (0.787) and FP score (0.767) followed by pMFT (0.755) and ppFS (0.743).

Conclusions: MRI-determined periprostatic FT combined with intraoperative FP score are correlated to post-prostatectomy EF. Based on the hypothesis that a thicker fascia forms a protective layer for the nerves, we recommend assessing FT preoperatively to counsel men for the odds of preserving EF after RARP.

Introduction

Prostate cancer (PCa) is the most common non-cutaneous cancer in men (1). Radical prostatectomy is an integral part in the management of localized PCa. Nevertheless, surgery induces damage to nerves bundles surrounding the prostate and is often associated with erectile dysfunction (ED). In an attempt to increase the quality of life of patients who value their erectile function (EF), a nerve-sparing prostatectomy is performed in confined PCa (2-4).

Initially, the periprostatic nerves were considered to run mainly dorsolaterally to the prostate, but more recent studies have demonstrated that nerves exist in the entire circumference of the (multi-layered) periprostatic fascia (5-8). Multiparametric Magnetic Resonance Imaging (mpMRI) could be helpful to virtually prepare the best nerve-sparing approach in a patient in order to improve EF (9-11).

Several scoring systems for nerve preservation have been proposed: among others the risk-stratified approach described by Tewari et al (12-13). We recently proposed an intraoperative scoring system that can be used by the urologist to document and quantitatively assess the extent of fascia preservation (FP) at different radial segments of the prostate (14). We reported that FP was predictive for EF, however, extensive nerve-sparing did not automatically result in better postoperative EF in all men. Therefore, other factors may determine EF. Other studies have shown that tension on the neurovascular structures surrounding the prostate adversely affect functional outcome (15-16).

We hypothesize that a thicker fascia may 1) provide a better natural protection of periprostatic nerves during robot-assisted laparoscopic radical prostatectomy (RARP) and 2) contain more periprostatic nerves. Both may result in better EF outcome. As such, a preoperative means of analysis of fascia thickness (FT) may have predictive value for postoperative EF. Aim of our study was to determine whether the thickness of the periprostatic fascia as assessed on preoperative MRI is correlated with EF in men with PCa who underwent a nerve-sparing RARP.

Materials and Methods

Patient population

The study was compliant with the Health Insurance Portability and Accountability Act while informed consent was waived for each patient. We retrospectively identified 106 patients between May 2010 and November 2013 who had localized PCa (cT1c – cT2c, Nx-N0, Mx-M0) and who were offered a 3tesla (3T) endorectal coil mpMRI prior to RARP (≥6 weeks after biopsies). Additionally, inclusion criteria were a preoperative International Index of Erectile Function-Erectile Function (IIEF-EF) (17) Questionnaire score ≥ 20, an intraoperatively determined FP score and at least 1 follow-up visit 6 months after prostatectomy in which EF was evaluated with the IIEF-EF score. Patients were excluded when they had any prior or current treatment for PCa, if prior transurethral resection of the prostate was performed, if there were factors excluding accurate reading of mpMRI such as movement artifacts and if there were contraindications for nerve preserving prostatectomy.

Surgical procedure-FP score assessment

All RARP procedures were performed by two experienced urologists with the da Vinci S(i) surgical robot system (Intuitive Surgical, Sunnyvale, CA, USA). During the procedures an attempt was made to preserve the periprostatic fascia tissue, as described in our previous study (14). In brief, the extent of preservation was scored intraoperatively at 12 positions circumferentially to the prostate. The FP score ranged from 0 – 12, scoring the intact fascia from base to apex on the dodecagon around the prostate

MRI Measurements and Image Analysis

A semi-automated macro in ImageJ was constructed to measure the fascia surface (FS) and the FT in TIFF-images. After manual delineation of prostate

and fascia outlines, 360 lines radiating out from the centre were generated: one for each of the 360 degrees. The periprostatic fascia was divided into 12 (30 degrees) parts, corresponding to the FP score dodecagon (Fig. 1). The distances from the intersection of the prostate contour to the intersection of the fascia boundary were collected, as well as the surface-area of the prostate, the total FS and the surface-area of the 12 different fascia regions. This semi-automatic method provided a standardized approach, while preserving the observer's ability to delineate the tissues. The midprostate level had the highest Intraclass Correlation Coefficient (ICC) among observers during the delineation process compared to the base and axial level (Fig. 2).

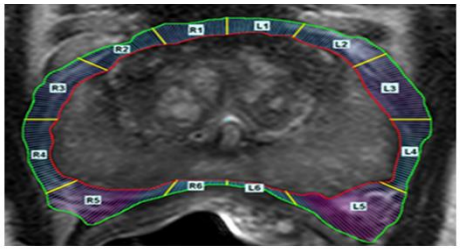

Fig. 1. T2-weighted transversal MR image at mid-prostate level with drawn contours and - clockwise - the 12 parts (corresponding with the FP score – 'L' stands for FP-region on the left side of the prostate and 'R' for the right side, respectively) consisted of 360 radial lines, color-coded for the prostate-fascia distance: pink = thick fascia, blue = thin fascia. FP, fascia preservation.

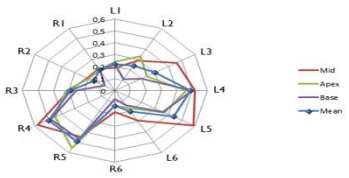

Fig. 2. ICC for median fascia distance per location (midprostate, apex and base) and per FP region for the different observers. Highest agreement in midprostate section (0.36; 0.31 and 0.26 respectively for apex and base). With

respect to the FP region: highest ICCs in L4, R4 and R5. Lowest ICCs in regions L6, R6 and R2. FP, fascia preservation; ICC, intraclass correlation coefficient.

Because normal distribution did not apply to the results of the delineations, the median values of the measured thicknesses were used. The median fascia thickness (MFT) per patient was defined as the sum of the median FT of the 12 regions on MRI. The preserved median fascia thickness (pMFT) was the sum of the median thicknesses of the fascia regions which were preserved; thus the pMFT is composed of both FT and FP score. The percentage of preserved median fascia thickness (ppMFT) was calculated as pMFT divided by MFT. The preserved fascia surface (pFS) was the sum of the FS which was preserved and the percentage of preserved fascia surface (ppFS) was calculated as pFS divided by FS.

Periprostatic nerves and blood vessels density assessment

To provide insight in the anatomy of the fascia regions, nerves and blood vessels were stained and measured in prostatectomy midsections of ten patients who underwent a non-nerve sparing RARP.

Outcome Assessment

The primary outcome was post-operative EF, based on the validated IIEF-EF at 12 months follow up. Men were subsequently divided in two groups; a group with ED (IIEF-EF score ≤19, n=66) and a group without ED (IIEF-EF score ≥20, n=40). Nine different factors were defined as possible predictors for postoperative ED: 1) age, 2) preoperative IIEF-EF score 3) FP score, 4) MFT, 5) pMFT, 6) ppMFT, 7) FS, 8) pFS and 9) ppFS.

Statistical Analysis

Comparison of clinical and pathologic characteristics between ED and non-ED groups was done with Mann-Whitney U Tests. The Spearman's rho correlation coefficient (r) and the linear regression analysis (r^2) were used to calculate correlations between the different variables measurements. A binary logistic regression analysis and the area under the curve (AUC) of the receiver operating characteristics (ROC) analysis were performed in order to determine the predictors of ED. Odds ratios (OR) and 95% confidence intervals (CI) were reported. Values of $p < 0.05$ were considered statistically significant. SPSS software ver. 22.0 (SPSS Inc., Chicago, IL) and the R statistical package (R Foundation for Statistical Computing, Vienna, Austria) were used to perform the statistical analysis.

Results

Periprostatic distribution of peripheral nerves and blood vessels

In the ten additional patients who underwent non-nerve sparing prostatectomy the nerves and blood vessels densities in the different FP regions were calculated (Fig. 3A-F). These immunohistochemical analyses revealed that on average the dorsolateral region (R4, R5, L4, L5) contained the thickest fascia, the most FS (47,7% of total amount), the highest peripheral nerve content (61,0% of total peripheral nerves) and the highest amount of blood vessels (52,5% of total number). Interestingly, a strong correlation was observed between the distribution of the peripheral nerves and the blood vessels ($R^2=0.94$, $p < 0.0001$). It has to be mentioned that a great variation was observed between patients. The variation in FT, FS, peripheral nerve density and blood vessel density is illustrated in Fig. 4.

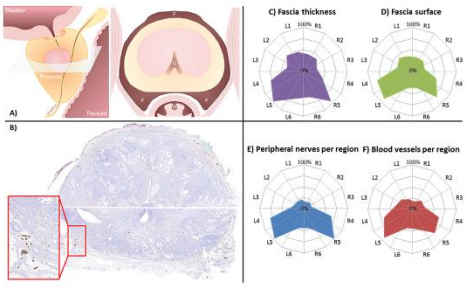

Fig. 3. A schematic picture of the prostate and a mid-prostate section. F: Fascia, R: Rectum, U: Urethra. B. A mid-prostate section stained with a s100-staining (nerve staining). C-F. Spiderplots which show the (C) FT (D) the FS (E) the peripheral nerve density (F) and the blood vessel density for the different FP regions of 10 patients who had a non-sparing prostatectomy. All graphs are normalized. FP, fascia preservation; FS, fascia surface; FT, fascia thickness.

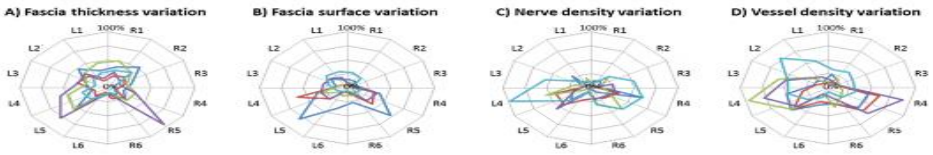

Fig. 4. These spiderplots show the variation in (A) FT, (B) FS, (C) peripheral nerve density and (D) blood vessel density per FP region for 5 individual patients. All graphs are normalized. FP, fascia preservation; FS, fascia surface; FT, fascia thickness.

All these patients received preoperative T2-weighted MRI of the prostate (Fig. 5A). Comparisons with the pathological findings indicated that the FT and FS derived from the ten associated MRI scans generated a similar distribution pattern (Fig. 5B-C). Quantitatively, however, the mean MFT and mean FS as defined at pathology were 1.41 (±0,45) mm and 181 (±60) mm^2, while the same specimens yielded values of 3.42 (±0,77) mm and 560 (±170) mm^2 on MRI, respectively. Comparing both datasets yielded a low correlation coefficient between MRI and immunohistology for both the FT (R^2 = 0.05) and the FS (R^2 = 0.50).

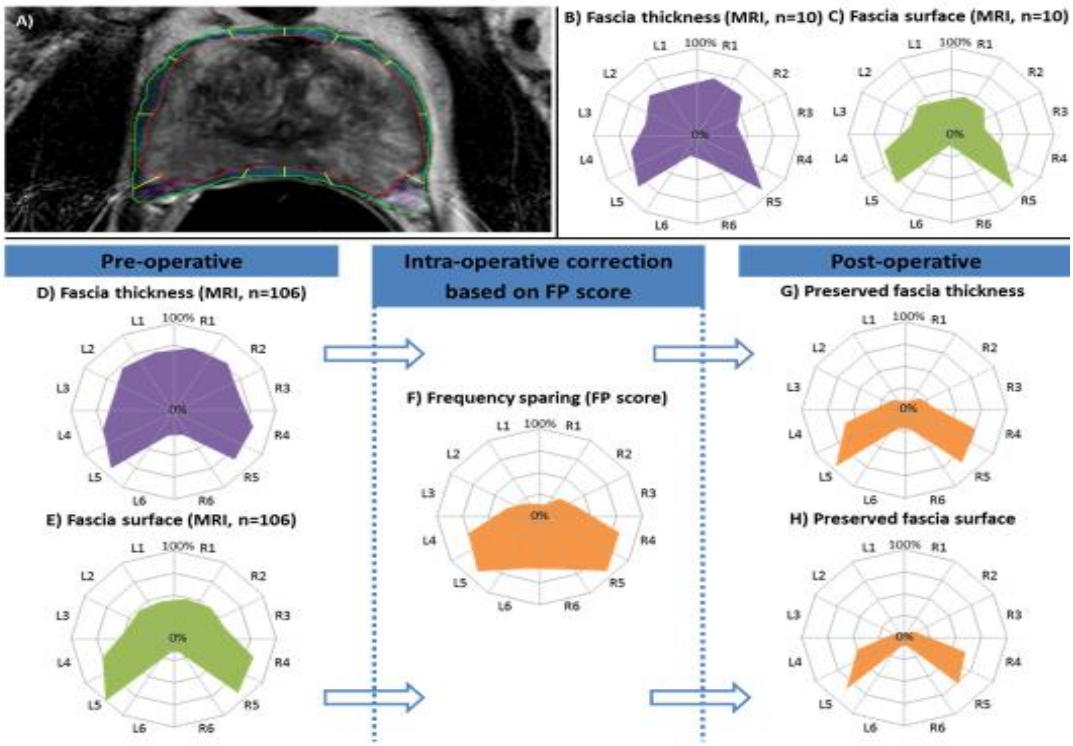

Fig. 5. A. A pre-operative MRI of the prostate, the boundary of the prostate and the fascia are drawn to determine the fascia thickness. B-C These spiderplots show the (B) FT and the (C) FS of the ten patients who underwent a non-sparing prostatectomy. D-E These spiderplots show the (D) FT and the (E) FS of the 106 patients who underwent (partly) fascia sparing prostatectomy. F This spiderplot shows how often the 12 FP regions are spared during the (partly) fascia sparing prostatectomy. G In this spiderplot the thicknesses (D) of the

spared regions (F) are summed up. H In this spiderplot the surface (E) of the spared regions (F) is summed up. All graphs are normalized. FP, fascia preservation; FS, fascia surface; FT, fascia thickness.

Preoperative MFT assessment

Clinical-pathologic features in the study population (106 patients) are presented in Table 1. The mean MFT and the mean FS defined on T2-weighted MRI were 3.75 (±0.95) mm and 633 (±206) mm^2, respectively. Five parameters were significantly higher ($p < 0.0001$) in patients without ED compared to those with ED, namely: FP score, pMFT, ppMFT, pFS and ppFS (Table 1).

Table 1. Summary of patient characteristics.

	Men without erectile dysfunction (n = 40)	Men with erectile dysfunction (n = 66)	*p value*
No. clinical stage (%) cT1c cT2a cT2b cT2c	 13 (32.5) 8 (20) 13 (32.5) 6 (15)	 19 (28.8) 15 (22.7) 16 (24.2) 16 (24.2)	
Mean age at time of RARP, yrs (SD)	61.3 (5.9)	61.2 (6.1)	0.945
Mean pre-operative IIEF-EF score (SD)	28.4 (2.1)	27.1 (3.0)	0.057
Mean prostate volume (TRUS), cc (SD)	42.4 (18.6)	42.7 (17.7)	0.924

Mean BMI, kg/ m² (SD)	25.7 (2.6)	26.6 (2.6)	0.096
Mean area of prostate, mm² (SD)	1350 (448)	1397 (449)	0.605
Resected Lymph nodes, No. (%)	11 (26.1)	24 (36.4)	0.352
Mean FP score (SD)	6.9 (2.3)	4.9 (2.7)	<0.001
Mean MFT, mm (SD)	47.1 (11.6)	43.7 (11.2)	0.053
Mean pMFT, mm (SD)	26.9 (10.2)	18.2 (10.2)	<0.001
Mean ppMFT (SD)	0.59 (0.2)	0.41 (0.2)	<0.001
FS, mm² (SD)	654 (219)	621 (198)	0,431
Mean pFS, mm² (SD)	397 (160)	287 (159)	<0.001
Mean ppFS (SD)	0.63 (0.2)	0.46 (0.19)	<0.001

Age, preoperative IIEF score, the MFT and the FS were not significantly different between patients with and without ED ($p = 0.945$, $p = 0.057$, $p = 0.053$ and $p = 0.431$, respectively). No significant correlation between median FT and BMI [$r = -0.072$, $p = 0.463$], age [$r = 0.123$, $p = 0.272$] and preoperative prostate volume [$r = 0.028$, $p = 0.778$] was observed, therefore we decided not to correct for these variables.

Based on the MR images the MFT and the mean FS per FP region were determined and plotted in Fig. 5D-E. Comparison of these plots revealed differences in the ventral region (R1-3, L1-3) of the prostate fascia. The fascia in the ventral region is as thick as the fascia in the dorsolateral region, however it contained less FS compared to the dorsolateral region.

Intraoperative FP score combined with preoperative FT

In all of the 106 patients who underwent (partly) sparing prostatectomy, one or more FP regions were spared; the FP score range was 1-12 (mean 5.7 ± 2.5). The frequency of sparing plotted per region is presented in Figure 5F, revealing that most sparing occurred in the dorsal region (R4-6, L4-6). On average 21.49 (±10.98) mm FT and 329 (±168) mm^2 FS were spared on a patient scale. In Figures 5G and 5H the spared FT and FS of the spared regions (based on FP score) is summed up, which showed that most fascia was preserved in the dorsolateral region.

Predictors for postoperative ED

In the univariate binary logistic regression analysis (Table 2) lower IIEF-EF score (OR 0.829, CI: 0.701-0.980, p = 0.028), lower FP score (OR 0.694, CI: 0.571-0.843, p < 0.001), lower pMFT (OR 0.923, CI: 0.884-0.963, p < 0.001), lower ppMFT (OR 0.007, CI: 0.001- 0.884, p < 0.001) and lower pFS (OR 0.996, CI: 0.993-0.998, p = 0.002) and lower ppFS (OR 0.009, CI: 0.001-0.095, p < 0.001) were predictors of ED. In the multivariate regression analysis lower FP score (OR 0.721, CI: 0.537-0.968, p = 0.03) and lower ppMFT (OR 0.001, CI: 0.000-0.374, p = 0.027) were independent predictors of ED.

Table 2. Univariate and multivariate binary logistic regression analysis of variables predicting ED outcome.

Variables	Univariate analysis			Bivariate analysis		
	OR	95% CI	*p value*	OR	95% CI	*p value*
Age	1.003	0.935-1.075	0.934			
IIEF-EF score	0.829	0.701-0.980	0.028	0.853	0.700-1.040	0.115

FP	0.694	0.571-0.843	<0.001	0.721	0.537-0.968	0.030
MFT	0.974	0.940-1.008	0.136			
pMFT	0.923	0.884-0.963	<0.001	1.035	0.906-1.182	0.617
ppMFT	0.007	0.001-0.084	<0.001	0.0001	0.000-0.374	0.027
FS	0.999	0.997-1.001	0.428			
pFS	0.996	0.993-0.998	0.002	0.997	0.989-1.005	0.441
ppFS	0.009	0.001-0.095	<0.001	3.67	0.284-4.737	0.106

The predictive value of the five factors which were different between the two groups (FP score, pMFT, ppMFT, pFS and ppFS) was assessed using ROC analysis. This analysis showed the highest AUC for ppMFT (0.787) and FP score (0.767) followed by pMFT (0.755), ppFS (0.743), and pFS (0.703). These findings indicate that the predictive value of the FP score can be further improved when the thickness (or to a lesser extent the surface) of the saved fascia regions is taken into account during the planning of the procedure.

ROC analysis with ED as outcome (cut-off IIEF-score ≤19) showed also that the AUC of pMFT remained 0.755 if the thickness of the regions R&L 1-3 was not taken into account. However, after removing the influence of the thickness of the regions R4 and L4, the AUC dropped to 0.724 and it dropped even further after removing the influence of the regions R5 and L5 (0.706). Hence, these results underline the importance of the dorsolateral region in the postoperative IIEF.

Cut-off IIEF-score

Patients were divided into groups (ED or no ED postoperatively) based on their IIEF-score, the cut-off IIEF-score ≤19 for ED was based on literature. When the cut-off was varied in the range IIEF-score ≤1 to ≤29 the predictive values of the five predictors from the previous ROC analysis varied, with an optimum at the cut-off IIEF-score ≤12 or ≤13. At this optimum, the AUC for the five factors (Fig. 6) which were significantly related to postoperative ED were: FP score (0.812), pMFT (0.834), ppMFT (0.818), pFS (0.777) and ppFS (0.815). The differences between the AUC values depended on the cut-off chosen, but were most consistent in the range of a cut-off IIEF-score ≤10 to ≤20. In this range, the mean difference in AUC-values between the FP score and pMFT was 0.015, whereby the pMFT proved to be a slightly stronger predictor than the FP score.

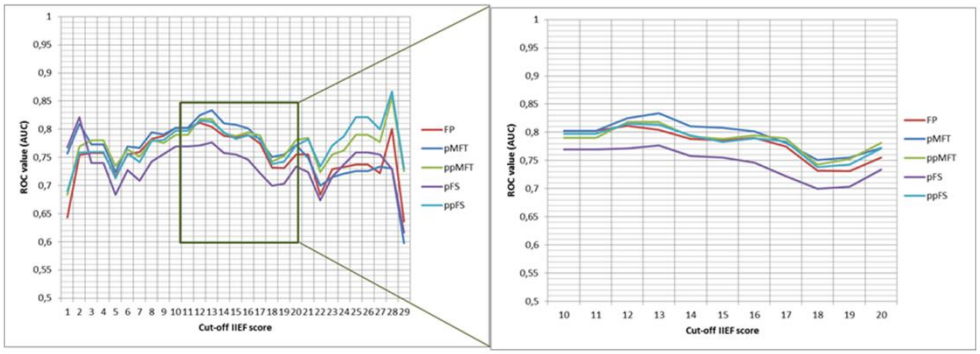

Fig. 6. The predictive value of the five factors which were significantly related to postoperative ED varied dependent on the cut-off chosen. The highest AUC values were reached with a cut-off IIEF-score ≤12 or ≤13. AUC, area under the curve; ED, erectile dysfunction; IIEF, International Index of Erectile Function-Erectile Function.

Discussion

To our knowledge, this is the first study that examines the correlation of preoperative MRI-assessed FT and intraoperative FP score with postoperative

EF. Preoperative MRI enabled quantification of periprostatic anatomy that allowed a better prediction of postoperative EF outcome. Patients without ED after nerve sparing prostatectomy had a thicker fascia on preoperative MRI compared with ED patients independent of the extent of nerve preservation, although this difference was at the edge of statistical significance ($p = 0.053$). Moreover, FT was not correlated with established prognostic factors of ED such as body mass index (BMI), age and preoperative prostate volume.

In order to find an explanation for the association between FT and ED we studied vessel and nerve density. We observed that there was poor correlation between histological- and MRI-determined FT while vessel and nerve density overlapped. Based on these observations from histology we studied the role of location of FP on outcome and we confirmed earlier findings that, regardless of FT sparing, the dorsolateral tissue is strongest correlated with improved erectile function outcome (14). We assume that FT itself contributes to preservation of EF by forming a solid, protective layer for the neurovascular bundles that withstands extensive traction and manipulation during surgery. Kwon et al. (18) made observations that support our hypothesis but did only assess the thickness of the dorsolateral fascia on the prostate where the neurovascular bundle was assumed. In our analysis we present data of the entire circumference of the prostate.

Based on the results of bivariate and ROC analyses FP score, ppMFT, pFMT and ppFS were the best predictors of postoperative EF preservation accounting for the observation that the preservation of a thicker and more dense fascia are inversely correlated with ED outcome. These observations emphasize our theory about the fascia as protective layer additionally enhanced by higher nerve density. Our method of measuring FT could be combined with the risk-stratified approaches such as the neural-hammock sparing of Tewari et al. (4) for optimal prediction of ED outcome.

Limitations

Several limitations to the present study are evident. We have not taken into account the intraoperative use of bipolar or monopolar coagulation or the use of surgical clips. To assess EF, we used the IIEF-EF questionnaire which does not take into account possible social-psychological issues as a reason for ED. In addition, the interobserver correlation for the FT assessment was poor to moderate, which could be attributed to the complex anatomy of the prostate and adjacent structures (6, 19). Interobserver variability in target definition has been demonstrated in a multitude of studies and at various anatomic sites (20-22). A more reproducible delineation of structures can be achieved by specific educational interventions (23-25). Similarly, the correlation between FT measurements on MRI and histology was poor.

Conclusions

Periprostatic FT determined in MR images combined with intraoperative FP score were correlated to postprostatectomy EF outcome. The MRI analysis indicated a large anatomical heterogeneity in FT between patients, as was the case in histologic evaluation of the fascia. This study is a step closer to provide a more personalized approach in counselling a patient who consider RARP as treatment for PCa.

References

1. R.L. Siegel, K.D. Miller, A. Jemal. Cancer Statistics, 2017, CA. Cancer. J. Clin. 67 (2017) 7-30.
2. A.T. Savera, S. Kaul, K. Badani, et al., Robotic radical prostatectomy with the "Veil of Aphrodite" technique: histologic evidence of enhanced nerve sparing, Eur. Urol. 49 (2006) 1065-73.
3. J.U. Stolzenburg, R. Rabenalt, M. Do, et al., Intrafascial nerve-sparing endoscopic extraperitoneal radical prostatectomy, Eur. Urol. 53 (2008) 931-40.
4. A. Tewari, J.O. Peabody, M. Fischer, et al., An operative and anatomic study to help in nerve sparing during laparoscopic and robotic radical prostatectomy, Eur. Urol. 43 (2003) 444-54.
5. G.M. Villeirs GM, K. L Verstraete, W.J. De Neve, G.O. De Meerleer., Magnetic resonance imaging anatomy of the prostate and periprostatic area: a guide for radiotherapists, Radiother. Oncol. 76 (2005) 99-106.
6. F.P. Secin, F.J Bianco. Surgical anatomy of radical prostatectomy: periprostatic fascial anatomy and overview of the urinary sphincters, Arch. Esp. Urol. 63 (2010) 255-66.
7. C. Eichelberg, A. Erbersdobler, U. Michl, et al., Nerve distribution along the prostatic capsule, Eur. Urol. 51 (2007) 105-10.
8. K.D. Sievert, J. Hennenlotter, I. Laible, et al., The periprostatic autonomic nerves--bundle or layer? Eur. Urol. 54 (2008) 1109-16.
9. M. de Rooij, E.H Hamoen, J.J Fütterer, et al., Accuracy of multiparametric MRI for prostate cancer detection: a meta-analysis, AJR. Am. J. Roentgenol. 202 (2014) 343-51.
10. T.D. McClure, D.J. Margolis, R.E. Reiter, et al., Use of MR imaging to determine preservation of the neurovascular bundles at robotic-assisted laparoscopic prostatectomy, Radiology. 262 (2012) 874-83.
11. K. Tanaka, K. Shigemura, M. Muramaki, et al., Efficacy of using three-tesla magnetic resonance imaging diagnosis of capsule invasion for decision-making about neurovascular bundle preservation in robotic-assisted radical prostatectomy, Korean. J. Urol. 54 (2013) 437-41.

12. A.K. Tewari, A. Srivastava, M.W. Huang, et al., Anatomical grades of nerve sparing: a risk-stratified approach to neural-hammock sparing during robot-assisted radical prostatectomy (RARP), BJU. Int. 108 (2011) 984-92.
13. O. Schatloff, S. Chauhan, A. Sivaraman, et al., Anatomic grading of nerve sparing during robot-assisted radical prostatectomy, Eur. Urol. 61 (2012) 796-802.
14. H.G. van der Poel, W. de Blok. Role of extent of fascia preservation and erectile function after robot-assisted laparoscopic prostatectomy, Urology. 73 (2009) 816-21.
15. K.J. Kowalczyk, A.C. Huang, N.D. Hevelone, et al., Effect of minimizing tension during robotic-assisted laparoscopic radical prostatectomy on urinary function recovery, World. J. Urol. 31 (2013) 515-21.
16. A.D. Asimakopoulos, V.E. Corona Montes, R. Gaston. Robot-assisted laparoscopic radical prostatectomy with intrafascial dissection of the neurovascular bundles and preservation of the pubovesical complex: a step-by-step description of the technique, J. Endourol. 26 (2012) 1578-85.
17. R.C. Rosen, A. Riley, G. Wagner, et al., The international index of erectile function (IIEF): a multidimensional scale for assessment of erectile dysfunction, Urology. 49 (1997) 822-30.
18. T. Kwon, C. Lee, J. Jung, C.S. Kim. Neurovascular bundle size measured on 3.0-T magnetic resonance imaging is associated with the recovery of erectile function after robot-assisted radical prostatectomy, Urol. Oncol. 35 (2017) 542.
19. V. Ficarra, G. Novara, T.E. Ahlering, et al., Systematic review and meta-analysis of studies reporting potency rates after robot-assisted radical prostatectomy, Eur. Urol. 62 (2012) 418-30.
20. J. Walz, A.L. Burnett, A.J. Costello, et al., A critical analysis of the current knowledge of surgical anatomy related to optimization of cancer control and preservation of continence and erection in candidates for radical prostatectomy, Eur. Urol. 57 (2010) 179-92.
21. E. Weiss, C.F. Hess. The impact of gross tumor volume (GTV) and clinical target volume (CTV) definition on the total accuracy in

radiotherapy theoretical aspects and practical experiences, Strahlenther. Onkol. 179 (2003) 21-30.

22. C.D. Fuller, J. Nijkamp, J.C. Duppen, et al., Prospective randomized double-blind pilot study of site-specific consensus atlas implementation for rectal cancer target volume delineation in the cooperative group setting, Int. J. Radiat. Oncol. Biol. Phys. 79 (2011) 481-9.
23. J. Kalpathy-Cramer, M. Awan, S. Bedrick, et al., Development of a software for quantitative evaluation radiotherapy target and organ-at-risk segmentation comparison, J. Digit. Imaging. 27 (2014) 108-19.
24. J.E. Bekelman, S. Wolden, N. Lee. Head-and-neck target delineation among radiation oncology residents after a teaching intervention: a prospective, blinded pilot study, Int. J. Radiat. Oncol. Biol. Phys. 73 (2009) 416-23.
25. X.A. Li, A. Tai, D.W. Arthur, et al., Variability of target and normal structure delineation for breast cancer radiotherapy: an RTOG Multi-Institutional and Multiobserver Study, Int. J. Radiat. Oncol. Biol. Phys. 73 (2009) 944-51.

8

Quantitative assessment of fascia preservation improves the prediction of membranous urethral length and inner levator distance on continence outcome after robot-assisted radical prostatectomy.

Grivas N, van der Roest R, Schouten D, Cavicchioli F, Tillier C, Bex A, Schoots I, Artibani W, Heijmink S, Van Der Poel H.

Neurourol Urodyn. 2018 Jan;37(1):417-425.

Abstract

Aims: To determine whether preoperative prostate/pelvic anatomical structures and intraoperative fascia preservation (FP) predict continence recovery after robot-assisted radical prostatectomy (RARP). **Methods:** Between January 2012 and March 2016, 439 prostate cancer (PCa) patients with normal preoperative continence were retrospectively included. FP score was defined as the extent of FP from base to apex of the prostate, quantitatively assessed by the surgeon. Anatomical prostate structures were measured on endorectal preoperative Magnetic Resonance Imaging. The International Consultation on Incontinence Questionnaire-Short Form (ICIQ-SF) was used to assess urinary incontinence (UI). Cox analysis was used to determine predictive factors for early continence recovery. Finally a binary logistic regression analysis was performed to develop a risk calculator. **Results:** At a median follow up of 12.1 months 50.8% of men reported UI. In the Cox multivariate analysis longer membranous urethral length (MUL; $P < 0.0001$; OR 1.309; CI 1.211, 1.415) and shorter inner levator distance (ILD; $P < 0.0001$; OR 0.904; CI 0.85, 0.961) were predictors of earlier continence recovery. In the multivariate binary logistic regression analysis longer MUL ($P < 0.0001$; OR 1.565, CI 1.362, 1.798), shorter ILD ($P < 0.0001$; OR 0.819, CI 0.742, 0.904) and higher FP score ($P=0.024$; OR 1.089, CI 1.011, 1.172) were independent predictors of continence outcome. The risk calculator predicted continence recovery between 1.3% and 99%. **Conclusions:** Preoperative longer MUL and shorter ILD, but also intraoperative FP independently improve continence recovery after RARP. The risk calculator could be used to identify patients at high risk of UI.

Introduction

Radical prostatectomy (RP) is the mainstay surgical treatment for localized prostate cancer (PCa) aiming to combine oncological control with urinary continence and erectile function preservation (1). The incidence of urinary incontinence (UI) is variable and difficult to assess due to the lack of a common definition and differences in the time and methodology of assessment (2). Robot-assisted radical prostatectomy (RARP) has shown lower postoperative UI rates compared to retropubic (RRP) (3.8% risk reduction) or laparoscopic radical prostatectomy (LRP) (4.6% risk reduction) with a UI incidence ranging from 4% to 31% at 12-months (3).

The factors associated with postoperative urinary continence after RARP are only partly understood (4). Besides surgical factors such as extent of nerve preservation and reconstruction techniques, pelvic floor anatomical variables such as membranous urethral length (MUL), urethral wall thickness, levator muscle thickness and inner levator distance (ILD) were found to correlate with urinary continence recovery (5,6). Multiparametric magnetic resonance imaging (mpMRI) can be used to non-invasively investigate the morphology and anatomy of the pelvic floor and assess the thickness of the multilayered peri-prostatic fascia which contains the neurovascular bundles (NVBs) (5,7).

Previously we proposed an intraoperative scoring system that can be used by the urologist to document and to quantitatively assess the extent of fascia preservation (FP) at different radial segments of the prostate (8). Using this system we did show that, FP was an independent predictor of continence recovery reducing the risk of UI at 6 months by > 60% when the peri-prostatic fascia was preserved at the lateral locations.

Aim of our study was to assess the role of intraoperative FP in combination with preoperative pelvic floor MRI measurements as predictive factors of any involuntary urine loss after RARP. In addition we recorded possible correlations of the examined parameters with the length of continence recovery and the severity of incontinence. Finally, a prognostic model for UI was developed.

Patients and Methods

Patients

We retrospectively identified 439 men with PCa who underwent preoperative staging MRI and intraoperatively FP assessment and RARP between January 2012 and March 2016. We included only men with localized PCa (cT1c – cT3a, Nx-N0, Mx-M0) and normal preoperative continence, based on the International Consultation on Incontinence Questionnaire-Short Form (ICIQ-SF) (9). Further selection criteria were: at least one follow up visit after RARP including ICIQ-SF assessment, no contraindication for MRI (e.g., pacemaker, history of allergic reaction to gadolinium, GFR <30 ml/min/1,73 m²), no prior or current treatment for PCa (eg radiotherapy, hormonal treatment or chemotherapy), no intra- or postoperative iatrogenic complications (e.g rectal injury, anastomotic insufficiency, repeated surgery due to bleeding), no overactive bladder symptoms, no external urethral sphincter scarring in urethroscopy and no medical therapy for incontinence.

The following demographic, clinical and surgical variables were recorded: age (years), prostate size (cm^3), body mass index (BMI, kg/m^2), preoperative prostate-specific antigen (PSA, ng/ml), Gleason sum score and clinical stage (cT).

Surgical Procedure and FP score assessment

A transperitoneal RARP was performed using the da Vinci S(i) surgical robot (Intuitive Surgical, Inc., Sunnyvale, CA, USA) as described earlier (8). Briefly, no cauterisation was used for the dissection of the distal parts of the prostatic fascia and prostate apex while the urethra was also transected with cold scissors. FP score was defined as the extent of fascia preservation from base to apex of the prostate, assessed by the surgeon after RARP (10). FP ranged from 0-12 according to the intact fascia on the dodecagon around the prostate (Fig. 1).

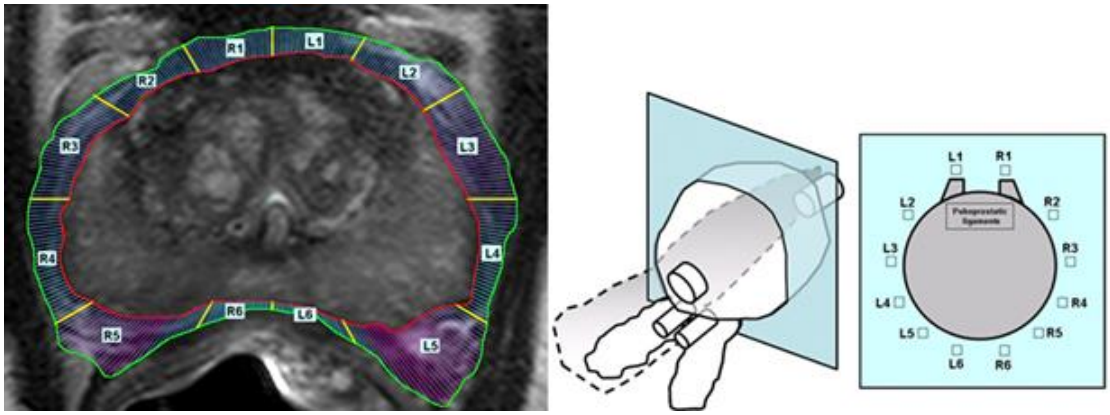

Fig 1. MRI image demonstrating the FT measurement; drawn contours and - clockwise - the 12 parts (corresponding with the FP score) consisted of 360 radial lines, color-coded for the prostate-fascia distance (the more pink, the thicker the fascia and the more blue, the thinner the fascia). Distribution of 12 levels of fascia preservation, corresponding FP-region with region on MRI ('L1' stands for FP-region 1 on the left side of the prostate, 'R1' stands for FP-region 1 on the right side of the prostate).[10] FT, fascia thickness; FP, fascia preservation.

Pelvic MRI Measurements

MRI was performed using a 3 tesla system (Philips, Best, the Netherlands) with an endorectal coil. T2-weighted (sagittal, axial and coronal plane; around 60 images), T1-weighted, diffusion-weighted images and Dynamic Contrast-Enhanced (DCE) images were obtained. For the standard DCE-MRI examination 15 ml of the contrast agent Dotarem (Gadoteric acid, concentration 0,5M) was administered intravenously. The axial T2 TSE sequence, with a slice thickness in the axial plane of 3 mm and matrix size of 512 × 512, was used for further analysis. Images were analysed with a DICOM viewer PACS (Carestream Health, Inc., Rochester, NY) and tagged image file format TIFF-images of the required slice of the prostate were saved for further analysis. All measurements were done by two observers blinded to outcome. The distance between posterior margin of bladder neck and seminal vesicles, the narrowest distance from inner border of levator muscle to urethra below the caudal margin of the prostatic apex (ILD), the length of the prostate, the MUL in the coronal and sagittal view, the levator and anterior sphincter thickness, the urethral and

prostate volume were measured.

Fascia thickness assessment

A semi-automated macro in ImageJ (Laboratory for Optical and Computational Instrumentation (LOCI), University of Wisconsin-Madison, USA) was constructed to measure FT in the TIFF images generated from the DICOM files. Manual delineation of prostate and fascia outlines was done at 12 circumferential positions surrounding the prostate and 360 lines radiating out from the centre were generated (Fig. 1). Hereafter, the periprostatic fascia was divided into 12 (30 degree) parts: each part corresponding to the aforementioned FP score dodecagon. Because normal distribution does not apply to the results of the delineations, the median length of FT of the 12 regions was used. The sum of these 12 median measurements was called total FT. The total saved fascia (i.e. the sum of the saved FT segments) was also calculated in order to combine FT and FP score and obtain an estimate of the volume of saved fascia tissue. Finally, we calculated a variable called the Median Fascia Ratio by dividing total saved fascia by the sum of the 12 parts of the total median FT in order to obtain an estimate of the percentage of the fascia volume that was saved.

Outcome Assessment

The primary outcome was postoperative incontinence, defined as any involuntary urine loss irrespective of inlay use or amount of urine loss, according to ICIQ-SF. The answers from ICIQ-SF result in a sum, with minimum score of 0, and maximum score of 21. Only patients who answered “never” on question 4a (When does urine leak?) were considered continent. To assess the severity of UI[11] the ICIQ-SF total scores were recoded into four levels of incontinence: slight (1–5), moderate (6–12), severe (13–18) and very severe (19–21). The form was completed by the patient preoperatively and at each follow-up visit i.e. every 6 months for the first 2 years after surgery and yearly thereafter.

Statistical analysis

Comparison of clinical and pathologic characteristics between the continence and incontinence group was done using the Student t test. Kaplan-Meier curve estimates using log-rank statistics were performed to compare the recovery of continence while Cox proportional hazards method for multivariate analyses was used to determine predictive factors for early continence recovery. In addition a binary logistic regression analysis was performed in order to create a predictive model for continence outcome. We evaluated the discrimination of a base model that included age, clinical stage, Gleason score, PSA and BMI to that of a model that included in addition the variables found significant in the multivariate, binary logistic regression analysis. Odds ratios (OR) and confidence intervals (CI) are reported. Discrimination was measured using the area under the curve (AUC) of the receiver operating characteristics (ROC) analysis and corrected for statistical optimism using bootstrap methods. Variables in the final model that exhibited a significant independent association with the outcome at a P-value of less than 0.05 were considered as risk factors. Finally, we developed an interactive risk calculator using the variables that exhibited a significant independent association with continence outcome. SPSS software ver. 22.0 (SPSS Inc., Chicago, IL) was used to perform the statistical analysis.

Results

Median follow up was 16 months (interquartile range: 12-24 months). Patient characteristics and preoperative MRI measurements are presented in Table 1. 50.8% of the patients reported any involuntary urinary loss at the end of follow up. Continent patients had longer mean MUL (12.9 mm vs 11.5 mm, $p < 0.0001$) as well as higher mean FT (49.1 mm vs 46.1 mm, $P = 0.035$) and FP score (4 vs 3.1, $P = 0.003$) and higher mean saved fascia (14.8 vs 11.8, $P = 0.017$) compared to incontinent patients. No difference in the rest of the demographic and MRI measurements was observed between the two groups.

Table 1. Summary of patient characteristics and MRI dimensions.			
	Continent men (n = 216)	Incontinent men (n = 223)	P-value

Mean age at surgery (years) (SD)	62.4 (6.3)	63.5 (6.1)	0.083
Mean BMI (kg/m^2) (SD)	26.1 (3.4)	26.6 (3.1)	0.12
Mean PSA (ng/ml) (SD)	9.5 (6.2)	10.3 (11.2)	0.321
No. clinical stage (%)			0.232
T1c	50 (23.1)	49 (22)	
T2	131 (60.6)	124 (55.6)	
T3	35 (16.2)	50 (22.4)	
Mean Gleason sum score (SD)	6.9 (0.8)	6.8 (0.9)	0.282
Mean total FT (mm) (SD)	49.1 (11.7)	46.9 (9.6)	**0.035**
Mean total saved fascia (mm) (SD)	14.8 (13.2)	11.8 (11.5)	**0.017**
% Mean Fascia Ratio (SD)	30.4 (25.2)	26.7 (25.3)	0.145
Mean FP score (SD)	4.0 (3.1)	3.1 (3.0)	**0.003**
Mean MRI variables (SD):			
MUL, sagittal view (mm)	12.9 (1.7)	11.5 (1.5)	**<0.0001**
MUL, coronal view (mm)	12.9 (1.6)	11.6 (1.6)	**<0.0001**
ILD (mm)	15.4 (2.2)	16.6 (2.6)	**<0.0001**
Prostate size (cm^3) (SD)	49.2 (68.1)	44.5 (19.3)	0.323
Prostate height (mm)	44.7 (7.5)	45.4 (7.7)	0.331
Bladder-seminal vesicles distance (mm)	5.0 (1.0)	4.9 (1.1)	0.129
Prostate length (anterior-posterior) (mm)	33.2 (7.5)	33.4 (8.5)	0.84
Prostate length (lateral) (mm)	51.6 (6.9)	52.0 (7.3)	0.578

Maximal urethra diameter (mm)	11.2 (1.9)	11.3 (1.8)	0.162
Right levator muscle thickness (mm)	11.2 (1.7)	11.4 (1.4)	0.426
Left levator muscle thickness (mm)	11.2 (1.9)	11.3 (1.8)	0.386
Anterior sphincter thickness (mm)	4.6 (0.8)	4.5 (0.7)	0.263
Urethral volume (cm^3)	99.9 (21.1)	101.5 (20.5)	0.404

Postoperative severity of incontinence

Regarding the severity of UI, most of the patients had slight and moderate (62.8% and 28.4%, respectively) while 8.4% and 0.4% of the patients had severe and very severe incontinence, respectively. We compared slight UI with moderate-severe UI. The severity was only correlated with lower FP score ($P < 0.0001$), shorter MUL ($P < 0.0001$) and lower total saved fascia ($P = 0.001$).

Predictors for postoperative duration of continence recovery

In the Cox univariate analysis (Table 2) higher FT (OR 1.014; CI 1.001, 1.027; $P = 0.036$), higher FP score (OR 1.045; CI 1.002, 1.090; $P = 0.041$), shorter ILD (OR 0.882, CI 0.835, 0.931; $P < 0.0001$) and longer MUL (OR 1.347; CI 1.258, 1.448; $P < 0.0001$) were predictors of shorter continence recovery time (Fig.2a and Fig. 2b). In the multivariate analysis only a longer MUL (OR 1.309; CI 1.211, 1.415; $P < 0.0001$) and shorter ILD (OR 0.904; CI 0.850, 0.961; $P = 0.001$) were independent predictors of earlier continence recovery.

Table 2. Cox univariate and multivariate analysis of clinical and MRI variables predicting continence recovery rate.						
Variables	Univariate			Multivariate		
	Odds	95% CI	P-value	Odds	95% CI	P-value
Age	0.986	0.966-1.007	0.203			
BMI	0.967	0.93-1.006	0.098			
PSA	0.991	0.975-1.008	0.308			
Clinical stage			0.52			
T2 vs T1	1.009	0.728-1.398	0.959			
T3 vs T1	0.352	0.528-1.255	0.352			
Gleason sum score	1.097	0.943-1.275	0.231			
Total FT	1.014	1.001-1.027	**0.036**	1.007	0.995-1.020	0.262
Total saved fascia	1.009	0.998-1.020	0.127			
% Fascia Ratio	1.173	0.676-2.033	0.571			
FP score	1.045	1.002-1.090	**0.041**	1.021	0.974-1.069	0.39
MUL, sagittal view	1.347	1.254-1.448	**<0.0001**	1,309	1.211-1.415	**<0.0001**
MUL, coronal view	1.293	1.200-1.393	**<0.0001**			
ILD	0.882	0.835-0.931	**<0.0001**	0.904	0.850-0.961	**0.001**
Prostate size	1.001	0.999-1.003	0.206			

Prostate height	0.995	0.978-1.013	0.607			
Bladder-seminal vesicles distance	1.032	0.916-1.664	0.602			
Prostate length (anterior-posterior)	1.000	0.984-1.017	0.963			
Prostate length (lateral)	0.995	0.976-1.013	0.566			
Maximal urethra diameter	0.947	0.862-1.041	0.261			
Right levator muscle thickness	0.978	0.911-1.050	0.537			
Left levator muscle thickness	0.985	0.918-1.056	0.661			
Anterior sphincter thickness	1.075	0.907-1.275	0.403			
Urethral volume	0.998	0.992-1.005	0.583			

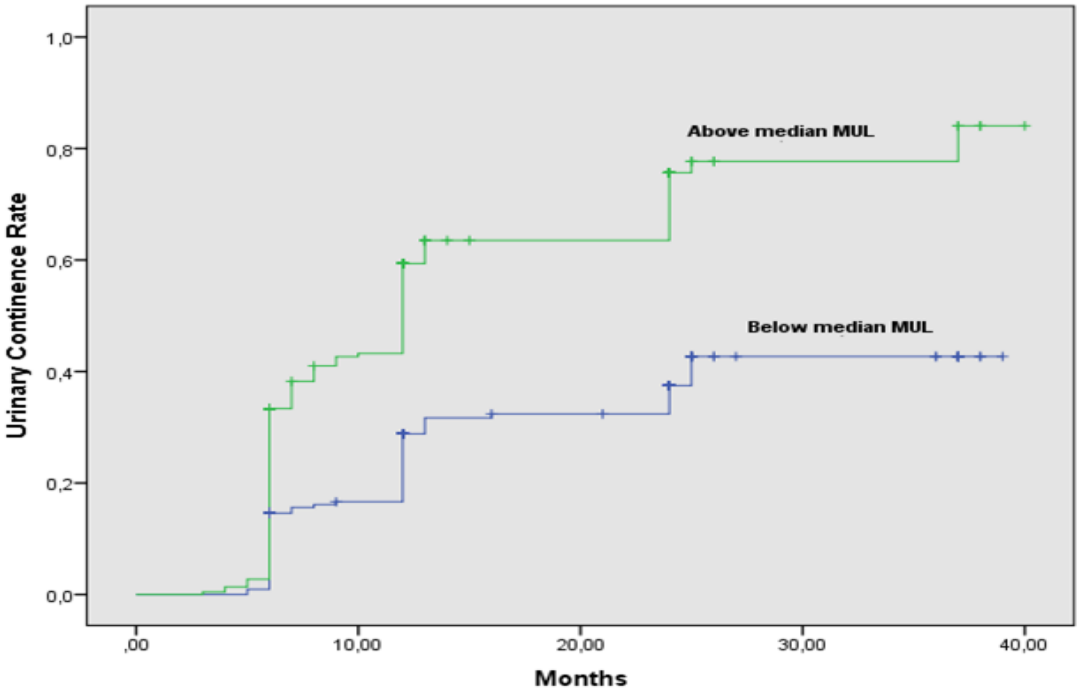

Fig 2a. Kaplan Meier curve of continence recovery rate, stratified by the median (12.1 mm) MUL (long rank test, P<0.0001).

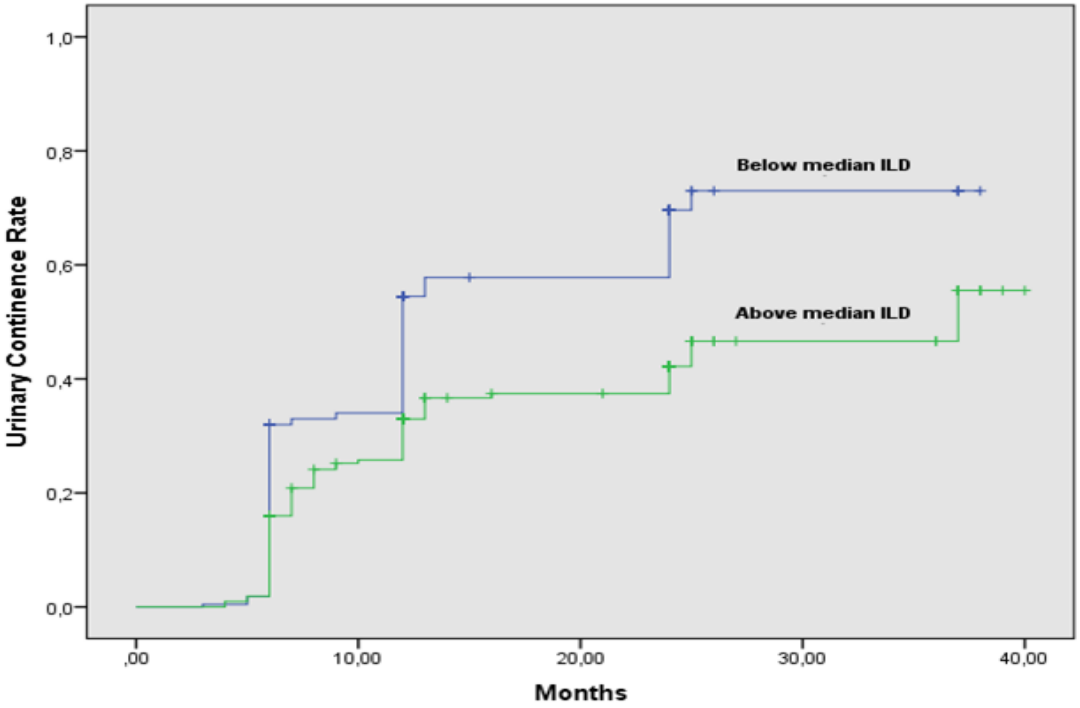

Fig 2b. Kaplan Meier curve of continence recovery rate, stratified by the median (15.8 mm) ILD (long rank test, P<0.0001).

Prediction model for postoperative continence

In the multivariate binary logistic regression analysis (Table 3) longer MUL (OR 1.565; CI 1.362, 1.798; P < 0.0001), shorter ILD (OR 0.819, CI 0.742, 0.904; P < 0.0001) and higher FP score (OR 1.089, CI 1.011, 1.172; P = 0.024) were independent predictors of continence outcome. The discrimination of the base model was low (bootstrap corrected AUC = 0.584) while it was significantly increased with the addition of FP score (AUC = 0.613), ILD (AUC = 0.694) and MUL (AUC = 0.779). In the developed predictive model, maximal nerve preservation (FP score = 12) improved the continence recovery by 5-30% points for all measures of MUL. A risk calculator based on FP score, MUL and ILD predicted continence recovery between 1.3% and 99% on a patient level (% continence propability=(EXP(-2,57+(0.472*MUL)+(0.107*FP)-(0.225*ILD))/(1+EXP(-2.57+(0.472*MUL)+(0.107*FP)-(0.225*ILD)))

Table 3. Univariate and multivariate binary logistic regression analysis of clinical and MRI variables predicting continence outcome.

Variables	Univariate			Multivariate		
	Odds	95% CI	P-value	Odds	95% CI	P-value
Age	0.974	0.945-1.004	0.084			
BMI	0.948	0.895-1.005	0.073			
PSA	0.989	0.968-1.011	0.327			
Clinical stage			0.26			
T2 vs T1c	1.035	0.651-1.647	0.883			
T3 vs T1c	0.686	0.382-1.231	0.206			

Gleason sum score	1.125	0.907-1.394	0.720			
Total FT (mm)	1.020	1.001-1.039	**0.036**	1.017	0.996-1.039	0.11
Total saved fascia (mm)	1.020	1.003-1.036	**0.018**			
% Median Fascia Ratio	1.784	0.819-3.888	0.145			
FP score	1.100	1.035-1.170	**0.002**	1.089	1.011-1.172	**0.024**
MUL, sagittal view	1.654	1.453-1.883	**<0.0001**	1.565	1.362-1.798	**<0.0001**
MUL, coronal view	1.583	1.393-1.799	**<0.0001**			
ILD	0.812	0.748-0.882	**<0.0001**	0.819	0.742-0.904	**<0.0001**
Prostate size	1.003	0.997-1.008	0.393			
Prostate height	0.988	0.964-1.012	0.331			
Bladder-seminal vesicles distance	1.145	0.961-1.364	0.13			
Prostate length (anterior-posterior)	0.988	0.974-1.021	0.84			
Prostate length (lateral)	0.998	0.967-1.019	0.577			
Maximal urethra diameter	0.908	0.793-1.039	0.162			
Right levator muscle thickness	0.959	0.865-1.063	0.425			

Left levator muscle thickness	0.957	0.865-1.057	0.385			
Anterior sphincter thickness	1.152	0.899-1.476	0.263			
Urethral volume	0.996	0.987-1.005	0.403			

Discussion

Prostate removal by any surgical method results in structural and functional changes of the components of the urinary sphincter complex which is inherently related to the structure and function of the membranous urethra. To improve post-prostatectomy continence, it remains crucial to know which pelvic floor structures and prostate fascia areas are associated with urine control. To our knowledge, our study is the first to investigate a quantitative measure of FP in combination with preoperative pelvic MRI measurements as prognostic factors for continence recovery after RARP.

In our cohort, patients with FT and FP score above the median values (39.7 mm and three, respectively) had significant higher chance to be continent at 12 months after RARP (34.4% vs 45.5% and 37% vs 50.8%, respectively) while maximal FP improved the continence recovery by 5-30% for all measures of MUL. A systematic review confirmed the association between FP and postoperative continence recovery (12). Moreover, in a meta-analysis of 51 articles, complete musculo-fascial reconstruction showed a 30% increase in urinary continence 3 months after RARP (13).

It remains unclear how FP improves postoperative continence. Urethral sphincter innervation, from pudendal nerve and pelvic plexus, is anatomically closely related to the prostate apex and it is often found to be adversely affected in men with postprostatectomy incontinence (13). There is also a debate about the role and extent of the contribution of the NVBs to the innervation of the external urethral sphincter. Murphy et al. reported that NVBs might not contain

any somatic nerve supply while Strasser et al. have shown that NVBs directly innervate the membranous urethra (14,15). In a multicenter study Steineck et al. have recently demonstrated that the preservation of both NVBs during RRP and RARP decreased the rate of UI by two times 1 year after surgery (16). These findings suggest that not only erectile function but also continence may benefit from more extensive nerve sparing procedures.

In addition to FP, we focused on soft tissue measurements of the distal sphincteric complex which consists of the rhabdosphincter, the peraurethral skeletal musculature and the membranous urethra (17). According to our median value of MUL (12.1 mm) continence recovery at 1 year was 17.3% and 47%, for patients with MUL below and above median, respectively. There is insufficient evidence to propose an exact cut-off value. A recent meta-analysis has shown that every extra millimeter of MUL is associated with 9% greater odd for return to continence (18). It is considered that an increased MUL could result in a greater amount of smooth muscle fibers and rhabdosphincter preservation potentially increasing the length of the urethral pressure profile and gaining muscle volume for postoperative training (19).

In accordance to Bodman et al. we found that levator thickness was not significantly associated with continence recovery, but a more narrow levator muscle closely to the urethra as expressed by a shorter ILD, was identified as an independent predictor of UI (6). It seems that there are men in whom the levator muscles are tightly round to the prostate apex and membranous urethra, whereas in others the levator fibers are looser and more anatomically distant. A smaller ILD may prevent bladder descent after prostatectomy thereby avoiding opening of the bladder neck and incontinence.

In our analysis, age and BMI were not predictors of UI. A possible explanation may be the fact that our patients were relatively fit with a median age of 63 years and with a relatively low preoperative BMI (median value: 26.1). Kadono et al. also have shown that age and BMI were not related to post-RARP UI in a cohort of 111 patients (20). On the other hand, Matsushita et al. in a sample of 2.500 patients have demonstrated higher age and higher BMI were independent predictors of UI at 6 and 12 months after prostatectomy (21).

No correlation was also found between preoperative prostate size and UI, possibly related to the low median volume (40 cm^3) in our patients. Similar

results have been reported by Kadono et al. and by Pettus et al. in a cohort of more than 3000 patiemts (20,22).

Our high incontinence rate of 50.8% could be attributed to the strict criteria we chose for continence definition. Others have found higher rates of continence recovery using 0-1 pad-use as definition of continence (3). Using any, even a minimal, amount of urine loss as definition for UI is justified by our previous finding confirming that any urine loss rather than diaper use affected many aspects of quality of life (8). In addition, in our population, no men underwent any form of reconstruction of the pelvic floor and our UI rates were similar to earlier reported analyses where no reconstruction (23) or only posterior vesicourethral reconstruction (24) was performed. Compared to the reconstruction of the posterior musculofascial plate of Denonvilliers fascia (Rocco stich), Student et al. have shown a 40% improvement in UI rate at 12 months after additionally including the fibres of the levator ani muscle, the retrotrigonal layer and the median dorsal raphe in the reconstruction of vesicourethral support (24). Moreover, vas deferens urethral support during RARP has been shown to improve early postoperative UI by 40% in a randomized study (25). Finally, Retzius-sparing RARP, which avoids all the Retzius structures involved in continence, achieved 96% continence rate at 12 months in a prospective study with 200 patients (26).

Limitations

The limitations of this study include those inherent to a retrospective analysis of prospectively collected data. Moreover, the selection of patients for FP was based on preoperative patients' factors, while preoperatively erectile function may have influenced the extent of preservation. We also lacked comorbidity data which could influence continence recovery, such as the rate of diabetic patients. There was also no possibility to record the amount of urinary leakage since no pad-test data were obtained. Still we feel that the well-defined population with meticulous QOL follow up avoids bias e.g. by missing data. A major limitation of MRI is its interobserver variability in the measurements while the endorectal probe might have had an impact on the soft tissue dimensions

measurements. We therefore cannot generalize our observations to mpMRI without an endorectal coil.

Conclusions

More extensive fascia preservation as well as longer MUL and shorter ILD independently predict improved continence recovery after RARP. A developed risk prediction model is of potential value to clinicians for patient counselling prior to surgery. Patients with a (preoperative) high risk of postoperative incontinence could be identified, in whom FP techniques could be applied, even in those where erectile function preservation is not needed. Further improvements and validation are needed before implementing this ‘continence’ prediction model in clinical practice.

References

1. Ficarra V, Sooriakumaran P, Novara G, et al. Systematic review of methods for reporting combined outcomes after radical prostatectomy and proposal of a novel system: the survival, continence, and potency (SCP) classification. Eur Urol 2012;61:541-8.
2. Eastham JA, Kattan MW, Rogers E, et al. Risk factors for urinary incontinence after radical prostatectomy. J Urol 1996;156:1707-13.
3. Ficarra V, Novara G, Rosen RC, et al. Systematic review and meta-analysis of studies reporting urinary continence recovery after robot-assisted radical prostatectomy. Eur Urol 2012;62:405-17.
4. Sandhu JS, Eastham JA. Factors predicting early return of continence after radical prostatectomy. Curr Urol Rep 2010;11:191-7.
5. Tienza A, Hevia M, Benito A, et al. MRI factors to predict urinary incontinence after retropubic/laparoscopic radical prostatectomy. Int Urol Nephrol 2015;47:1343-9.
6. von Bodman C, Matsushita K, Savage C, et al. Recovery of urinary function after radical prostatectomy: predictors of urinary function on preoperative prostate magnetic resonance imaging. J Urol 2012;187:945-50.
7. Sievert KD, Hennenlotter J, Laible I, et al. The periprostatic autonomic nerves--bundle or layer? Eur Urol 2008;54:1109-16.
8. van der Poel HG, de Blok W, Joshi N, van Muilekom E. Preservation of lateral prostatic fascia is associated with urine continence after robotic-assisted prostatectomy. Eur Urol 2009;55:892-900.
9. Avery K, Donovan J, Peters TJ, et al. ICIQ: a brief and robust measure for evaluating the symptoms and impact of urinary incontinence. Neurourol Urodyn 2004;23:322-30.
10. van der Poel HG, de Blok W. Role of extent of fascia preservation and erectile function after robot-assisted laparoscopic prostatectomy. Urology 2009;73:816-21.
11. Klovning A, Avery K, Sandvik H, Hunskaar S. Comparison of two questionnaires for assessing the severity of urinary incontinence: The

ICIQ-UI SF versus the incontinence severity index. Neurourol Urodyn 2009;28:411-5.

12. Heesakkers J, Farag F, Bauer RM, et al. Pathophysiology and Contributing Factors in Postprostatectomy Incontinence: A Review. Eur Urol 2016 Oct 6. pii: S0302-2838(16)30666-2. doi: 10.1016/j.eururo.2016.09.031. [Epub ahead of print]
13. Hollabaugh RS Jr, Dmochowski RR, Kneib TG, Steiner MS. Preservation of putative continence nerves during radical retropubic prostatectomy leads to more rapid return of urinary continence. Urology 1998;51:960-7.
14. Murphy DG, Costello AJ. How can the autonomic nervous system contribute to urinary continence following radical prostatectomy? A "boson-like" conundrum. Eur Urol 2013;63:445-7.
15. Strasser H, Bartsch G. Anatomic basis for the innervation of the male pelvis. Urologe A 2004;43:128-32.
16. Steineck G, Bjartell A, Hugosson J, et al. Degree of preservation of the neurovascular bundles during radical prostatectomy and urinary continence 1 year after surgery. Eur Urol 2015;67:559-68.
17. Nguyen L, Jhaveri J, Tewari A. Surgical technique to overcome anatomical shortcoming: balancing post-prostatectomy continence outcomes of urethral sphincter lengths on preoperative magnetic resonance imaging. J Urol 2008;179:1907-11.
18. Mungovan SF, Sandhu JS, Akin O, et al. Preoperative Membranous Urethral Length Measurement and Continence Recovery Following Radical Prostatectomy: A Systematic Review and Meta-analysis. Eur Urol 2017;71:368-378.
19. Chang JI, Lam V, Patel MI. Preoperative Pelvic Floor Muscle Exercise and Postprostatectomy Incontinence: A Systematic Review and Meta-analysis. Eur Urol 2016;69:460-7.
20. Kadono Y, Ueno S, Kadomoto S, et al. Use of preoperative factors including urodynamic evaluations and nerve-sparing status for predicting urinary continence recovery after robot-assisted radical prostatectomy: Nerve-sparing technique contributes to the reduction of postprostatectomy incontinence. Neurourol Urodyn 2016;35:1034-1039.

21. Matsushita K, Kent MT, Vickers AJ, et al. Preoperative predictive model of recovery of urinary continence after radical prostatectomy. BJU Int 2015;116:577-83.
22. Pettus JA, Masterson T, Sokol A, et al. Prostate size is associated with surgical difficulty but not functional outcome at 1 year after radical prostatectomy. J Urol 2009;182:949-55.
23. Tewari A, Jhaveri J, Rao S, et al. Total reconstruction of the vesico-urethral junction. BJU Int 2008;101:871-7.
24. Student V Jr, Vidlar A, Grepl M, et al. Advanced Reconstruction of Vesicourethral Support (ARVUS) during Robot-assisted Radical Prostatectomy: One-year Functional Outcomes in a Two-group Randomised Controlled Trial. Eur Urol 2016 Jun 6. pii: S0302-2838(16)30201-9. doi: 10.1016/j.eururo.2016.05.032. [Epub ahead of print]
25. van der Poel HG, De Blok W, Van Muilekom HA. Vas deferens urethral support improves early post-prostatectomy urine continence. J Robot Surg 2012;6:289-94.
26. Galfano A, Di Trapani D, Sozzi F, et al. Beyond the learning curve of the Retzius-sparing approach for robot-assisted laparoscopic radical prostatectomy: oncologic and functional results of the first 200 patients with ≥ 1 year of follow-up. Eur Urol 2013;64:974-80.

Summary

The local lymph nodes (LN) status is a major prognostic factor in prostate cancer (PCa). The low sensitivity of imaging techniques, the toxicity of extended pelvic lymph node dissection (ePLND) and the need to identify occult lymphatic metastases have encouraged the exploration of the sentinel node (SN). Sentinel node biopsy (SNB) is a minimal invasive technique with the advantage of histopathologic examination and confirmation of metastatic nodal disease resulting in a more accurate staging, avoiding the toxicity of ePLND.

Accurate PCa staging is critical in guiding a patient's treatment decision and it could prevent both under- and overtreatment. Local staging with multiparametric (mp)-MRI has become widely available and provides new diagnostic means to assess the local extent of prostate tumours. Another new application of MRI is the classification of benign prostate hyperplasia (BPH) patterns. Moreover, MRI has been used for non-invasively investigating the morphology and anatomy of the pelvic floor in order to assess the thickness of the multilayered peri-prostatic fascia which contains the neurovascular bundles (NVBs). These findings can be used for the preoperative prediction of functional results of radical prostatectomy, such as urinary incontinence (UI) and erectile dysfunction (ED).

Chapter 1 is a general introduction focusing on the role of SNB for determining LN status and the role of MRI for BPH classification, local staging of prostate cancer and prediction of UI and ED.

Chapter 2 assessed the efficacy of robotic-assisted laparoscopic sentinel lymph node dissection (SLND) to select those patients with PCa who would benefit from additional pelvic external beam radiation therapy and long-term androgen deprivation therapy (ADT). The 5-year biochemical recurrence (BCR)-free and metastasis free survival (MFS) rates for node negative (pN0) patients were 67.9% and 87.8%, respectively. The corresponding values for node positive (pN1) patients were 43% and 66.6%. The PSA level and number of removed SLNs were independent predictors of BCR and MFS, and pN status was an additional independent predictor of BCR. Patients in the higher quartiles of Kattan nomogram prediction of BCR had better than expected outcomes.

The complication rate from SLND was 8.9%. In conclusion, high staging accuracy of SLND is accompanied by low morbidity. The better than expected outcomes observed in the lower quartiles of BCR prediction suggest a role for SNB as a potential selection tool for the addition of pelvic radiation therapy and ADT in pN1 patients.

Chapter 3 evaluated the BCR after robot-assisted radical prostatectomy (RARP) and ePLND in PCa patients, stratified by the application of SNB. The results were compared with the predictions of the updated Memorial Sloan Kettering Cancer Center (MSKCC) nomogram. The 5-year BCR-free survival rate was 80.5% and 69.9% in the ePLND+SNB and ePLND group, respectively. At multivariate analysis, PSA, primary Gleason grade > 3, seminal vesicle invasion and higher number of removed and positive nodes were independent predictors of BCR in the ePLND group. In the ePLND+SNB group only the number of positive nodes was independent predictor of BCR. The overall accuracy of MSKCC nomogram was higher in the ePLND+SNB compared to the ePLND group. However, the nomogram was underestimating the probability of BCR-free status in the ePLND+SNB group, while the ePLND group was performing as predicted. However, our results should be interpreted cautiously, given the non-randomized nature and the selection bias of the study.

Chapter 4 aimed to externally validate the Winter nomogram and examines its performance in patients undergoing ePLND, ePLND combined SNB and SLND only. The results were compared with the MSKCC) and updated Briganti nomograms. Based on the area under the curve (AUC), the performance of Briganti nomogram (0.756) in the ePLND group was superior to both the MSKCC (0.744) and Winter nomogram (0.746). The Winter nomogram, however was the best predictor of LNI in both the ePLND+SNB (0.735) and sLND (0.709) populations. In the calibration analysis, all nomograms showed better accuracy in the low/intermediate risk patients while in the high-risk population an overestimation of the risk for LNI was observed.

Chapter 5 analyzed the staging accuracy of 3 tesla (3T) mp MRI by comparing the imaging report of seminal vesicle invasion (SVI) with the tissue histopathology. The additional value in the existing prediction models and the

role of radiologists' experience were examined. In the overall cohort, sensitivity, specificity, positive predictive value (PPV) and negative predictive value (NPV) for SVI detection on MRI were 75.9%, 94.7%, 62% and 97% respectively. Based on our sub-analysis, the radiologist's expertise improved the accuracy demonstrating a sensitivity, specificity, PPV and NPV of 85.4%, 95.6%, 70.0% and 98.2%, respectively. In the multivariate analysis PSA, primary Gleason Score (GS) 4 or 5 (OR 3.671, p = 0.007) and Partin estimates were significant predictors of SVI. When MRI results were added to the analysis, a significant prediction of SVI was observed (OR 45.9, p < 0.0001).

Chapter 6 investigated the association between BPH patterns, classified by preoperative mpMRI, with lower urinary tract symptoms (LUTS) or continence, preoperatively and after RARP. BPH patterns were significant predictors of preoperative LUTS. Prostates with pedunculated enlargement and bilateral transition zone (TZ) and/or retrourethral enlargement (pattern 5) gave more symptoms compared to bilateral TZ and retro-urethral enlargement (pattern 3) and bilateral TZ enlargement (pattern 1), while pattern 3 was additionally associated with more voiding symptoms compared to pattern 1. None of the BPH patterns were predictive of postoperative LUTS and continence. Independent predictors of continence at 12 months were lower preoperative PR25-LUTS score (P = .022) and longer membranous urethral length (P = .025).

Chapter 7 reports the correlation of preoperative fascia thickness (FT) and intraoperative fascia preservation (FP) with erectile function (EF) after nerve-sparing RARP. The neurovascular bundle is covered in the periprostatic fascia. To assess the role of the periprostatic fascia dimension and functional outcome periprostatic fascie dimension were measured on MRI.Median fascia thickness (MFT) per patient was defined as the sum of the median FT of 12 MRI regions. The preserved MFT (pMFT) was the sum of the saved MFT. The percentage of pFMT (ppMFT) was also calculated. Fascia surface (FS) was measured on MRI and it was combined with FP score resulting in preserved FS (pFS) and percentage of pFS (ppFS). FP score, pMFT and ppFS were significantly lower (p < 0.0001) in patients with ED. In the multivariate regression analysis lower FP score (odds ratio [OR] 0.721, p = 0.03) and lower ppMFT were independent

predictors of ED. ROC analysis showed the highest area under the curve for ppMFT (0.787) and FP score (0.767) followed by pMFT (0.755) and ppFS (0.743).

Chapter 8 examined whether preoperative prostate/pelvic anatomical structures and intraoperative FP predict continence recovery after RARP. In the Cox multivariate analysis, longer membranous urethral length (MUL) and shorter inner levator distance (ILD) were predictors of earlier continence recovery. In the multivariate binary logistic regression analysis longer, shorter ILD and higher FP score were independent predictors of continence outcome.

Samenvatting

De lokale lymfeklier (LN) status is een belangrijke prognostische factor bij prostaatkanker (PCa). De lage gevoeligheid van de beeldvormingstechnieken, de toxiciteit van uitgebreide bekken-lymfeklierdissectie (ePLND) en de noodzaak om occulte lymfekliermetastasen te identificeren, hebben de exploratie van schildwachtklier (SN) methoden gestimuleerd. De selectieve schildwachtklierbiopsie (SNB) heeft het voordeel van histopathologisch onderzoek en bevestiging van metastatische nodale ziekte resulterend in een meer nauwkeurige stadiëring, met het potentieel om de toxiciteit van ePLND te verminderen.

Nauwkeurige PCa-stadiering is van cruciaal belang bij de behandelkeuzes van een patiënt en kan zowel onder- als overbehandeling voorkomen. De diagnostiek naar lymfekliermetastasen staat ter discussie met name omdat het betrouwbaar vaststellen van microscopische metastasen vooralsnog preoperatief niet mogelijk is. Beeldvorming van lymfeklieren wordt dan ook alleen nog geadviseerd bij mannen met een verhoogde kans op macroscopische metastasen. De zogenaamde schildwachtklier methode (SNB) maakt het mogelijk om gericht die lymfklieren te verwijderen en pathologisch te onderzoeken met de grootste kans op (microscopische) metastasen. Deze methode wordt al veel toegepast bij borstkanker, peniskanker en het melanoom en blijkt veel gevoeliger dan beeldvorming. De preciese rol SNB bij prostaatkanker is nog niet bekend.

Lokale stadiëring met multiparametrische (mp-)MRI is breed beschikbaar geworden en biedt nieuwe diagnostische middelen om de lokale omvang van prostaattumoren te beoordelen. Een andere nieuwe toepassing van MRI is de classificatie van goedaardige prostaathyperplasie (BPH) -patronen. Bovendien is MRI gebruikt voor het niet-invasief onderzoeken van de morfologie en anatomie van de bekkenbodem om de dikte van de meerlagige peri-prostatische fascia te bepalen die de neurovasculaire bundels (NVB's) bevat. Deze bevindingen kunnen worden gebruikt voor de preoperatieve voorspelling van functionele resultaten van radicale prostatectomie, zoals urine-incontinentie (UI) en erectiestoornissen (ED).

Hoofdstuk 1 is een algemene introductie gericht op de rol van SNB voor het bepalen van de LN-status en de rol van MRI voor BPH-classificatie, lokale stadiëring van prostaatkanker en voorspelling van UI en ED.

In **Hoofdstuk 2** onderzochten we de effectiviteit van de laparoscopische schildwachtklier lymfeklierdissectie (SLND) om prostaatkankerpatiënten te selecteren die baat zouden hebben bij extra externe bekkenbestraling op de lymfklieren en langdurige androgeendeprivatie therapie (ADT). De 5-jaars biochemische recidief (BCR) -vrije en metastasevrije overleving (MFS) voor kliermetastase-negatieve (pN0) patiënten was respectievelijk 67,9% en 87,8%. De overeenkomstige waarden voor lymfekliermetastase-positieve (pN1) patiënten waren 43% en 66,6%. Het PSA-niveau en het aantal verwijderde SLN's waren onafhankelijke voorspellers van BCR en MFS en de pN-SNB-status was een aanvullende onafhankelijke voorspeller van BCR. Patiënten in de hogere kwartielen van de Kattan-nomogramvoorspelling van BCR hadden beter dan verwachte resultaten. In 8,9% van de patienten die een SLND ondergingen ontstond een complicatie door de ingreep. Concluderend ging de hoge nauwkeurigheid van SLND-stadiering gepaard met een lage morbiditeit. De beter dan verwachte resultaten waargenomen in de onderste kwartielen van de BCR-voorspelling suggereren een rol voor SNB als selectie voor patienten voor bekkenbestraling en ADT.

In **Hoofdstuk 3** evalueerden we de BCR na robot-geassisteerde radicale prostatectomie (RARP) en ePLND bij PCa-patiënten, gestratificeerd naar de toepassing van SNB. De resultaten werden vergeleken met de voorspellingen van het bijgewerkte nomogram van het Memorial Sloan Kettering Cancer Center (MSKCC) voor voorspelling van prognose. De 5-jaars BCR-vrije overleving was respectievelijk 80,5% en 69,9% in de ePLND + SNB-groep versus de ePLND-groep. Bij multivariate analyse waren de preoperatieve PSA, primaire Gleason graad > 3, zaadblaasjesinvasie en een hoger aantal verwijderde en positieve klieren onafhankelijke voorspellers van BCR in de ePLND-groep. In de ePLND + SNB-groep was alleen het aantal gevonden klieren met metastasen een onafhankelijke voorspeller van BCR. De algehele

nauwkeurigheid van het MSKCC-nomogram was hoger in de ePLND + SNB vergeleken met de ePLND-groep. Het nomogram onderschatte echter de kans op BCR-vrije status in de ePLND + SNB-groep, terwijl in de ePLND-groep de voorspelling correct was. Deze observatie suggereert een therapeutisch voordeel van het toevoegen van de SNB aan de ePLND. Een mogelijke verklaring hiervoor zou kunnen zijn dat door het toevoegen van SNB er betere detectie en verwijdering mogelijk was van klieren die metastasen bevatten. Onze resultaten moeten echter voorzichtig worden geïnterpreteerd, gezien de niet-gerandomiseerde aard en de selectiebias van het onderzoek.

Het Winter nomogram voorspelt de kans op een positieve SNB bij patienten met prostaatkanker. Het onderzoek beschreven in **Hoofdstuk 4** had tot doel om het Winter nomogram extern te valideren in onze patientenpopulatie en de voorspelling van het nomogram te onderzoeken bij patiënten die ePLND, ePLND gecombineerd, alleen SNB en SLND ondergingen. De resultaten werden vergeleken met de MSKCC en de bijgewerkte Briganti nomogrammen. Op basis van het oppervlak onder de curve (AUC) in de ROC-curve analyse was de voorspelling met het Briganti nomogram (0,756) in de ePLND-groep superieur aan zowel het MSKCC (0,744) als het Winter-nomogram (0,746). Het Winter nomogram was echter de beste voorspeller van LNI in zowel de ePLND + SNB (0,735) en sLND (0,709) populaties. In de kalibratieanalyse vertoonden alle nomogrammen een betere nauwkeurigheid bij patiënten met laag / intermediair risico, terwijl in de patientenpopulatie met een hoog risico een overschatting van het risico op LNI werd waargenomen.

In **Hoofdstuk 5** analyseren we nauwkeurigheid van 3 tesla (3T) mp-MRI voor de preoperatieve detectie van ingroei van tumor in de zaadblaasjes (SVI). We vergelijken de preoperatieve mpMRI met de weefselhistopathologie van de prostatectomie. De toegevoegde waarde in de bestaande voorspellingsmodellen en de rol van de ervaring van radiologen werden onderzocht. De sensitiviteit specificiteit, positief voorspellende waarde (PPV) en negatief voorspellende waarde (NPV) voor SVI-detectie op MRI waren respectievelijk 75,9%, 94,7%, 62% en 97%. In de subanalyse naar de ervaring van de radioloog verbeterde de expertise van de radioloog de nauwkeurigheid met een sensitiviteit, specificiteit, PPV en NPV van respectievelijk 85,4%,

95,6%, 70,0% en 98,2%. In de multivariate analyse waren het PSA, een primaire Gleason graad 4 of 5 (OR 3,671, p = 0,007) en het Partin-nomogram voorspelling significante voorspellers van SVI. Wanneer MRI-resultaten aan de analyse werden toegevoegd, werd een zeer significante voorspelling van SVI waargenomen (OR 45,9, p <0,0001).

In **Hoofdstuk 6** onderzochten we de associatie tussen BPH-patronen, geclassificeerd met preoperatieve mp-MRI en plasklachten (LUTS) en urinecontinentie, zowel pre-operatief als na RARP bij mannen met een geschat preoperatief prostaatvolume > 50 cc. BPH-patronen op mpMRI waren gecorreleerd met pre-operatieve LUTS. Mannen met een middenkwab of met bilaterale overgangszone (TZ) en/of retro-urethrale vergroting (patroon 5) hadden preoperatief ernstigere symptomen dan mannen met bilaterale TZ en retro-urethrale vergroting (patroon 3) en bilaterale TZ-uitbreiding (patroon 1). Patroon 3 werd bovendien geassocieerd met meer mictiesymptomen in vergelijking met patroon 1. Geen van de BPH-patronen was voorspellend voor postoperatieve LUTS en continentie. Onafhankelijke voorspellers van continentie na 12 maanden waren een lagere pre-operatieve PR25-LUTS-score (P = 0,022) en een langere membraneuze urethrale lengte (P = 0,025).

In **Hoofdstuk 7** onderzochten we de correlatie tussen pre-operatieve fasciedikte (FT) op mpMRI en intra-operatief fasciabehoud (FP) met erectiele functie (EF) na zenuwsparende RARP. De neurovasculaire bundel naast de prostaat loopt door de periprostatische fascie. Om de rol van de dikte van de periprostatische fascie en de functionele uitkomsten na prostatectomie te bepalen werd de dikte van deze fascie gemeten op de preoperatieve mp-MRI voor prostatectomie. Mediane fasciadikte (MFT) gemeten op 12 locaties rond de prostaat met mpMRI werd gedefinieerd als de som van de mediane periprostatische fascie dikte (FT). De behouden MFT (pMFT) was de hoeveelheid gespaarde periprostatische fascie na de prostatectomie. Het percentage gespaarde fascie (ppMFT) werd ook berekend als: pMFT/MFT. Naast gemeten dikte van de fascie werd ook het fascie-oppervlak (FS) gemeten op mpMRI. Door deze meting te combineren met de geschatte hoeveelheid gespaarde periprostatische fascie (FP-score) werd de hoeveelheid (pFS) en het percentage gespaarde fasie (ppFS) berekend. FP-score, pMFT, en ppFS

waren significant lager (p <0,0001) bij patiënten met postoperatief ED. In de multivariate regressieanalyse waren een lagere FP-score (odds ratio [OR] 0.721, p = 0.03) en een lager ppMFT onafhankelijke voorspellers van ED. ROC-analyse toonde het hoogste gebied onder de curve voor ppMFT (0,787) en FP-score (0,776) gevolgd door pMFT (0,705) en ppFS (0,743).

In **Hoofdstuk 8** beschreven we het onderzoek naar of de pre-operatieve anatomische structuren van de prostaat en het bekken en intra-operatieve FP het continentieherstel na RARP voorspelden. In de Cox multivariate analyse waren langere membraneuze urethra lengte (MUL) en kortere binnenste levator afstand (ILD) voorspellers van eerder herstel van continentie. In de multivariate binaire logistische regressieanalyse waren een langere MUL, een smallere ILD en een hogere FP-score onafhankelijke voorspellers van de continentie-uitkomst na prostatectomie.

Aknowledgements

I am grateful to European Association of Urology (EAU) for the support with EAU Scholarship Programme. I am also extremely grateful to my Promotor Professor Simon Horenblas, all the staff urologists in NKI and especially dr. Esther Wit and dr. Axel Bex, the fellows; dr Teele Kuusk, the residents, the surgical nurses and Urology department's secretary for their tolerance, support and kind help in whatever I asked during my stay in Netherlands. A special note should be done for my co-promotor, dr. Henk van der Poel for the research and surgical opportunities that he offered to me and the endless hours he spent assisting and guiding me, starting in 2014 with his positive reply to my email application to come in NKI and still continuing with this thesis and many other research projects.

I would also like to express my deepest regards to the colleagues from Radiology Department, and especially Professor Regina Beets-Tan, dr Stijn Heijmink for being also my co-promotor and dr Ivo Schoots for their valuable support and guidance from my first days in NKI and for their crucial role as co-authors in most of the studies of this thesis. Not to forget dr Floris Pos from Radiation Oncology Department, dr Jeroen de Jong from Pathology Department and dr Fijs van Leeuwen from Leiden University Medical Centre who were co-authors in many of the studies included on this thesis.

Finally I would like to express my regards to my wife and small daughter for their tolerance and support expecially during my 1 year stay in NKI.

About the author

Dr Nikolaos Grivas graduated from Medical School in University of Ioannina, Greece in 2006 and in 2013 he finished his PhD study at the same University. He completed his urology training in Hatzikosta General Hospital of Ioannina, Greece in 2014. Recently he finished his fellowship in the Urology Department of Netherlands Cancer Institute, NKI-Avl in Amsterdam. He stayed 1 year in this center of excellence where he was trained in the robotic urological surgery and involved in many research projects with main focus in the fields of sentinel nodes and functional/oncological outcomes after robot-assisted radical prostatectomy. Currently he is a Consultant Urologist in Hatzikosta General Hospital of Ioannina and he is scientifically affiliated with Netherlands Cancer Institute, NKI-Avl.

The last 3 years he is an associate member of European Association of Urology (EAU) guidelines panel of Urolithiasis. He is also a member of Young Academic Urologists (YAU) Robotics group. He has received 5 awards at three European congresses and in 2016 he received the Best Young Urologist Award in Greece. He has 30 publications in peer-reviewed journals while he is a reviewer for 16 urological journals. He also belongs to the editorial board of 8 urological journals. He has also received Scholarships from the Greek Urological Association and European Association of Urology. Finally, he has performed over 40 oral presentations and invited speeches in many international conferences. For his fellowship in which he performed the presented research, he received the prestigious EAU-schollarship award 2017.